Higgs vacuum decay and implications for the Standard Model

Katie Marie Marshall

Thesis submitted for the degree of
Doctor of Philosophy

School of Mathematics, Statistics & Physics
Newcastle University
Newcastle upon Tyne
United Kingdom

September 2019

For Mum, Dad and Hollie.

Acknowledgements

This research was made possible by financial support from the Science and Technology Facilities Council.

I'd like to thank my primary supervisor Ian Moss for all the help, support, advice, and most of all patience over the last four years, without which I'd still probably be debugging the first program I ever wrote for this project. Also, my second supervisor Gerasimos Rigopoulos, for his help and alternate perspectives that often provided clarity. Thanks also to Ruth Gregory, Leo Cuspinera and Florent Michel for the discussions and collaborative work that made this thesis possible.

Over in Canada, thank you to the Perimeter Institute for hosting me for seven fantastic weeks and being the highlight of my PhD experience, while back home I'd like to thank my fellow PhD students in the department and all of PhD 6, especially Francesca for the coffee, Sophie for the LaTeX help and seemingly limitless supply of stationery, and Marios for being the challenge that sometimes I needed.

Thank you also to the cosmology group at Newcastle, especially Paul McFadden not only for his talks, but for agreeing to examine this thesis, for which I also thank my external examiner, Elizabeth Winstanley.

Outside of academia, I have to say thank you to Mum and Dad, for whom vacuums are Dysons and bubbles are found in Aeros, but have always been supportive and helped make the course of this PhD run smoother. Special thanks to Kayla, Beth, Kelly and Izzy for the company and friendship I needed to keep me going, no matter the distance.

Abstract

The confirmed discovery of the Higgs boson in 2012 raises some intriguing cosmological questions about the fate of the false vacuum and what this means for the Standard Model. Quantum field theory allows for the existence of metastable fields where a potential develops a lower energy state, or true vacuum, at large field values where the energy is lower than its local minimum, or false vacuum, value. The most recent measurements of the Higgs and top masses suggest this is the case for the Higgs potential.

A phase transition may occur through the process of quantum tunnelling, resulting in the nucleation of a rapidly expanding true vacuum bubble on a false vacuum background. Such a bubble may have devastating consequences for the universe if it expands to cover all of space. The fact that this has clearly not yet happened allows us to put constraints on our model for vacuum decay and provides insight into Beyond Standard Model physics.

Using methods from Euclidean field theory, we find the tunnelling rates of toy model potentials as well as a close approximation to the Higgs in various spacetimes. We first investigate tunnelling in asymptotically flat space before applying a similar method to false vacuum decay in de Sitter space, also incorporating the effects of back reaction.

Two different potentials are considered to investigate vacuum decay in a Randall-Sundrum braneworld: a quartic potential with two well defined vacua, and a Higgs-like potential closely approximating the Higgs at high energies. Vacuum decay is studied for fields living on a 4-dimensional brane in RS2, and the presence of a fifth dimension is found to have little influence on the decay rate.

We further use these potentials to look at the case of vacuum decay seeded by the presence of a black hole in five dimensions. By comparing the tunnelling rate with the Hawking evaporation, it is found that small black holes at high energy scales can catalyse vacuum decay. The energy scales needed to form such black holes may potentially be reached in the most energetic of cosmic ray collisions.

Finally, we look at the negative modes of O(4) and black hole instantons and find that instantons seeded by a black hole characteristically have a single negative mode. For O(4) instantons at energies close to the Planck scale, an infinite stack of negative modes arises, raising the question of how this is to be interpreted.

Contents

List of Figures

Chapter 1

Introduction

The existence of the Higgs boson was first proposed in 1964 – an excitation of the Higgs field that provides a mechanism by which other particles are granted mass[1]. Some time after this proposal, the subject of vacuum decay began to attract interest in the 1970s, with work by Sidney Coleman and others investigating the "fate of the false vacuum" [2], [3]. When considering the fate of our universe, these two topics become inextricably linked. If the Higgs field is metastable, then a spontaneous phase transition may result in, as Coleman put it, "the ultimate ecological catastrophe". This dramatic claim refers to the phenomenon of vacuum decay – if a field occupies a local minimum energy state, then there exists a non-zero probability of a spontaneous transition to a lower energy state.

Consideration of this possibility for a scalar field was initiated in the Soviet Union with Kobsarev, Okun and others investigating the formation of bubbles in metastable vacua [4],[5]. These bubbles form when a field occupying a local minimum energy state (known as the false vacuum) transitions to a lower energy state (the true vacuum). A bubble where the field is near to its true vacuum value nucleates at the transition site, before expanding very rapidly at speeds asymptotically approaching the speed of light to eventually swallow up all of space. The region contained inside this bubble has a lower vacuum energy and therefore different physics to the region outside, justifying Coleman's claim that such an event would indeed be an ecological catastrophe were such a bubble to swallow up Earth.

A methodology for calculating the likelihood of such a phase transition was developed by Coleman [2], and later extended to incorporate gravity by Coleman and de Luccia [3]. For a potential with two minima separated by a barrier, a transition from the higher to lower minimum may spontaneously occur through the process of quantum tunnelling. The transition rate Γ is given by

$$\Gamma = Ae^{-B} \tag{1.1}$$

where the prefactor A is a constant and B is the difference in actions between an instanton and the false vacuum. In the Coleman-de Luccia formalism, semi-classical (or instanton) solutions to the field's equations of motion are known as the bounce. Finding these instanton solutions provides a technique for investigating the decay rate of metastable vacua, including the Higgs.

In 2012, experiments at CERN confirmed the existence of the Higgs boson. Our current understanding suggests that the Higgs field is indeed metastable [6]. More accurate measurements of the Higgs and top quark masses are needed to determine the shape of the potential with greater certainty, but it is likely that the Higgs occupies a false vacuum state.

This raises some intriguing cosmological questions about physics beyond the Standard Model and the fate of our universe. The effects of such a transition may be felt across Hubble volumes or even larger scales, and a rapidly expanding vacuum bubble could have major consequences for the universe depending on whether it expands to cover all space or remains contained within a local horizon. An average decay time on the order of 10^9 years may be cause for concern, or it may be possible that true vacuum bubbles were formed during inflation. Evolution of the Higgs field during inflation has been previously studied by Espinosa *et al.* [7] and draws the conclusion that while the bubbles may initially be innocuous during the period of inflation, they could later expand to swallow all of space.

It is therefore of considerable interest to answer the question of how likely it is for a phase transition to occur, and what factors may enhance or suppress the transition rate. By first considering a toy model potential in Coleman's thin wall approximation, we develop numerical techniques to calculate B in Minkowski space, which is covered in section two.

The effect of back-reaction on the tunnelling rate and the interaction of a massive field with the spacetime curvature is considered in chapter three. We investigate tunnelling in de Sitter space and consider the effects of the self-coupling parameters in the potential and the rescaled Planck mass M_p.

Chapter four gives the potentials that we consider in the later chapters of this thesis: a quartic potential with two well-defined minima, and a logarithmic potential that closely approximates the Higgs potential at high energies.

Our techniques for calculating tunnelling rates are then applied to the Higgs field in chapter five, where we look at the influence of a fifth dimension on the bounce when the Higgs field is localised to a four-dimensional brane in a five-dimensional Randall-Sundrum

braneworld. Chapter six continues to investigate vacuum decay rates in RS2 with the addition of a black hole in the bulk.

The negative modes of Coleman-de Luccia instantons and how to interpret these are examined in chapter seven. The main scenario we consider is for O(4) instantons in empty space, and results are also included for vacuum decay seeded by a black hole. This presents the first look at negative modes of instantons with curvature coupling and we give a new result for the negative mode in the thin wall approximation.

In chapter eight, we summarise the conclusions we are able to draw from this study of vacuum decay and consider where future work in this field may lead.

Chapter 2

The Coleman-de Luccia Instanton

2.1 Metastable vacua and true vacuum bubbles

Investigation of vacuum decay began in the 1970s, when Kobsarev, Okun and Voloshin first considered the possibility in *Bubbles in metastable vacuum* [5]. This paper examined the case of two energy states with different energy density, and found that the higher vacuum was almost stable in terms of a possible phase transition to the lower. In the case where a phase transition occurs, a bubble of the lower vacuum energy state would be produced. The upper and lower vacua are now known as the false and true vacuum respectively. This paper looked at the possibility of vacuum decay for a Klein-Gordon field with the Lagrangian density

$$\mathscr{L} = \frac{1}{2}(\partial\phi)^2 - V(\phi) \tag{2.1}$$

A previous paper by Zeldovich, Kobsarev and Okun [4] had looked at the case where $V(\phi)$ is a symmetric potential

$$V(\phi) = \lambda^2(\phi^2 - \eta^2)^2 \tag{2.2}$$

where λ and η are constants. This potential produces two degenerate vacuums at $-\eta$ and $+\eta$ where $V(\phi) = 0$. The domains with $\phi = +\eta$ and $\phi = -\eta$ are separated by walls with thickness $\sqrt{2}/\eta$ and a surface mass density

$$\mu = \frac{4\sqrt{2}}{3}\lambda\eta^3 \tag{2.3}$$

This established that the walls can form bubbles which collapse under the action of the surface tension. For a potential with degenerate vacua, there is no difference in energy densities to trigger a spontaneous phase transition. Kobsarev *et al.* considered phase transitions for an asymmetric potential. In this case, the transition rate is related to the difference in actions between the false and true vacua according to

$$\Gamma = Ae^{-B} \tag{2.4}$$

A method for finding the action B was presented by Coleman in *Fate of the false vacuum: semiclassical theory* [2]. The method for finding the co-efficient A was dealt with in a second paper [8]. We will come back to the prefactor A later.

2.2 Vacuum decay from Euclidean Field Theory

In *Fate of the false vacuum* [2], Coleman presented a methodology for finding the instanton solutions for a quantum field theory with two vacuum states with different energy densities.

To begin constructing this methodology, first consider a particle of unit mass moving in one spatial dimension under the influence of potential $V(x)$. Imagine, in the classical version of this system, the particle is in a stable equilibrium at $x = 0$. However, in the quantum picture, quantum corrections render this state unstable. Field theory can give rise to a similar situation. Consider the theory of a scalar field in four dimensions with the Lagrangian,

$$\mathscr{L} = \frac{1}{2}\partial_\mu\phi\partial^\mu\phi - V(\phi). \tag{2.5}$$

The potential $V(\phi)$ has two unequal minima, referred to by Coleman as ϕ_+ (the higher state) and ϕ_- (the lower state). The higher of these energy states is known as the false vacuum, and the lower, the true vacuum.

The probability of a phase transition from the false to true vacuum is considered in terms of barrier penetration. Coleman develops a methodology by looking at barrier penetration in many dimensions for a particle of unit mass, and then extends this to Euclidean field theory (imaginary time). To investigate the evolution of the field in imaginary time, we make the substitution

$$t = i\tau \tag{2.6}$$

where t is the real time and τ is imaginary time. The Euclidean action is defined as minus the analytic continuation of (2.5) to imaginary time,

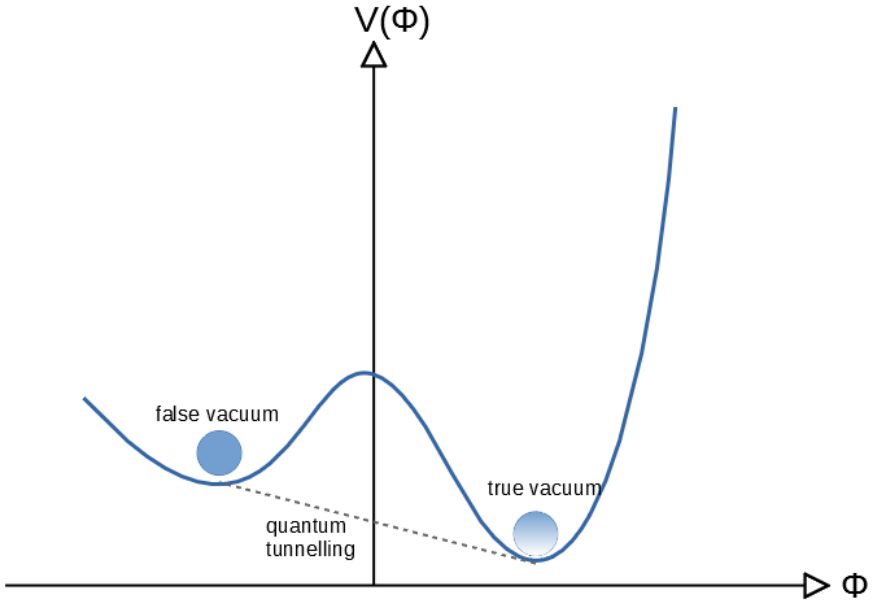

Figure 2.1: A potential with degenerate minima where it is possible for a phase transition from false to true vacuum to occur via quantum tunnelling.

$$S_E = \int d^4x \left[\frac{1}{2}\partial_\mu\phi\partial^\mu\phi + V(\phi)\right] \tag{2.7}$$

The equation of motion for the field with a solution known as the "bounce" is

$$\left(\frac{\partial^2}{\partial\tau^2} + \nabla^2\right)\phi = V'(\phi) \tag{2.8}$$

where the prime denotes differentiation with respect to ϕ. The boundary conditions for the bounce are

$$\lim_{\tau\to\pm\infty}\phi(\tau,\mathbf{x}) = \phi_+, \tag{2.9}$$

and

$$\frac{\partial\phi}{\partial\tau}(0,\mathbf{x}) = 0. \tag{2.10}$$

The action S_E will be used to determine the tunnelling exponent in equation (2.4):

$$S_E = \int d\tau d^3x \left[\frac{1}{2}\left(\frac{\partial\phi}{\partial\tau}\right)^2 + \frac{1}{2}(\nabla\phi)^2 + V\right]. \tag{2.11}$$

For B to be finite, the field must approach its false vacuum value at infinity. This imposes

the condition

$$\lim_{|x|\to\pm\infty} \phi(\tau, \mathbf{x}) = \phi_+, \tag{2.12}$$

This condition has a physical interpretation: quantum fluctuations cause a bubble of true vacuum to nucleate at the site of the transition, while at locations far away from this site, the field existing in the false vacuum remains unaffected.

It can be shown that the bounce is always O(4) symmetric, ie. ϕ is only a function of ρ where $\rho = \sqrt{|x|^2 + \tau^2}$. Therefore, the Euclidean action simplifies to

$$S_E = 2\pi^2 \int_0^\infty \rho^3 d\rho \left[\frac{1}{2}(\phi'^2) + V(\phi)\right]. \tag{2.13}$$

The prime denotes differentiation with respect to ρ. The equation of motion becomes

$$\phi'' + \frac{3}{\rho}\phi' = \frac{dV}{d\phi}. \tag{2.14}$$

The tunnelling exponent B in (2.4) is given by the difference in actions between the false vacuum and the bounce.

$$B = S_E(\phi) - S_E(\phi_+) \tag{2.15}$$

After tunnelling, the field inside the bubble evolves according to the classical field equation

$$-\frac{\partial^2\phi}{\partial t^2} + \nabla^2\phi = V'(\phi). \tag{2.16}$$

where t is the real time, and the bubble rapidly expands.

2.3 The thin wall approximation

In his first paper on the subject of vacuum decay [2], Coleman gives a method for finding instanton solutions where the bounce looks like an O(4) spherically symmetric bubble nucleating with a thin wall separating the region of true vacuum inside the bubble from the false vacuum background. The radius of the bubble is assumed to be large compared to the characteristic variational scale of the field ϕ.

To implement this method, Coleman begins by considering an even function of ϕ, $V_+(\phi)$,

$$V_0(\phi) = V_0(-\phi) \tag{2.17}$$

with minima at points $\pm a$,

$$V_0'(\pm a) = 0 \tag{2.18}$$

V_0 is a function chosen such that $V_0(\phi_+) = V_0(\phi_-)$ and $dV_0/d\phi$ vanishes at both ϕ_+ and ϕ_-. We define the difference between the two vacua ϵ

$$\epsilon = V(\phi_+) - V(\phi_-) \tag{2.19}$$

and write V as

$$V(\phi) = V_0(\phi) + O(\epsilon) \tag{2.20}$$

The equation of motion for the approximate ϕ is

$$\phi'' = \frac{dV_0}{d\phi} \tag{2.21}$$

This discards the term proportional to ϕ' in equation (2.14) which will be justified later. (2.21) admits a first integral,

$$\left[\frac{1}{2}(\phi')^2 - V_0\right]' = 0 \tag{2.22}$$

Its value is determined by the condition that $\phi(\infty)$ is the false vacuum ϕ_+:

$$\frac{1}{2}(\phi')^2 - V_0 = -V_0(\phi_\pm) \tag{2.23}$$

$\bar{\rho}$ is the point at which ϕ is the average of its two extreme values:

$$\int_{(\phi_+ + \phi_-)/2}^{\phi} d\phi [2(V_0 - V_0(\phi_\pm))]^{-1/2} = \rho - \bar{\rho} \tag{2.24}$$

$\bar{\rho}$ is assumed to be large compared to the length scale on which ϕ varies. If $\bar{\rho}$ is large, the bounce looks like a bubble of true vacuum embedded in the false vacuum, separated by a wall. This wall is small in thickness compared to the radius of the bubble, hence, we use a thin wall approximation to find instanton solutions.

Coleman determines $\bar{\rho}$ by computing the action B and imposing the condition it is stationary under variations of $\bar{\rho}$. The integration can be broken down into three parts: inside the wall, outside the wall, and within the wall itself.

Outside the wall:

$$B_{outside} = 0 \tag{2.25}$$

Inside the wall:

$$B_{inside} = -\frac{\pi^2}{2}\bar{\rho}^4\epsilon \tag{2.26}$$

Within the wall, in the thin wall approximation:

$$B_{wall} = 2\pi^2\bar{\rho}^3 \int d\rho \left[\frac{1}{2}\phi'^2 + V_0(\phi) - V_0(\phi_+)\right] \tag{2.27}$$

The tension in the bubble wall, σ, can be written as

$$\sigma = 2\int d\rho \left[V_0(\phi) - V_0(\phi_+)\right]. \tag{2.28}$$

Then, $B_{wall} = 2\pi^2\bar{\rho}\sigma$. We can now compute the action of the bounce

$$B = -\frac{1}{2}\pi^2\bar{\rho}^4\epsilon + 2\pi^2\bar{\rho}^3\sigma \tag{2.29}$$

This is stationary at

$$\bar{\rho} = 3\sigma/\epsilon \tag{2.30}$$

This quantity becomes large when ϵ is small. Therefore, for potentials with a small difference between the two minima, we can justify eliminating the ϕ'/ρ term in (2.14).

We can draw the following conclusions about the behaviour of the action depending on the form of the potential, and therefore the likelihood of the field to transition:

- B decreases and the tunnelling rate is enhanced when ϵ becomes large.
- The thickness of the bubble wall is increased by decreasing the size of the barrier.

We now know

$$B = 27\pi^2\sigma^4/2\epsilon^3 \tag{2.31}$$

The bounce has been used in the thin wall approximation to calculate a tunnelling coefficient that gives the probability of a bubble of true vacuum nucleating within the false vacuum. The bounce can also be used to describe the bubble evolution in real time. The surface $t = 0$ is the intersection of Euclidean space (imaginary) and Minkowski space (real time). The time derivative of ϕ on this surface is zero at the point the bubble materialises.

In this thin wall approximation, all of the energy released from the true vacuum to the false vacuum goes into driving the acceleration of the thin wall as the bubble expands.

Having established this model for vacuum decay in flat space, Coleman later with de Luccia modified the theory to incorporate gravity [3]. We will return to this later, but first we can revisit the other variable in the tunnelling equation: the co-efficient A.

2.4 First quantum corrections

Coleman's second paper with Callan [8] dealt with the co-efficient A in the tunnelling equation.

The specific value of A varies depending on the form of the potential V, though its contribution to the tunnelling rate is exponentially smaller than that of the action B. Therefore, throughout this thesis B will be the primary consideration when finding transition rates, though we will briefly look at A here and its relevance to the modes of the bounce.

The prefactor A comes from summing over the eigenvalues of all the perturbations about the bounce. It is obtained using a method based on functional integration, and ultraviolet divergences are removed using the usual renormalisation in perturbation theory.

Coleman and Callan present a method for obtaining A based on a sum over all the energy eigenstates. We can again consider the case of a particle of unit mass moving in one spatial dimension under the influence of the potential $V(x)$. The position eigenstates of the particle $|x_i>$ and $|x_f>$ appear in the Euclidean version of Feynman's sum over histories.

$$\langle x_f|e^{-HT/\hbar}|x_i\rangle = N\int [dx]e^{-S/\hbar} \tag{2.32}$$

In this equation, on the left hand side H is the Hamiltonian and T is a positive number, while on the right, N is a normalisation factor and S is the Euclidean action. Note, here $\hbar$ is not set equal to one. If we expand in a complete set of energy eigenstates

$$H|n\rangle = E_n|n\rangle, \tag{2.33}$$

Then

$$\langle x_f|e^{-HT/\hbar}|x_i\rangle = \sum_n e^{-E_nT/\hbar}\langle x_f|n\rangle\langle n|x_i\rangle. \tag{2.34}$$

The leading term in this expression for large T tells us the energy and wavefunction of the lowest lying energy eigenstate.

The Euclidean action S is

$$S = \int_0^T dt \left[\frac{1}{2} \left(\frac{dx}{dt} \right)^2 + V \right] \tag{2.35}$$

where $x(t)$ obeys the boundary conditions $x(0) = x_i$ and $x(T) = x_f$.

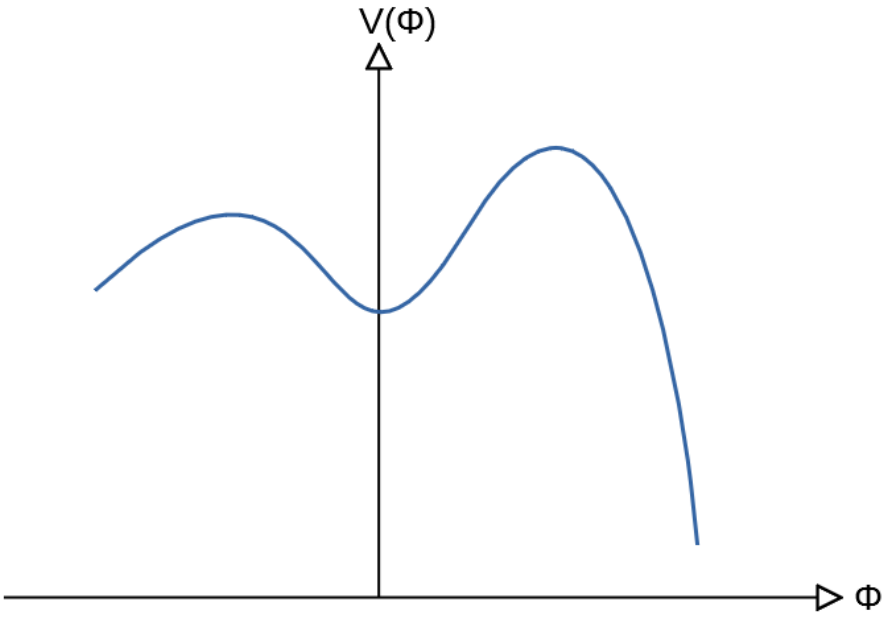

Figure 2.2: The Euclidean form of a potential with false and true vacua.

The total decay rate Γ can be found by summing the probability of decay from all the individual bounce solutions. The term "bounce" comes from the behaviour of a particle in the Euclidean form of a potential with a shape such as in fig. 2.2 (the potential is upside-down compared to fig. 2.1). The particle can begin at the top of the hill, bounce off the potential on the right, and return to the top of the hill. The bounce has energy $E = 0$ and the centre of the bounce is defined as the point where $dx/dt = 0$. If we denote the action of a bounce by B, then we can use equation (2.22) to express the action using the potential V

$$B = \int_{-\infty}^{\infty} dt (d\bar{x}/dt)^2 \tag{2.36}$$

$$= \int_0^{\sigma} dx [2V(x)]^{\frac{1}{2}} \tag{2.37}$$

where σ is the second zero of V (further explanation is given in [8].

By translation invariance, the centre of the bounce (ie. the point at which the bubble nucleates) can be anywhere along the t axis. For a very large time interval T, a bounce centred anywhere in the interval of integration is an approximate stationary point of the functional integrand. Therefore, there can be n separate bounces spaced out along an interval of length T, with centres at $t_1...t_n$, where $T > t_1 > t_2... > t_n > 0$. The functional integral can be evaluated by summing over all these configurations. Coleman and Callan do this by assembling the factors that go into this expression and then performing the summation.

For n bounces, the total Euclidean action is nB, which takes care of the exponential for the action.

To evaluate the determinant for the path integral, we find the product of contributions from large time intervals surrounding each bounce and the even larger time intervals where $x = 0$ surrounding each bounce. This gives

$$\left[\frac{\omega}{\pi}\right]^{\frac{1}{2}} e^{-\omega T} K^n \tag{2.38}$$

where K is defined by demanding that this expression give the right answer for one bounce and ω^2 is defined to be $V''(0)$.

Finally, an integration if performed over the locations of each of the centres of the bounce:

$$\int_0^T dt \int_0^{t_1} dt_2 ... \int_0^{t_{n-1}} dt_n = T^n/n! \tag{2.39}$$

The summation is now performed:

$$\sum_{n=0}^{\infty} \left[\frac{\omega}{\pi}\right]^{\frac{1}{2}} e^{-\omega T} \frac{(Ke^{-B}T)^n}{n!} = \left[\frac{\omega}{\pi}\right]^{\frac{1}{2}} \exp[-\omega T + Ke^{-B}T] \tag{2.40}$$

The total probability of decay comes from summing the probabilities of decay due to each bubble solution. For a single bubble solution, evaluating the path integral gives a contribution to A of the form

$$I_{\text{bubble}} \approx \frac{1}{2} i\Omega T \left|\frac{\det' S_E''[x_b]}{\det S_E''[x_{\text{fv}}]}\right|^{-1/2} \left(\frac{B}{2\pi}\right)^{1/2} e^{-B} I_{\text{fv}}, \tag{2.41}$$

where S_E'' is the second functional derivative of the Euclidean action, $\det'$ denotes the determinant with zero modes omitted, and I_{bubble} and I_{fv} are the actions of the bubble and false vacuum respectively. The factors Ω and T for the total volume and time period

arise from the zero modes, along with a Jacobian factor $(B/2\pi)^{1/2}$. This bounce solution has a vanishing derivative and is a saddle point of the Euclidean action. The second variational derivative of the action at the bounce has exactly one mode with a negative eigenvalue, which gives rise to a factor of i in the contribution to A (a more rigorous derivation of this result is given by Coleman and Callan in [8]). This would become i^n if there were n negative modes, which is explored later in chapter seven.

Summing the contributions to A from all possible bubble solutions gives a final decay probability per unit time

$$\Gamma = (B/2\pi)^{1/2} \left| \frac{\det'[-\partial_t^2 + V''(\bar{x})]}{\det[-\partial_t^2 + \omega^2]} \right| e^{-B}[1 + O(\hbar)]. \tag{2.42}$$

While the prefactor A is only considered in chapter seven of this thesis in relation to the negative modes of instantons, its contribution to the total decay rate is worth mentioning. Estimates for the prefactor A have been investigated previously by Strumia and Tetradis using a coarse-grained potential (a simplified form of the potential where microscopic detail can be smoothed over below the coarse-graining scale) in [9], which drew the following conclusions:

- The main role of A is to remove the dependence on the coarse-graining scale in high-temperature phase transitions.
- A always enhances the tunnelling rate.
- In strongly first-order phase transitions, B gives the dominant contribution to the decay process.
- A makes a greater contribution to the decay process for progressively weaker first-order phase transitions.

2.5 The Coleman-de Luccia instanton

Coleman's paper I [2] established a semiclassical theory for the decay of metastable vacua. In paper II [3], this theory is extended to include the effects of gravitation. While gravity and vacuum decay act on vastly different scales, when considering the evolution of the bubble, gravitational effects become significant.

We will now present a method for finding instanton solutions incorporating gravitation. As in the theory without gravity, consider a scalar field defined by the action,

$$S = \int d^4x \frac{1}{2}((\partial\phi)^2 - V(\phi)), \tag{2.43}$$

where $V(\phi)$ is a potential with two non-degenerate local minima $\phi_{\pm}$. A bubble is produced as a result of a transition from ϕ_+ to ϕ_-. When the bubble nucleates, the energy released by conversion of false vacuum to true is proportional to the volume of the bubble, and therefore so is the Schwarzchild radius associated with this energy.

Gravitation affects vacuum decay and vacuum decay affects gravitation. Incorporating gravitational effects into the theory, a scalar field is defined by the action,

$$S = \int d^4x\sqrt{-g}\frac{1}{2}[g^{\mu\nu}(\partial\phi)^2 - V(\phi) - (8)\pi G)^{-1}R], \tag{2.44}$$

where R is the curvature scalar. A cosmological constant can be introduced into the action by adding a constant to V. Once vacuum decay occurs, the cosmological constant inside the bubble is different from the one outside, fundamentally changing the structure of the spacetime for the true vacuum. The effects of backreaction on decay rates are discussed in section two.

Experimental observations confirm our universe is flat with a very small cosmological constant [10]. We therefore have two scenarios to consider: (1) that we live in a false vacuum where a phase transition has yet to occur, and the shape of the spacetime in any true vacuum bubble would be AdS; or (2) we live in a universe in which vacuum decay has already occurred, and the resulting spacetime in the true vacuum bubble is flat after tunnelling. Measurements of the Higgs mass that find the field to be metastable [6], [11] rule out the second of these scenarios.

To expand Coleman's model for vacuum decay to incorporate gravity, we begin with the bounce solution. We can reasonably assume that gravitation does not break the symmetries of the scalar problem, and the bounce will therefore be invariant under four-dimensional rotations.

In this model, we first construct a general rotationally invariant Euclidean metric. Define a radial curve to be a curve of fixed angular co-ordinates. Choose the radial co-ordinate ξ to measure distance along radial curves.

$$ds^2 = d\xi^2 + \rho(\xi)^2 d\Omega^2 \tag{2.45}$$

where $d\Omega^2$ is the element of distance on a unit three-sphere of volume $2\pi^2$ and ρ gives the radius of curvature of each three-sphere.

The scalar field equation is

$$\phi'' + \frac{3\rho'}{\rho}\phi' = \frac{dV}{d\phi} \tag{2.46}$$

where the prime denotes $d/d\xi$. The Einstein equation

$$G_{\xi\xi} = -\kappa^2 T_{\xi\xi} \tag{2.47}$$

becomes

$$\rho'^2 = 1 + \frac{1}{3}\kappa^2\rho^2\left(\frac{1}{2}\phi'^2 - V\right) \tag{2.48}$$

where $\kappa = 8\pi G$.

The action of the field incorporating gravity is

$$S_E = 2\pi^2 \int d\xi \left(\rho^3(\frac{1}{2}\phi'^2 + V) + \frac{3}{\kappa^2}(\rho^2\rho'' + \rho\rho'^2 - \rho)\right). \tag{2.49}$$

From this, we will now construct the bounce in the thin wall approximation. Trivially, inside the wall, ρ is replaced with ξ. Comparing the field equations with and without gravity, the co-efficient of the ϕ' term in the gravitational case is now ρ'/ρ rather than $1/\rho$. Therefore, in the thin wall approximation we can copy (2.24) and replace ρ.

$$\int_{(\phi_+ + \phi_-)/2}^{\phi} d\phi[2(V_0 - V_0(\phi_\pm))]^{-1/2} = \xi - \bar{\xi} \tag{2.50}$$

Once we have ϕ, we can solve the Einstein equation (2.48) to find ρ. We choose the integration constant

$$\bar{\rho} = \rho(\bar{\xi}) \tag{2.51}$$

This is the radius of curvature of the wall separating the false and true vacua.

The action S_E can be integrated by parts to give

$$S_E = 2\pi^2 \int d\xi \left(\rho^3(\frac{1}{2}\phi'^2 + V) - \frac{3}{\kappa^2}(\rho\rho'^2 + \rho)\right) \tag{2.52}$$

It is not necessary to introduce any surface term to the action – B is the difference between two actions where the solutions agree at infinity, and these surface terms will therefore cancel in the calculation of the bounce action.

We can now use (2.48) to replace ρ'^2:

$$S_E = 2\pi^2 \int d\xi \left(\rho^3 V - \frac{3\rho}{\kappa^2}\right) \tag{2.53}$$

So far in this subsection, we have not yet implemented the thin wall approximation in our calculations incorporating gravitation. Now we will evaluate B. The action is divided up

into three parts as before.

Outside the wall:

$$B_{outside} = 0 \tag{2.54}$$

Within the wall, ρ can be replaced with $\bar{\rho}$ and V with V_0:

$$B_{wall} = 4\pi^2\bar{\rho}^3 \int d\xi [V_0(\phi) - V_0(\phi_+)] \tag{2.55}$$

Inside the wall, ϕ is constant, hence,

$$d\xi = d\rho(1 - \frac{1}{3}\kappa\rho^2 V)^{-1/2} \tag{2.56}$$

and

$$B_{inside} = -\frac{12\pi^2}{\kappa} \int_0^{\bar{\rho}} \rho d\rho [1 - \frac{1}{3}\kappa\rho^2 V(\phi_-)]^{1/2} - (\phi_- \to \phi_+) \tag{2.57}$$

When considering vacuum decay in relation to our universe, there are two possibilities: we are either living in a pre-transition universe waiting for vacuum decay to occur, or alternatively, vacuum decay has already happened at some point in the past and we live in the universe with the new vacuum energy that results from it.

Our current understanding of the Higgs field allows us to rule out this second scenario and conclude that our universe exists in a metastable vacuum. However, Coleman and de Luccia considered the post-apocalyptic scenario for a more general scalar field.

2.5.1 Case 1

The first special case Coleman and de Luccia consider is that we currently live in a universe after vacuum decay, where our present spacetime in the true vacuum is flat having decayed from a de Sitter false vacuum. The energy densities of the false and true vacua are:

$$V(\phi_+) = \epsilon, V(\phi_-) = 0 \tag{2.58}$$

The action B is stationary at the bubble radius

$$\bar{\rho} = \frac{12\sigma}{4\epsilon + 3\kappa\sigma^2} \tag{2.59}$$

$$= \frac{\bar{\rho_0}}{1 + (\bar{\rho_0}/2\Lambda)^2}. \tag{2.60}$$

The action can be expressed in terms of the action without gravitation, B_0

$$B = \frac{B_0}{[1 + (\bar{\rho}/2\Lambda)^2]^2}. \tag{2.61}$$

where $B_0 = 27\pi^2\sigma^4/2\epsilon^3$ is the decay exponent in the absence of gravity.

2.5.2 Case 2

The second special case considered is that we're living before a vacuum decay event has happened in our region of space. In this scenario, we live in a flat universe with zero energy density at the false vacuum, while the true vacuum has negative energy density and the spacetime inside the bubble is anti-de Sitter. The energy densities for the false and true vacua are:

$$V(\phi_+) = 0, V(\phi_-) = -\epsilon \tag{2.62}$$

B is stationary at

$$\bar{\rho} = \frac{\bar{\rho_0}}{1 - (\bar{\rho_0}/2\Lambda)^2} \tag{2.63}$$

The action is

$$B = \frac{B_0}{[1 - (\bar{\rho}/2\Lambda)^2]^2} \tag{2.64}$$

Without gravitation, the thin wall approximation is valid when $\bar{\rho}$ is large compared to the length scale of variation of ϕ. In the case with gravity, $1/\rho$ in the ϕ' term in the field equations is replaced with ρ'/ρ. This is the quantity that must be small at the wall.

We can test whether this is small using the Einstein equations. From equation (2.48), we have,

$$\frac{\rho'^2}{\rho^2} = \frac{1}{\rho^2} + \frac{\kappa}{3}\left(\frac{1}{2}\phi'^2 - V\right) \tag{2.65}$$

The left hand side is small if both terms on the right are small. The first term $1/\rho$ is small as in the non-gravitational case. In the second term, $\left(\frac{1}{2}\phi'^2 - V\right)$ is approximately constant throughout the wall, and has zero magnitude on one side of the wall and magnitude ϵ on the other. It would therefore be an overestimate to replace this quantity with ϵ everywhere – the second term becomes $(1/\Lambda)^2$.

The thin wall approximation is valid if both $\bar{\rho}$ and Λ are large compared to the characteristic scale on which ϕ varies, which does not place a restriction on the ratio $\bar{\rho}/\Lambda$ that measures the importance of gravitation.

Coleman and Callan consider two special cases. In the first case, for a field decaying into

our present vacuum, gravitation increases the likelihood of a bubble materialising (B gets smaller) and decreases the radius of the bubble at the point of materialisation (ρ gets smaller).

In the second case, for a field decaying from our present vacuum, the opposite is true. The presence of gravitation introduces a cosmological constant Λ and makes bubble nucleation less likely while the radius of the bubble increases. Vacuum decay can be quenched completely when $\bar{\rho_0} = 2\Lambda$, where $\bar{\rho}$ is the bubble radius before incorporating gravitational effects.

This can be explained by considering the energy of the bubble. For vacuum decay to occur, the nucleating bubble must have zero energy – the sum of a negative volume term and a positive surface term. In the case without gravity, it is always possible to create a zero energy bubble regardless of how small ϵ is, provided $\bar{\rho}$ is large. The volume/surface ratio in this case allows the bubble to have zero energy.

When including gravitation, the negative energy density inside the bubble leads to a distortion of the spacetime geometry in such a way as to diminish the volume/surface ratio. It is therefore possible that, for sufficiently small ϵ, no bubble will ever have zero energy regardless of the size of $\bar{\rho}$.

2.6 Negative mode solutions

As a result of the first quantum corrections in [8], a characteristic feature of vacuum decay is the emergence of a negative mode of field perturbations corresponding to a scaling of the bubble radius up or down. In chapter seven, we address the problem of infinitely many such modes occurring for tunnelling in asymptotically de Sitter space.

For the case with a negative mode, a solution to the field equations can be found by considering a potential with degenerate minima

$$V_0 = \frac{1}{4}\lambda\phi^2(\phi - \phi_{tv})^2 \tag{2.66}$$

where the field has its true vacuum value at $\phi = \phi_{tv}$. For this potential, the field equation is,

$$\frac{1}{2}\phi'^2 = V_0(\phi) \tag{2.67}$$

Which then permits a solution for ϕ of the form,

$$\phi = \frac{1}{2}\phi_{tv}(1 - \tanh\kappa(r - R)) \tag{2.68}$$

where r is the radial co-ordinate with the centre of the bubble at $r = 0$ and R is the bubble radius. By differentiating 2.68 and defining $\theta = \kappa(r - R)$ we can write ϕ' as

$$\phi' = \frac{1}{2}\phi_{tv}\kappa\,\mathrm{sech}^2\,\theta \tag{2.69}$$

Substituting into 2.67 gives

$$\frac{1}{2}\phi'^2 = \frac{1}{8}\phi_{tv}\kappa^2\,\mathrm{sech}^2\,\theta \tag{2.70}$$

$$\begin{aligned} \frac{1}{4}\lambda\phi^2(\phi^2 - \phi_{tv}^2) &= \frac{1}{4}\lambda\phi_{tv}^2(1 - \tanh\theta)^2\frac{1}{4}\lambda\phi_{tv}^2(1 + \tanh\theta)^2 & (2.71)\\ &= \frac{1}{64}\lambda\phi_{tv}^2(1 - \tanh^2\theta)^2 & (2.72) \end{aligned}$$

Hence κ is given by

$$\kappa^2 = \frac{1}{8}\lambda\phi_{tv}^2 \tag{2.73}$$

The action per unit area of the bubble wall, σ, can be found by performing an integration of the potential

$$\sigma = \int_0^{\phi_{tv}} \sqrt{\frac{1}{2}\lambda\phi^2(\phi^2 - \phi_{tv}^2)}d\phi \tag{2.74}$$

We can now substitute (2.68) and (2.72) to express κ in terms of σ.

$$\kappa = \frac{3\sigma}{\phi_{tv}^2} \tag{2.75}$$

In chapter seven, we revisit this solution for ϕ to explore the negative modes of O(4) and black hole instantons.

Chapter 3

Tunnelling with toy model potentials

3.1 Tunnelling in flat space

Numerical techniques for investigating decay rates are developed from Coleman and de Luccia's formalism for finding instanton solutions using Euclidean field theory. To build these techniques, the first case considered is one where the gravitational back reaction is ignored. This has the metric:

$$ds^2 = dt^2 - dx^2 - dy^2 - dz^2. \tag{3.1}$$

To convert this metric to the Euclidean space we will work in, we make the replacement $t = ir$ where r is the imaginary time. In polar co-ordinates the metric can be written in terms of r:

$$ds^2 = dr^2 + r^2(d\chi^2 + \sin^2\chi(d\theta^2 + \sin^2\theta d\phi^2)) \tag{3.2}$$

For a vacuum to be metastable, there must exist a barrier in the potential through which the field can tunnel, the height of which will determine the bubble wall thickness (see fig. 3.1).

The method to find instanton solutions numerically implements a means of testing whether an estimate for ϕ at the centre of the bubble, ϕ_0, "undershoots" or "overshoots", as defined by Coleman in [2]. The explanation of this considers a particle moving in the potential subject to a viscous damping force. If the initial position of this particle is properly chosen, it will come to rest at ϕ_{fv}, the value of ϕ in the false vacuum, at minus infinity.

We will return to this explanation later when considering the implementation of numerical methods.

Depending on particle physics parameters such as the Higgs mass, the Higgs potential may feature a false vacuum and a potential barrier. The precise location of the true vacuum is either not known, or a second local minimum might not exist. The potentials we will use in later chapters give close approximations to the Higgs potential at large field values. To begin developing our methods to find instanton solutions numerically, we will first consider a toy model potential with two well-defined minima, the lower of which is located at $V(\phi) = 0$, thus placing the true vacuum in flat space.

$$V(\phi) = \frac{1}{2}m^2\phi^2 - \frac{1}{4}\lambda\phi^4 + \frac{1}{6}g\phi^6 \tag{3.3}$$

m is the scalar field mass while g and λ are self coupling parameters. The number of free parameters can be reduced by rescaling. First we choose to define $\phi = \phi'/P$ and $V = V'/Q$ and substitute this into equation (3.3):

$$V' = QV = \frac{Q}{2}m^2\frac{\phi'^2}{P^2} - \frac{Q}{4}\lambda\frac{\phi'^4}{P^4} + \frac{Q}{6}g\frac{\phi'^6}{P^6} \tag{3.4}$$

We then make the substitutions $m' = Qm^2/P^2$ and $\lambda' = Q\lambda/P^4$. By setting $m' = \lambda' = 1$, we can rewrite the remaining coupling parameter as $g' = m^6 g/\lambda^3$. The prime is then dropped. Our rescaled potential is therefore

$$V(\phi) = \frac{1}{2}\phi^2 - \frac{1}{4}\phi^4 + \frac{1}{6}g\phi^6 \tag{3.5}$$

This resembles the potential considered by Coleman in [2] in that both minima are well defined and that a bubble is expected to nucleate close to the minimum of the true vacuum.

The Euclidean field equation is

$$\phi'' + \frac{3}{r}\phi' - \frac{dV}{d\phi} = 0 \tag{3.6}$$

Our numerical methods are concerned with computing the quantity B in the usual tunnelling equation

$$\Gamma = Ae^{-B}. \tag{3.7}$$

(Coleman gives the exponent here as $-B/\hbar$, but we will choose to set $\hbar = 1$ for all

calculations.)

While the factor A has a small contribution to the tunnelling rate, B dominates the decay process and will be the primary concern throughout this thesis. Therefore, the numerical methods used to solve the field equations do not include a computation of A.

3.2 Numerical methods

After tunnelling, the field assumes a value ϕ_0 close to its true vacuum value ϕ_{tv} at the centre of the nucleated bubble, while the field remains in the false vacuum at large r. A regular solution must have ϕ' vanish at $r = 0$. We can therefore impose the boundary conditions:

$$\phi'(0) = 0 \tag{3.8}$$

$$\lim_{r\to\infty} \phi(r) = \phi_{fv} \tag{3.9}$$

Numerical calculation of the exact instanton solutions implements a shooting method. This requires making an initial estimate for the field value at the centre of the bubble $\phi(0) = \phi_0$, and an integration over r is then performed until either of the following conditions are met:

$$\phi < 0 \tag{3.10}$$

$$V(\phi) - \frac{1}{2}\phi'^2 > 0 \tag{3.11}$$

An instanton solution exists when both conditions are met simultaneously, thus satisfying the boundary conditions. If both conditions are not met, the initial estimate for ϕ_0 is adjusted accordingly depending on whether it "overshoots" or "undershoots". Coleman defines these terms in [2] depending on whether the field begins too far to the left or right of ϕ_{tv}, such as in fig. 3.1.

Returning to Coleman's explanation in terms of a particle moving in the potential, if the initial position is chosen to the right of ϕ_0 but sufficiently close to the turning point, the particle will overshoot and pass ϕ_{fv} at a finite time. On the other hand, should the initial position be chosen too far to the left of ϕ_0, the particle will never reach ϕ_{fv} and thus undershoots.

The beginning estimate for ϕ_0 is selected by choosing two points ϕ_{Left} and ϕ_{Right} between which ϕ_0 is expected to lie, and taking the midpoint $\phi_M = (\phi_L + \phi_R)/2 = \phi_0$. This starting estimate must be lie between the top of the barrier and the true vacuum. A numerical integration of ϕ between $r = 0$ and $r = \infty$ is then performed, stopping when

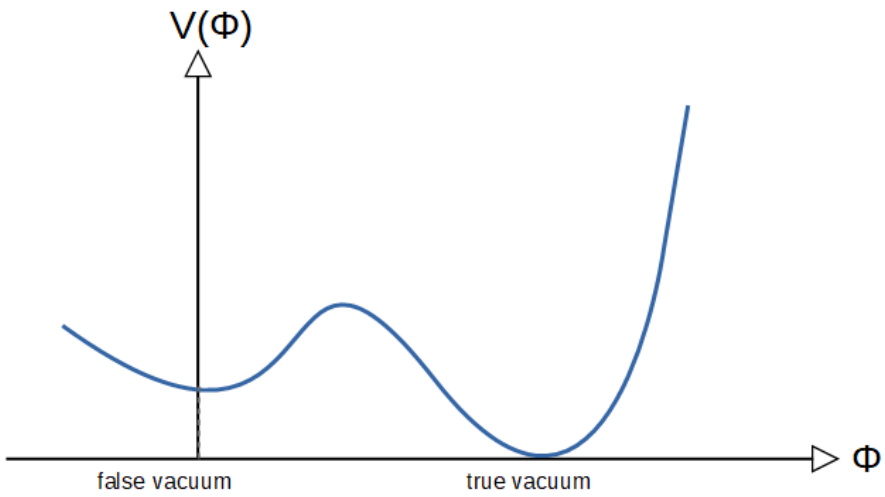

Figure 3.1: An example potential with false and true vacua, where the true vacuum is located at $V(\phi) = 0$.

r becomes very large. If the starting point chosen is too far to the right, there is not enough friction to slow down the field and satisfies the stopping condition 3.10 before the integration completes. This is considered an "overshoot" and a new estimate is chosen by reassigning $\phi_L = \phi_M$.

Similarly, if the starting point chosen is too far to the left, the field hits the potential and never reaches $\phi = 0$, satisfying the stopping condition 3.11 before the integration completes. This is considered an "undershoot" a new estimate is chosen by reassigning $\phi_R = \phi_M$. This process is repeated until the above conditions are met simultaneously to a desired accuracy and the actual value of for ϕ_0 can be assumed to lie close to the actual value.

3.3 Bubble profiles and action

The above method can be used to obtain the bubble profile for a single bounce solution, and also to investigate the effects of the self-coupling on the action B. For tunnelling in flat space, fig. 3.2 shows the evolution of the field during tunnelling when g=0.1. The thin wall approximation applies when the radius of the bubble R is much larger than the thickness of the bubble wall, which can be seen to be the case.

From fig. 3.3 it can be seen that there is a smooth increase in B as g is increased, meaning a stronger coupling suppresses the tunnelling rate. The location of the second minimum places a limit on the maximum value of $g < 3/16$ in order for the field not to tunnel beyond the minimum. However, the thin wall approximation breaks down before reaching

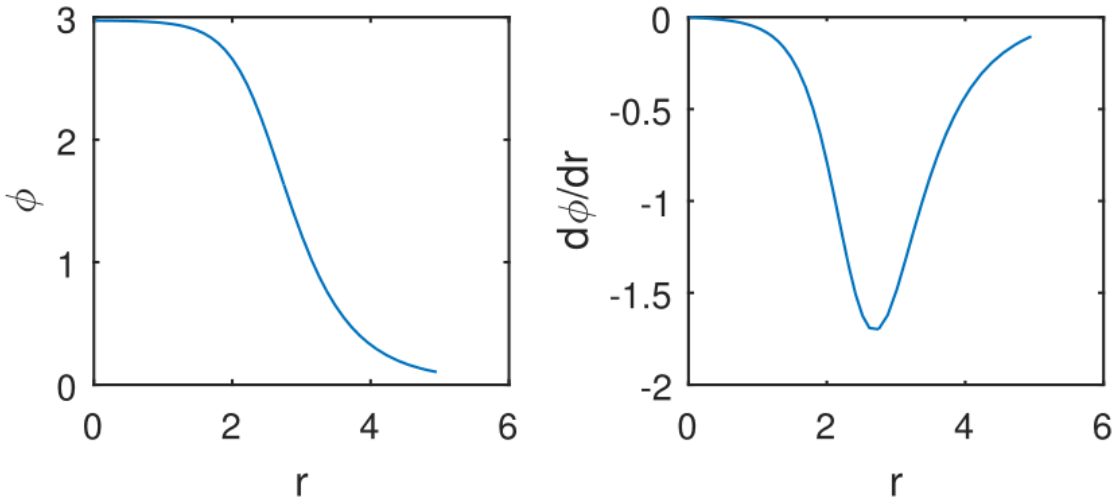

Figure 3.2: The change in ϕ and ϕ' with distance r from the center of the bubble when g=0.1. At this value of g we can see that the bubble's radius R is smaller than the thickness of its wall, determined by the steepness of the slope.

this point. Beyond a certain value of g, R becomes larger than the thickness of the bubble wall and the semiclassical approximation is no longer valid. This can be seen from the cut-off in fig. 3.2 beyond which numerical solutions could not be obtained.

3.4 Tunnelling between de Sitter vacua

So far, we have established a general methodology for calculating instanton solutions in order to obtain B and applied this to phase transitions in flat space. We will now consider tunnelling between de Sitter vacua where the spacetime within the bubble is also curved.

In curved space, the scale factor a now plays a role and the decay process is subject to back reaction. We will investigate the decay of a metastable field in 4-dimensional curved space that has curvature constant $k = 1$. Our metric is

$$ds^2 = dr^2 + a(r)^2[d\chi^2 + \sin^2\chi(d\theta^2 + \sin^2\theta d\phi^2)] \tag{3.12}$$

where $a(r)$ is the scale factor as a function of imaginary time r. Here we embed a two-sphere space within a three-sphere. This spacetime is chosen due to its O(4) symmetry and has a finite volume that will give a finite bounce action.

The spacetime evolves as the field tunnels through the barrier. The Euclidean Lagrangian

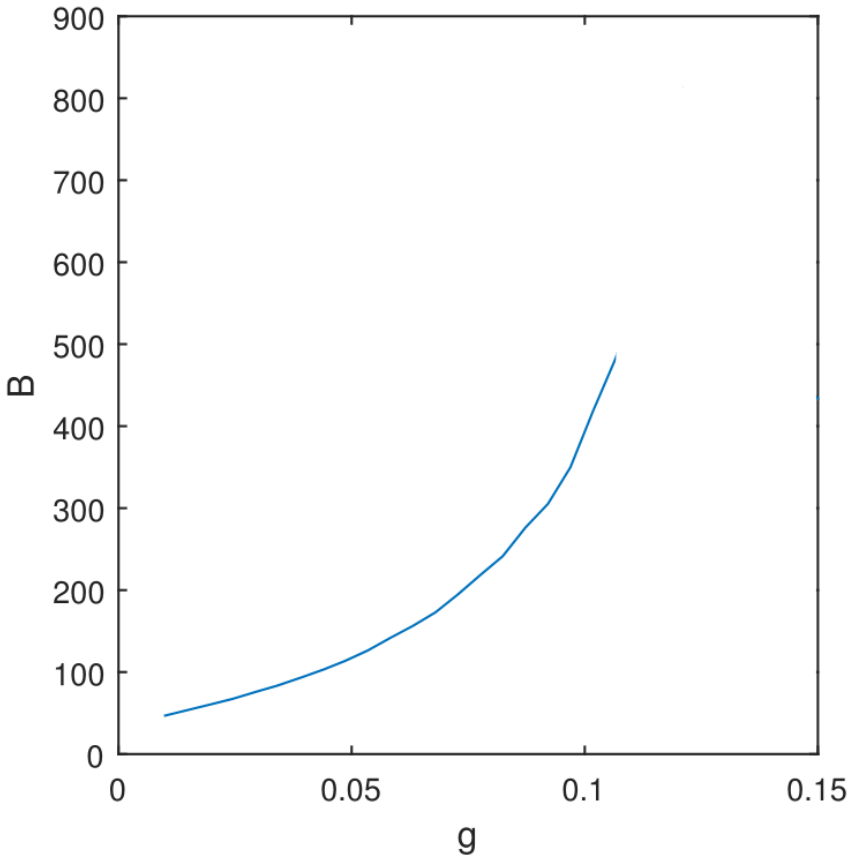

Figure 3.3: The tunnelling exponent B can be obtained over a range of g.

density for the bounce is given by

$$\mathscr{L} = \left(-\frac{RM_p^2}{2} + \frac{1}{2}(\nabla\phi)^2 + V(\phi)\right)\sqrt{|g|} \tag{3.13}$$

$$= 2\pi\left[-3M_p^2(ka + aa'^2) + a^3\left(\frac{1}{2}\phi'^2 + V(\phi)\right)\right] \tag{3.14}$$

Where R is the Ricci curvature tensor and the curvature constant $k = 1$. Primes denote differentiation with respect to r.

To avoid further calculations at this stage that are necessary to approximate the Higgs, we will again use a toy model potential with two well defined local minima. This allows the effects of back reaction to be observed as the relevant free parameters are varied. The form we choose for V is similar to the potential considered for the flat space case, with an additional parameter V_0.

$$V(\phi) = \frac{1}{2}m^2\phi^2 - \frac{1}{4}\lambda\phi^4 + \frac{1}{6}g\phi^6 + V_0 \tag{3.15}$$

m is the field mass while λ and g are self coupling parameters. V_0 is a non-zero quantity that tunes the potential such that $V(0) = V_0$, thus placing the false vacuum in de Sitter space while the spacetime inside the true vacuum bubble has a smaller potential and hence a smaller curvature. Rescaling allows us to set $m = \lambda = 1$ and therefore leaves two free parameters remaining in the potential: the rescaled Planck mass M and a constant V_0. We also have one free parameter from the Einstein equations: the self-coupling parameter g.

The Euclidean field equations are:

$$0 = \phi'' + 3\frac{a'}{a}\phi' - \frac{dV}{d\phi} \tag{3.16}$$

$$0 = 1 - a'^2 - 2aa'' - \frac{a^2}{M^2}\left(\frac{1}{2}\phi'^2 + V(\phi)\right) \tag{3.17}$$

where the prime denotes differentiation with respect to r.

3.4.1 Free parameters

There are three free parameters: V_0, M, and g. A fourth parameter is the de Sitter radius L, which gives the size of a "false" vacuum universe. This is dependent on V_0 and M according to $V_0 = -3M_p^2/L^2$ and is absorbed into the V_0 scaling. M is the rescaled reduced Planck mass such that $M^2 = \lambda M_p^2/m^2$. These parameters determine the shape of the potential, and therefore affect the tunnelling rate.

With the scale factor a coming into play and the instanton is finite, we no longer integrate between $r = 0$ and $r = \infty$, but impose boundary conditions based on the topology of the spacetime.

$$\phi'(0) = 0 \tag{3.18}$$

$$\phi_{\text{final}} = 0 \tag{3.19}$$

$$a(0) = 0 \tag{3.20}$$

$$a_{\text{final}} = 0 \tag{3.21}$$

Note that, from equation (3.17), $a'(0) = 1$.

In practice the complete integration is now performed between the two points where $a(r) =$

0. However, the transition between the false and true vacuums will occur long before this integration completes at $a = 0$.

We integrate the Lagrangian between $r_0 = 0$ and $r_1 < r_{final}$ to get the action of the bounce, given by

$$S_E = 2\pi^2 \int_0^{r_1} \left[-\frac{1}{3M^2}(a + aa'^2) + a^3 \left(\frac{1}{2}\phi'^2 + V(\phi) \right) \right] dr \tag{3.22}$$

The tunnelling exponent B in this case is given by

$$B = S_E - S_{FV} \tag{3.23}$$

where S_E is the bounce action and S_{FV} is the action for the false vacuum given by a change of variable from r to a' in equation (3.22). The action of the false vacuum is

$$\begin{aligned} S_{FV} &= 2\pi^2 \int_{a'(0)}^{a'(r_0)} \frac{18M^4 a'^2}{V_0} da' && (3.24) \\ &= 2\pi^2 \left[\frac{6M^4 a'^3}{V_0} \right] && (3.25) \\ &= \frac{12\pi^2 M^4}{V_0}(a'(r_0)^3 - 1) && (3.26) \end{aligned}$$

3.4.2 Evolution of the field and back reaction

Varying the parameters V_0, M, and g allows the effects of back reaction on ϕ to be observed. The back reaction can be reduced by increasing V_0, which reduces the relative difference between the two minima and increases the thickness of the bubble wall. The effect of variations in V_0 and M are shown in figures 3.6 and 3.7.

In the false vacuum, the scale factor a relates to r according to

$$a(r) = L\sin((r - r_0)/L) \tag{3.27}$$

where L is the de Sitter radius and r_0 is r at the centre of the bubble. At small r, this can be approximated as $a(r) \approx r$. The comparison between this and the numerical solution is shown in Fig. 3.4 (top right).

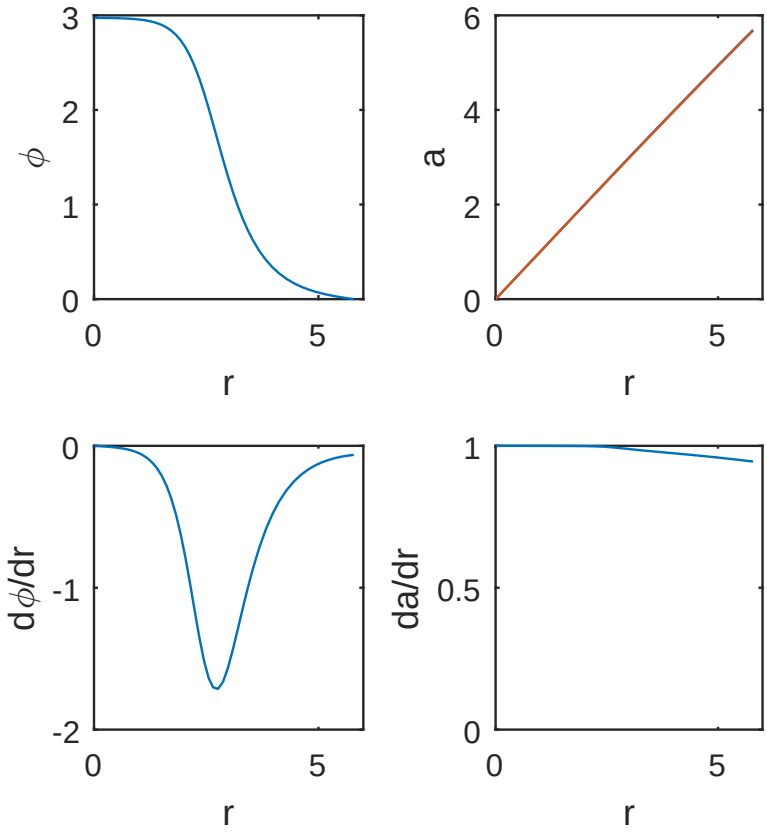

Figure 3.4: Plots of ϕ, ϕ', a and a' against r with the parameters $V_0 = 4$, $M_p = 20$, $g = 0.10$. The top left plot shows the profile of a thin wall ;bble, where the field approaches zero as r goes to infinity. Also plotted (red) in the top right is an analytical approximation for a at small values of r, $a = L\sin((r - r_0)/L)$, which perfectly matches the numerical calculation.

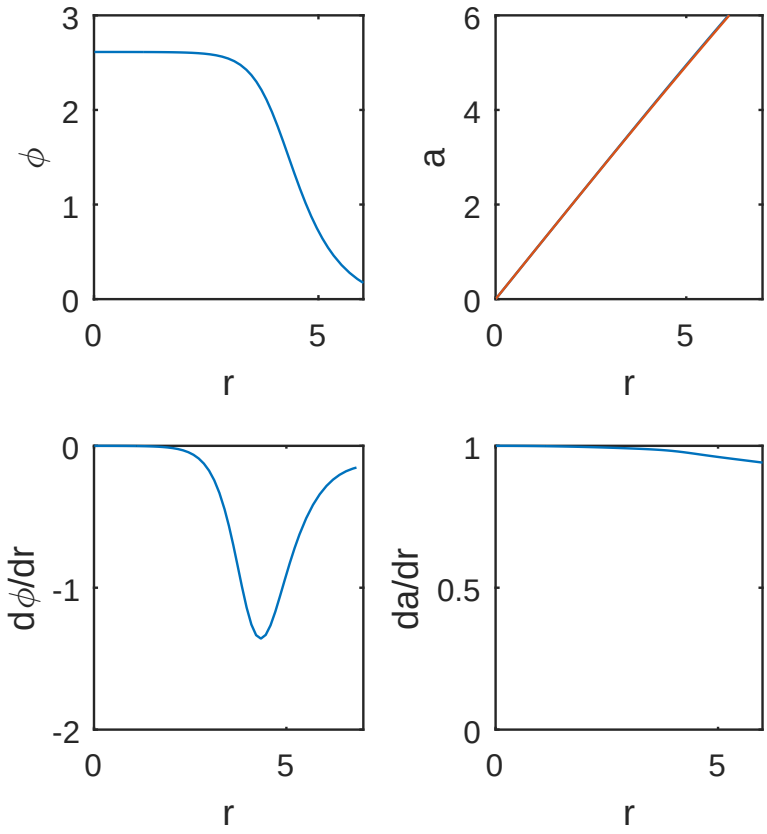

Figure 3.5: Plots of ϕ, ϕ', a and a' against r with the parameters $V_0 = 4$, $M = 20$, $g = 0.125$. Contrasted with figure (3.4), it can be seen that increasing g by 0.025 has increased the radius of the bubble and decreased the absolute difference between the two vacua, which is consistent with the case in flat space.

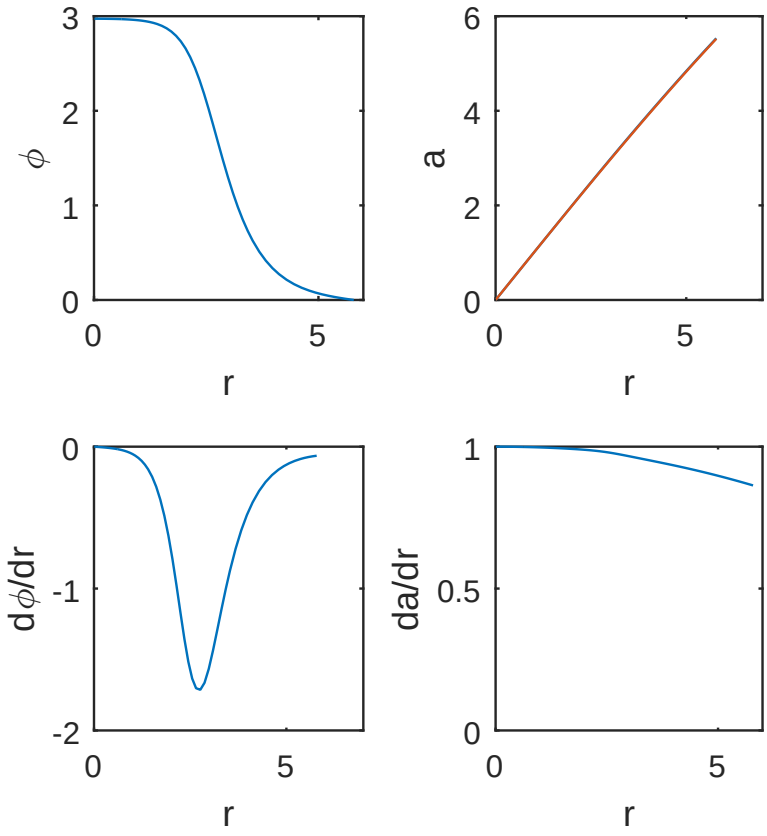

Figure 3.6: Plots of ϕ, ϕ', a and a' against r with the parameters $V_0 = 10$, $M = 20$, $g = 0.10$.

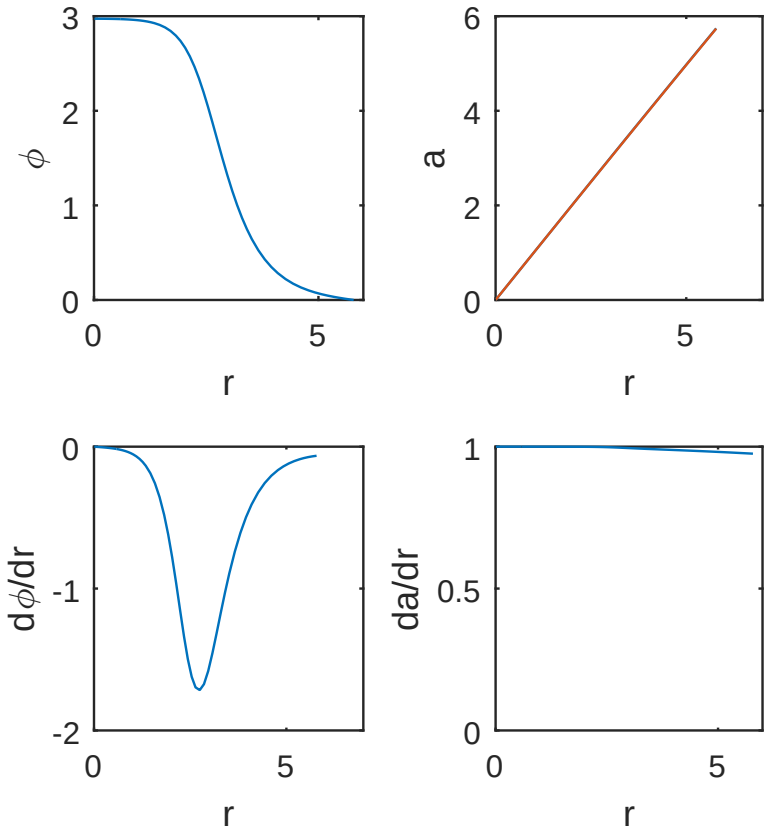

Figure 3.7: Plots of ϕ, ϕ', a and a' against r with the parameters $V_0 = 4$, $M = 30$, $g = 0.10$.

Chapter 4

Higgs approximations

4.1 Approximations to the Higgs potential

There has been a recent resurgence of interest in applications of vacuum decay to the standard model Higgs field [12, 13, 14, 15, 16, 17, 18]. In the following sections, we will consider various scenarios for vacuum decay with a potential that closely approximates the Higgs at large field values.

The standard model Higgs field is an SU(2) doublet Φ. The Higgs potential has the bare form

$$V(\Phi) = -\mu^2|\Phi|^2 + \lambda|\Phi|^4 \tag{4.1}$$

where λ is determined experimentally from measurements of the Higgs and top quark masses. The potential is symmetric under SU(2) field transformations, and at large field values it is often described as having a Mexican hat shape. Fig. 4.1 shows the real and imaginary parts of the field Φ.

The Higgs potential at large $|\Phi|$ includes quantum corrections and can be expressed in terms of an effective self-coupling λ_{eff} and field $\phi = \frac{1}{2}|\Phi|$

$$V(\phi) = \frac{1}{4}\lambda_{\text{eff}}\phi^4 \tag{4.2}$$

where λ_{eff} is a parameter greater than zero for stability. One and two-loop calculations in renormalisation group theory can be used to obtain estimates for λ_{eff} and allow for close approximations to the Higgs potential at large field values. Computations of the first next-to-next-to-leading order analysis of the Standard Model Higgs potential were presented in

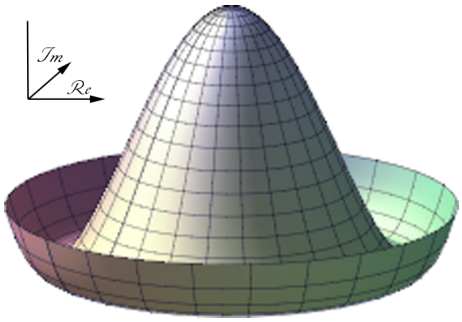

Figure 4.1: Shape of the Higgs potential at low energy. For a fixed value of λ the potential is shown against the real and imaginary parts of the first component of Φ.

[11], giving the two-loop QCD and Yukawa contributions to the effective coupling λ_{eff}. At high energies, λ_{eff} becomes negative.

While the Standard Model Higgs potential has the general features of a false vacuum and a potential barrier, its specific form is dependent on the values of the Higgs and top quark masses, currently measured as $M_H = 125.1 \pm 0.14GeV$ and $M_t = 172.9 \pm 0.4GeV$ [19]. The quantum corrected Higgs potential can decrease at large field values and destabilise the present day 246 GeV minimum. For top masses in the range $171 - 174$GeV, Higgs instability sets in at scales from $10^{10} - 10^{18}$ GeV. This instability scale, Λ, is very sensitive to particle physics parameters and possible new physics that lead to a metastable false vacuum [11, 20, 21].

In the metastable scenario, vacuum decay rates are strongly exponentially suppressed and the lifetime of the false vacuum is far too long to be cause for concern. However, the possibility of black holes seeding vacuum decay at an enhanced rate has recently been considered [22, 23, 24, 25, 26, 27, 28, 29]. In these cases, vacuum decay is very rapid. Chapter five of this thesis looks at Higgs vacuum decay in a Randall-Sundrum braneworld, while chapter six considers vacuum decay on the brane in the presence of a black hole. Chapter seven investigates the negative modes of true vacuum bubbles. In the following chapters, we will consider two different potentials: one is a quartic potential, with two well defined minima, while the other is a logarithmic potential closely approximating the Higgs at large field values.

4.1.1 Quartic potential

The quartic potential that appears in the later chapters of this thesis has the form,

$$V_q(\phi) = \frac{1}{4}\lambda_q\phi^4 - \frac{1}{3}\lambda_q(\phi_m + \phi_t)\phi^3 + \frac{1}{2}\lambda_q\phi_m\phi_t\phi^2, \tag{4.3}$$

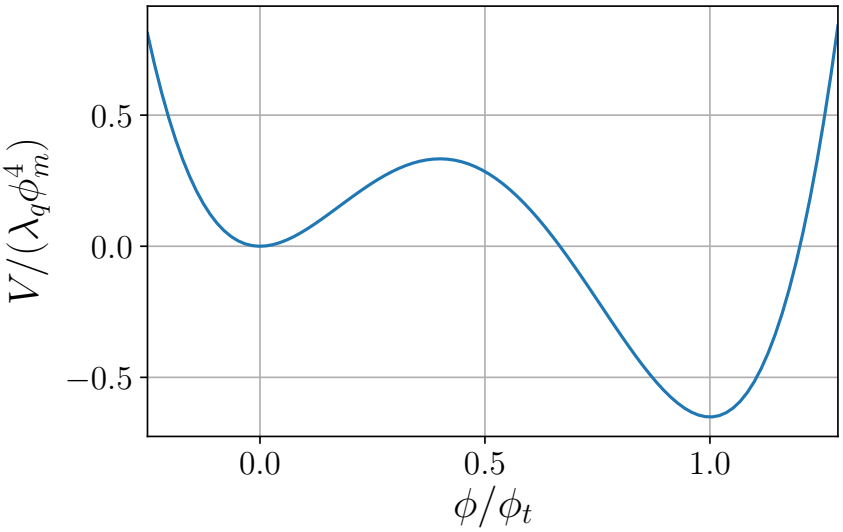

Figure 4.2: Plot by Florent Michel. Quartic potential (4.3) for $\phi_m = M_p/10$, $\phi_t = M_p/4$, and $\lambda_q = 10/3$.

which has been parametrised by the field values ϕ_m at the maximum and ϕ_t at the non-zero minimum. The parameter λ_q sets the overall scale. The origin $\phi = 0$ is a false vacuum, and ϕ_t is the true vacuum when $\phi_t > 2\phi_m$. One example is shown in the Fig. 4.2.

While our numerical calculations do not rely on the thin wall approximation, this can provide a useful check for the results. The thin wall approximation is valid when $\phi_t \sim 2\phi_m$.

For this potential, where the false vacuum is located at $V = 0$, the spacetime inside the true vacuum bubble is anti-de Sitter. An important parameter in this picture is the AdS radius ℓ, defined as

$$\ell^2 = -\frac{3M_p^2}{V(\phi_t)}. \tag{4.4}$$

We expect gravitational back-reaction to become important when the bubble radius is comparable to the AdS radius. In the thin-wall approximation, the 'flat-space' bubble radius is $R_0 = 3\sigma/\epsilon$ and we can obtain the ratio [1]

$$\frac{R_0}{\ell} = \frac{1}{\sqrt{2}}\frac{\phi_t}{M_p}\left(1 - 2\frac{\phi_m}{\phi_t}\right)^{-1/2}. \tag{4.5}$$

Note that this is independent of the overall scale parameter λ_q. It is possible to scan through different values of R_0/ℓ by fixing ϕ_m/ϕ_t and scanning through different values of ϕ_t, with the effects of back reaction becoming significant when $R_0/\ell \sim 1$.

[1] see chapter two for a calculation of σ

4.1.2 Logarithmic potential

The second potential we consider uses two-loop quantum corrections to closely approximate this Higgs. This potential is defined in terms of an effective coupling λ_{eff}:

$$V(\phi) = \frac{1}{4}\lambda_{\text{eff}}(\phi)\phi^4. \tag{4.6}$$

with a running coupling constant $\lambda_{\text{eff}}(\phi)$ that becomes negative at some crossover scale Λ_ϕ. Vacuum decay depends on the shape of the potential barrier in the Higgs potential around this instability scale, and in order to explore the likelihood of decay it is useful to use an analytic fit to λ_{eff}. The effective coupling is determined by renormalisation group methods and depends on low-energy particle masses, with strong dependence on the Higgs and top quark masses.

In [25], a two parameter fit to λ_{eff} was used to obtain a Higgs-like potential, where one of the parameters was closely related to the crossover scale. It was found that the dependence of the instanton action on the potential was strongly dependent on this parameter, but very weakly dependent on the second parameter, which was more related to the shape of the potential at low energy.

Two loop calculations of the running coupling λ give a high-energy approximation

$$\lambda_{\text{eff}} = g\left\{\left(\ln\frac{\phi}{M_p}\right)^4 - \left(\ln\frac{\Lambda}{M_p}\right)^4\right\} \tag{4.7}$$

Here, $\Lambda > 0$ is the scale at which the coupling and the potential vanish while g is strictly a positive number. A local minimum is located at $\phi = 0$. The approximate next-to-next-to-leading order calculations given by [11] are used to determine g for different values of the top quark mass. An example potential is given in Fig. 4.3 with top mass $M_t = 172GeV$, while a plot of the function λ_{eff} for three different choices of (g, Λ) are shown in Fig. 4.4.

The height of the Higgs potential barrier is small compared to Λ^4, meaning the bubbles produced have thick walls. The Higgs values inside the bubble are smaller then the false vacuum value beyond the barrier, but do not reach a true vacuum. Inside the bubble, the potential is roughly of order Λ^4 and the bubble size is of order Λ^{-1}, so that the 'effective' value of R_0/ℓ in this case is around Λ/M_p.

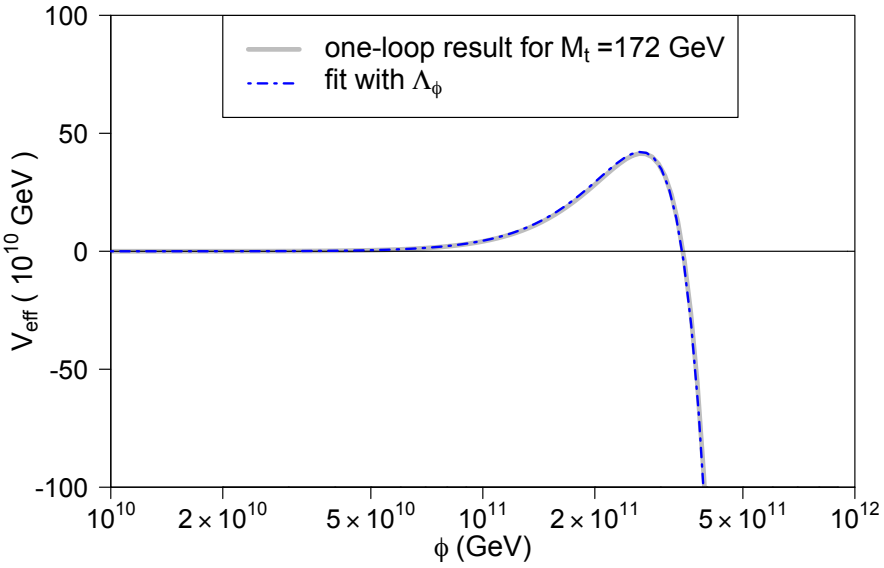

Figure 4.3: The Higgs potential calculated numerically at one loop order for top quark mass $M_t = 172\,\text{GeV}$ and the approximate potential using (4.7) with values of g and Λ_ϕ chosen for the best fit.

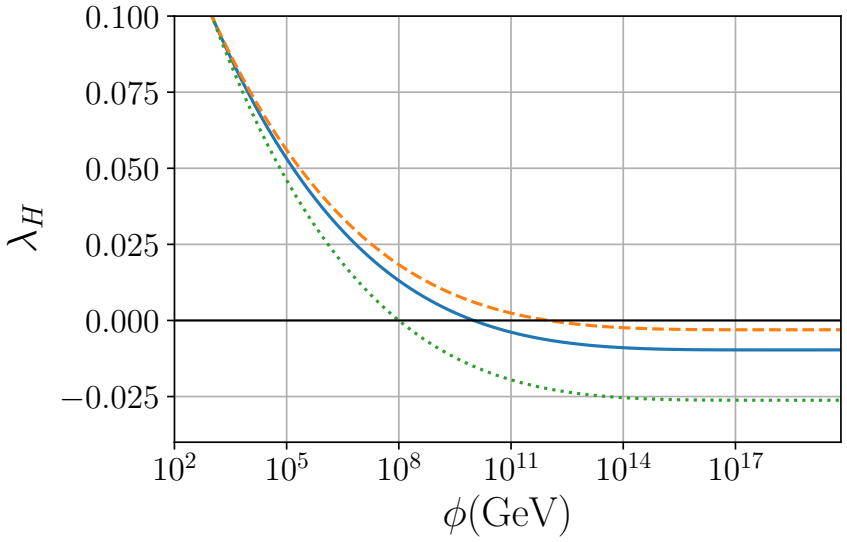

Figure 4.4: Plot by Florent Michel. The effective coupling is denoted by $\lambda_{\text{eff}} = \lambda_H$ for the Higgs-like potential (4.7) for $\Lambda = 10^8\text{GeV}$ (green, dotted), $\Lambda = 10^{10}\text{GeV}$ (blue, continuous), and $\Lambda = 10^{12}\text{GeV}$ (orange, dashed), and q chosen so that $\lambda(\phi = 10^3\text{GeV}) = 0.1$.

Chapter 5

Vacuum decay on the brane

This chapter presents work previously posted to arXiv:1907.11046 [hep-th], by L. Cuspinera, R. Gregory, Ruth,K. M. Marshall, and I. G. Moss, (2019). "*Higgs Vacuum Decay in a Braneworld.*"

5.1 Vacuum decay in a Randall-Sundrum braneworld

First order phase transitions in a Randall-Sundrum braneworld in de Sitter space have previously been investigated by Davis and Brechet [30], using Coleman and de Luccia's thin wall approximation to find bounce solutions. It was found that when the potential is smaller in magnitude than the brane tension, this gives the standard four dimensional result. In this chapter, we will use the CdL formalism to find exact instanton solutions for a potential that closely approximates the Higgs at high energies, and show that the four dimensional result is also reproduced when the space is asymptotically flat.

There are two variants of the Randall-Sundrum braneworld [31, 32], referred to as RS1 and RS2. Both versions describe the universe in terms of a five dimensional anti-de Sitter bulk where the Standard Model is localised on a 3+1 brane or branes. The RS1 model features two branes, the Planck brane and the TeV brane embedded in a five dimensional bulk at a fixed distance apart, with the particles of the Standard Model residing on the TeV brane. In the RS2 model shown in fig. 5.1, the geometry remains the same, but only the Planck brane is presumed to exist. The Standard Model particles are localised on the brane while gravity acts across the five-dimensional bulk. We will use the RS2 model to build our picture of higher-dimensional vacuum decay with black holes.

In this model, the field is located on a four dimensional brane where the Standard Model lives, while the brane is placed in a five dimensional bulk which has anti-de Sitter radius ℓ.

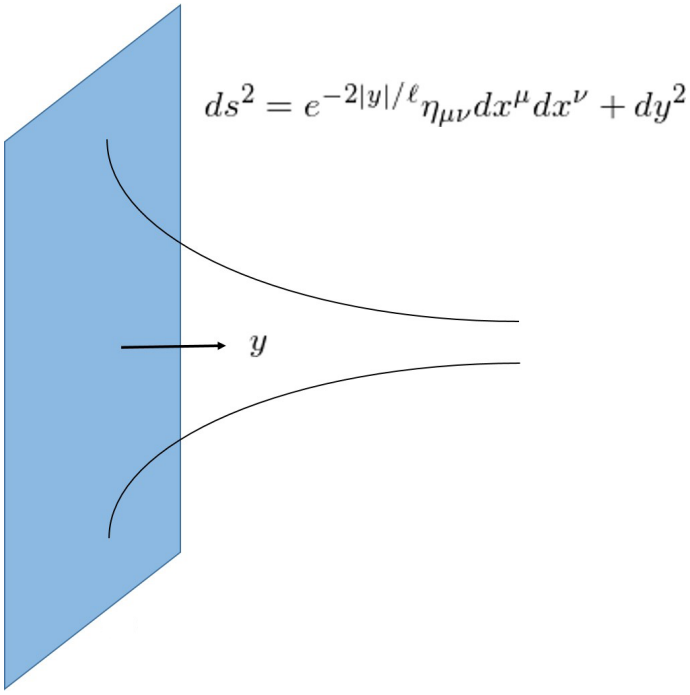

Figure 5.1: A Randall-Sundrum braneworld featuring a single brane. ℓ is the AdS radius and the brane tension σ is tuned so that the brane is flat in the false vacuum. Diagram by Leopoldo Cuspinera.

The tunnelling exponent B for decay rates on the brane will have contributions from both the brane and bulk. For a braneworld with a Z_2 symmetric bulk, the Euclidean action is given by $S_E = S_E^{(Bulk)} + S_E^{(brane)}$.

The action of the field in the bulk is

$$S_E^{(Bulk)} = \frac{1}{2\kappa_5^2}\int d^5x\sqrt{g}\left(-R^{(5)} + 2\Lambda_5\right) \tag{5.1}$$

while the action on the brane is

$$S_E^{(brane)} = \int d^4x\sqrt{h}\left(\frac{1}{2}(D\phi)^2 + V(\phi) + \sigma\right) \tag{5.2}$$

The induced metric on the brane is $h_{ab} = g_{ab} - n_a n_b$ where n_a is the normal to the brane. As in the Randall-Sundrum model, $\Lambda_5 = -6/\ell^2$ and the brane cosmological constant $\sigma = 6/\kappa_5^2\ell$.

Davis and Brechet implemented Coleman's thin wall approximation in order to find instanton solutions. They found that if the potential is smaller than the brane tension, this returns (to leading order) the standard four dimensional results. This is unsurprising, as

in the case of small curvature, gravity on the brane should reduce to standard relativity in four dimensions. If the potential is larger than the brane tension, then the effects of brane gravity become significant and are found to enhance vacuum decay in all cases.

In the next chapter, we will find exact solutions for the bounce on an RS2 brane when space is asymptotically flat, and compare the results with the case studied here.

5.2 Instanton solutions in RS2

Here we will consider the case of vacuum decay in RS2 with the Standard Model localised to a single Planck brane. We take a field living on a four-dimensional brane embedded in a five-dimensional bulk with anti-de Sitter radius ℓ. The brane tension in five dimensions is $\sigma = 6/\kappa_5^2\ell$ where $\kappa_5^2 = 8\pi G_N \ell$, found by taking the trace of $\Sigma_{\mu\nu}$. G_N is the standard Newton constant in four dimensions, related to the five dimensional gravitational constant by $G_N = G_5\ell$. The negative curvature of spacetime causes a localisation of the graviton on the brane, the background solution being a brane with energy and tension equal and precisely tuned to the bulk cosmological constant, giving a flat brane at $z = 0$:

$$ds^2 = e^{-2|z|/\ell}\eta_{\mu\nu}dx^\mu dx^\nu - dz^2 \tag{5.3}$$

where $\ell^2 = -6/\Lambda_5$ is the AdS curvature scale. The local negative curvature of the bulk supports the brane tension σ for a brane with curvature tensor $K_{\mu\nu}$, that is assumed by symmetry to be equal on both the positive $^+$ and negative $^-$ sides of the brane. σ that is easily calculated from the Israel junction conditions [33]:

$$K^+_{\mu\nu} = -\frac{1}{\ell}\eta_{\mu\nu} \quad \Rightarrow \qquad K^+_{\mu\nu} - K^+\eta_{\mu\nu} = \frac{3}{\ell}\eta_{\mu\nu} = 4\pi G_5\sigma\eta_{\mu\nu} \tag{5.4}$$

One can add energy momentum to the brane, a cosmological fluid, or a perturbative localised source. In all cases, the intuitive visualisation of brane matter is that it causes the braneworld to bend as first pointed out by Garriga and Tanaka [34] (see also [35, 36]).

For the single 4D brane in RS2, the metric is

$$ds^2_{brane} = d\tau^2 + a(\tau)^2 d\Omega_3^2, \quad \phi = \phi(\tau) \tag{5.5}$$

equation (5.1) is the Euclidean action for the bulk given in [30]. The bulk metric in AdS can be rewritten as

$$ds^2_{bulk} = hdt^2 + h^{-1}dr^2 + r^2 d\Omega_3^2 \tag{5.6}$$

where $h = 1 + (r^2/l^2)$ [37]. On the brane, $r = a(\tau)$.

For a field on the brane, we will find bounce solutions to the field equations and calculate transition rates. The probability of a phase transition is given by the usual form of Γ

$$\Gamma = Ae^{-B}. \tag{5.7}$$

The Euclidean action for the brane in equation (5.2) can be rewritten as

$$S_E = -\frac{1}{2\kappa_5^2}\int_{M^+} d^4x\,(R - 2\lambda) - \frac{1}{\kappa_5^2}\int_{\partial M^+} d^4x K + \int_{\partial M^+} d^4x \left(\frac{1}{2}(D\phi)^2 + V + \sigma\right). \tag{5.8}$$

where K is the brane curvature, ∂M denotes boundary terms, and the superscript $^+$ refers to the positive side of the brane. In line with the Randall-Sundrum model, we take a cosmological constant for the five-dimensional bulk, $\Lambda_5 = -6/\ell^2$ and $\sigma = 6/\kappa_5^2\ell$ for the brane.

The tunnelling exponent B is found by applying the usual method from Coleman and de Luccia's formalism for finding instanton solutions to the field equations [3]. It is possible to evaluate our form of B numerically without using the thin wall approximation.

In the standard 4-dimensional case without a brane, the field equations are

$$0 = \ddot{\phi} + 3\frac{\dot{a}}{a}\phi' - \frac{dV}{d\phi} \tag{5.9}$$

$$\ddot{a} = \frac{8\pi G_5 a}{3\ell}(\dot{\phi}^2 + V) \tag{5.10}$$

For our model in five dimensions where the brane has mirror symmetry, the equations of motion can be derived from the Israel junction conditions. A full derivation is given in Appendix A. Integrating the stress-energy tensor for the brane, we define a surface stress tensor

$$\Sigma_{\mu\nu} = \int T_{\mu\nu} dl \tag{5.11}$$

where the stress-energy tensor $T_{\mu\nu}$ is integrated across the brane. The junction condition is

$$K^+_{\mu\nu} = 4\pi G_5 \ell[\Sigma_{\mu\nu} - \frac{1}{3}\Sigma h_{\mu\nu}] \tag{5.12}$$

where the curvature $K^+_{\mu\nu} = K^-_{\mu\nu}$ is the same each side of the boundary. The extrinsic

curvature K is

$$K = -\frac{4\pi G_5}{3}\Sigma \tag{5.13}$$

We will use the curvature component $K_{\chi\chi}$ to derive the equations of motion for the field, where the subscript χ denotes spatial components. We use an ansatz for the field:

$$\phi = \phi(\tau) \tag{5.14}$$

$$(\nabla\phi)^2 = \dot{\phi}^2 \tag{5.15}$$

The trace Σ is given by

$$\Sigma = -\left(\dot{\phi}^2 + 4V + 4\sigma\right) \tag{5.16}$$

while $\Sigma_{\chi\chi}$ can also be written

$$\Sigma_{\chi\chi} = -a^2\left(\frac{1}{2}\dot{\phi}^2 + V + \sigma\right) \tag{5.17}$$

By symmetry from $K^+_{\chi\chi} = K^-_{\chi\chi}$ we can write

$$8\pi G_5(\Sigma_{\chi\chi} - \frac{1}{3}\Sigma g_{\chi\chi}) = 2K_{\chi\chi} \tag{5.18}$$

$$\tag{5.19}$$

The curvature $K_{\chi\chi}$ is found from the metric on the brane by taking the non-zero Christoffel symbols and defining a normal vector n_i

$$K_{\chi\chi} = h^a_\chi h^b_\chi \left(n_{a,b} - \Gamma^c_{ab} n_c\right) \tag{5.20}$$

$$= \Gamma^c_{\chi\chi} n_c \tag{5.21}$$

$$= \Gamma^t_{\chi\chi}\dot{r} - \Gamma^r_{\chi\chi}\dot{t} \tag{5.22}$$

Substituting this into the junction condition, we arrive at an equation of motion for the field in terms of $\dot{a}$ (see Appendix A).

$$1 - \dot{a}^2 = \left(\frac{8\pi G_5}{3\ell}\right)^2 a^2\left(\frac{6}{4\pi G_5 \ell}\left(V - \frac{1}{2}\dot{\phi}^2\right) + a^2\frac{4}{3}\pi G_5\left(V - \frac{1}{2}\dot{\phi}^2\right)^2\right) \tag{5.23}$$

Differentiating this with respect to τ gives us an equation of motion for the field in terms of $\ddot{a}$.

$$\ddot{a} = \frac{8\pi G_5 a}{3\ell}(\dot{\phi}^2 + V) + \frac{a}{3}(4\pi G_5)^2\left(V - \frac{1}{2}\dot{\phi}^2\right)\left(\frac{1}{3}V + \frac{5}{6}\dot{\phi}^2\right) \tag{5.24}$$

while the second field equation has the same form as the 4-dimensional case without the brane.

$$0 = \ddot{\phi} + 3\frac{\dot{a}}{a}\dot{\phi} - \frac{dV}{d\phi} \tag{5.25}$$

The boundary conditions are:

$$\text{when } \tau = 0,\ \phi = \phi_b,\ a = 0,\ \dot{a} = 1 \tag{5.26}$$

$$\text{as } \tau \to \infty,\ \phi \to \phi_{fv},\ a \to \tau + c \tag{5.27}$$

with ϕ_b denoting ϕ at the centre of the bubble. Note the presence of a constant c in the boundary condition $a \to \infty$.

It is also worth noting that the critical RS brane (with $V = \dot{\phi} = 0$) has $\dot{a} \equiv 1$. This leads to the brane trajectory

$$r(\tau) = a(\tau)\ , \qquad t(\tau) = \frac{\ell}{2}\log(1 + \tau^2/\ell^2) \tag{5.28}$$

This is a less familiar form for the critical RS brane, obtained because we are solving for the brane in bulk global coordinates, rather than the usual Poincare patch. The trajectory can easily be transformed to its familiar form (5.3) using

$$e^{z/\ell} = \frac{e^{t/\ell}}{\sqrt{1 + r^2/\ell^2}}\ , \qquad x^i = e^{z/\ell} r n_4^i \tag{5.29}$$

where n_4 is the unit vector in 4 dimensions.

5.3 Choice of potentials

We recall the Higgs-like potential from chapter four (4.2)

$$V(\phi) = \frac{1}{4}\lambda_{\text{eff}}(\phi)\phi^4 \tag{5.30}$$

with an effective coupling

$$\lambda_{\text{eff}} = g\left\{\left(\ln\frac{\phi}{M_p}\right)^4 - \left(\ln\frac{\Lambda}{M_p}\right)^4\right\} \tag{5.31}$$

and the quartic potential

$$V_q(\phi) = g\left[\frac{\phi^4}{4} - \frac{\phi^3}{3}(\phi_V + \phi_M) + \frac{\phi^2}{2}\phi_V\phi_M\right] \tag{5.32}$$

where ϕ_M is the value of ϕ at the top of the barrier, and ϕ_V is the field at the true vacuum. Both of these will be considered to calculate vacuum decay rates on the brane.

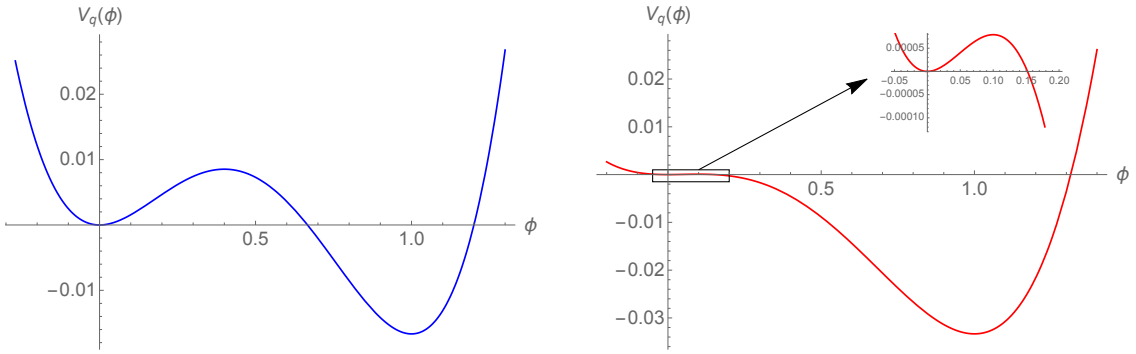

Figure 5.2: The V_q potentials referred to in the text. On the left in blue with $\phi_M = 0.4$, and $\phi_V = 1$ (with $M_p = 1$), corresponding to a well-defined bubble wall. On the right in red the potential more closely approximated the Higgs potential, with $\phi_M = 0.1$, and corresponds to a thick wall bubble.

In each case, we integrate (5.24) from the centre of the instanton, $\tau = 0$, looking for a solution that asymptotes the flat critical RS trajectory (5.28). However, note that because we set boundary conditions at $\tau = 0$ of $a = 0$, $\dot{a} = 1$ and $\dot{\phi} = 0$, the flat geometry at large τ is $\phi \to \phi_{\rm fv}$, $a \to \tau + c$ – integrating through the bubble wall produces an offset in the value of r relative to t. While this is not particularly relevant to the form of the bubble solution, for which $a(\tau)$ is important, it is a crucial observation for the computation of the action, as we will return to in the next section.

The quadratic potential (5.32) is particularly useful for exploring the variation from thin to thick bubble walls, and for varying backreaction strengths. To illustrate this, we present results for two representative potentials, one giving a strongly backreacting thin wall, with parameter values $g = 1, \phi_V = M_p, \phi_M = 0.4M_p$, and the other a weakly backreacting thick wall with parameter values $g = 1/2, \phi_V = M_p, \phi_M = 0.1M_p$; in both cases the Planck scales are $M_5 = 0.4$ in five dimensions and $M_p = 1$ in four dimensions, hence the bulk AdS lengthscale is $\ell = 1/M_5^3 = 125/8$. Fig. 5.2 shows the potential V_q for these two choices of parameters; note the thin wall potential (shown in blue) has a significant potential barrier between the vacua, but less well represents a Higgs-type potential, whereas the thick wall potential (shown in red) more closely resembles the Higgs potental, having a very small barrier relative to the global minimum.

The scalar field solution is shown in fig. 5.3, and demonstrates clearly the distinction between the potentials: the thin wall has a clear, sharp transition from false to true

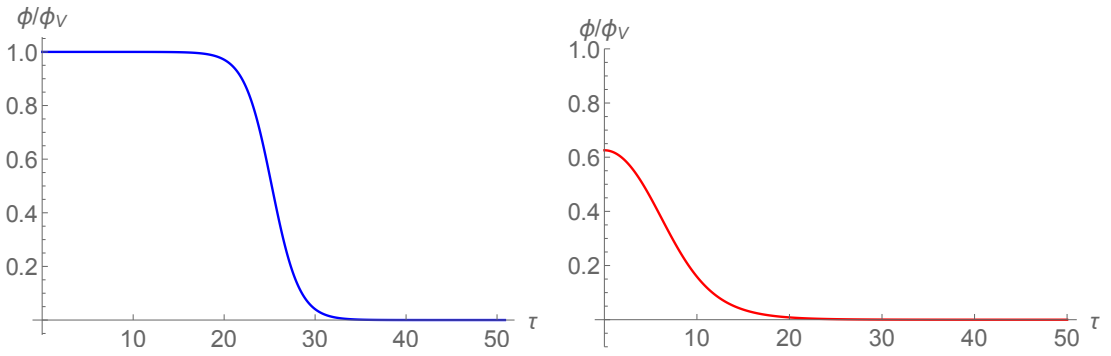

Figure 5.3: The scalar field solution for the potentials shown in fig. 5.2. Once again, blue corresponds to the thin wall bubble, here clearly seen as a step in ϕ, and red to the thick wall bubble.

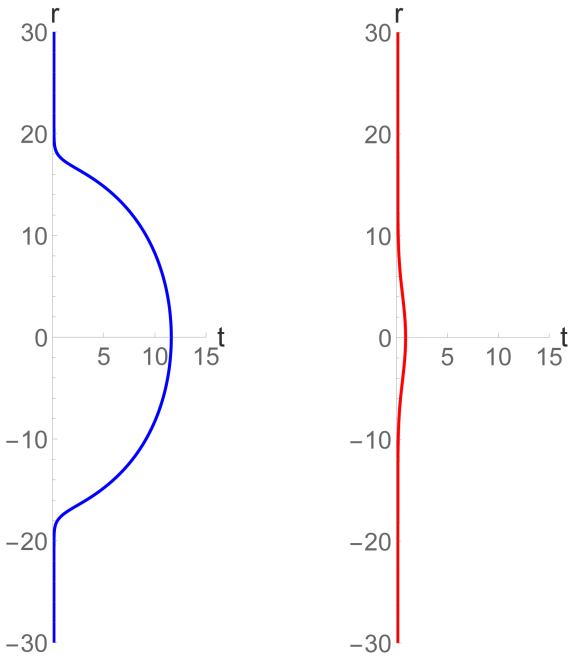

Figure 5.4: The geometry of the brane with bubble embedding shown in Poincare coordinates, as is usual for the flat RS brane. Right: embedding for a thin wall bubble. Left: embedding for a thick wall bubble. On the brane, r is given by $r = a(\tau)$ and $(\dot{t} = (h - \dot{(}r)^2)^{1/2}/h, \dot{r}^2$ is given by equation (5.23)

vacuum around $\tau \sim 25$, whereas the thick wall does not even reach the true vacuum by the centre of the bubble. The effect of the bubble on the embedding of the brane is shown in fig. 5.4. The strongly backreacting thin wall brane shows the transition between the flat RS critical asymptotic false vacuum brane, and the sub-critical true vacuum AdS embedding in the interior of the brane. The weakly interacting thick wall has a much less significant displacement, and does not reach the spherical shape of the sub-critical brane.

5.4 The bounce action in RS2

We use the action computed by Davis and Brechet [30] for the instanton on the brane to calculate B, which is found from the difference in actions inside and outside the bubble:

$$B = S_E(\phi) - S_E(\phi_{fv}) \tag{5.33}$$

For both the false and true vacuum regions, S_E is the total action combining contributions from the bulk (S_B)and brane (S_b).

$$S_E = S_{(b)} + S_{(B)} \tag{5.34}$$

Using the field equation (5.25), the bulk part of the action can be written as

$$S_E^{(B)} = \frac{2\pi^2}{3\ell^2} \int d\tau \frac{a^5}{h} \ell^2 \left(V - \frac{\dot{\phi}^2}{2} + \frac{6}{\kappa_5^2 \ell} \right) \tag{5.35}$$

From the trace of the junction condition, the brane part of the action reduces to

$$S_E^{(b)} = \frac{-2\pi^2}{3\ell^2} \int d\tau a^3 \left(V - \frac{\dot{\phi}^2}{2} + \frac{6}{\kappa_5^2 \ell} \right) \tag{5.36}$$

The overall bounce action B is therefore found by combining (5.35) and (5.36) and subtracting the false vacuum action from the action inside the bubble.

$$B = S_E^{(B)}(\phi) + S_E^{(b)}(\phi) - S_E^{(B)}(\phi_{fv}) + S_E^{(b)}(\phi_{fv}) \tag{5.37}$$

$$S_E^{(B)}(\phi) + S_E^{(b)}(\phi) = \frac{2\pi^2}{3\ell^2} \int d\tau \left(\frac{a^5}{h} - a^3 \ell^2 \right) \left(V - \frac{\dot{\phi}^2}{2} + \frac{6}{\kappa_5^2 \ell} \right) \tag{5.38}$$

At the false vacuum $V = 0$ and $\dot{\phi} = 0$. As $\tau \to \infty$, $a \to \tau + c$ where c is an unknown constant. The action computed from this is infinite, and therefore it is not possible to perform the subtraction in equation (5.37) because τ has a different meaning for the false vacuum and for the bubble.

To address this problem, we can write the equations of motion to express $\dot{a}$ and $\dot{\phi}$ in terms of a implicitly, thus removing the c:

$$S_E^{(b)} = \frac{-2\pi^2}{3\ell^2} \int da \frac{a^3}{(h)\dot{a}} \left(V - \frac{\dot{\phi}^2}{2} + \frac{6}{\kappa_5^2 \ell} \right) \tag{5.39}$$

At the false vacuum, $a = \tau$ and $V - \frac{\dot{\phi}^2}{2} = 0$. (5.37) can now be rewritten as

$$\begin{aligned} S_E(\phi) - S_E(\phi_{fv}) &= \frac{2\pi^2}{3} \int d\tau \left[\left(\frac{a^5}{h} - a^3 \ell^2 \right) \left(\frac{V - \dot{\phi}^2/2}{\dot{a}} \right) + \frac{6\ell}{\kappa_5^2} \left(\frac{1}{\dot{a}} - 1 \right) \right] & (5.40) \\ &= \frac{2\pi^2}{3} \int d\tau \frac{a^3}{h} \left[\frac{6\ell}{\kappa_5^2} (\dot{a}_b - 1) + \frac{\dot{\phi}^2}{2} + V \right] & (5.41) \end{aligned}$$

where $\dot{a}_b$ is the rate of change of a inside the bubble.

5.5 Equations of motion

Recall from equation (5.9) – (5.25) the equations of motion on the brane are

$$\begin{aligned} 0 &= \ddot{\phi} + 3\frac{\dot{a}}{a}\phi' - \frac{dV}{d\phi} & (5.42) \\ \frac{1 - \dot{a}^2}{a^2} &= \frac{8\pi G_5}{3} \left(V - \frac{1}{2}\dot{\phi}^2 \right) + \frac{4\pi G_5}{3} \left(V - \frac{1}{2}\dot{\phi}^2 \right)^2 & (5.43) \\ \ddot{a} &= \frac{8\pi G_5 a}{3} (\dot{\phi}^2 + V) + \frac{a}{3} (4\pi G_5)^2 \left(V - \frac{1}{2}\dot{\phi}^2 \right) \left(\frac{1}{3} V + \frac{5}{6}\dot{\phi}^2 \right) & (5.44) \end{aligned}$$

with the boundary conditions

$$\begin{gathered} \text{when } \tau = 0,\ \phi = \phi_b,\ a = 0,\ \dot{a} = 1 \\ \text{as } \tau \to \infty,\ \phi \to \phi_{fv},\ a \to \infty \end{gathered}$$

where the field has value $\phi = \phi_b$ at the centre of the bubble. Solving equation (5.42) and equation (5.44) gives the instanton solutions. In the ordinary 4D case without the brane, the equations of motion are

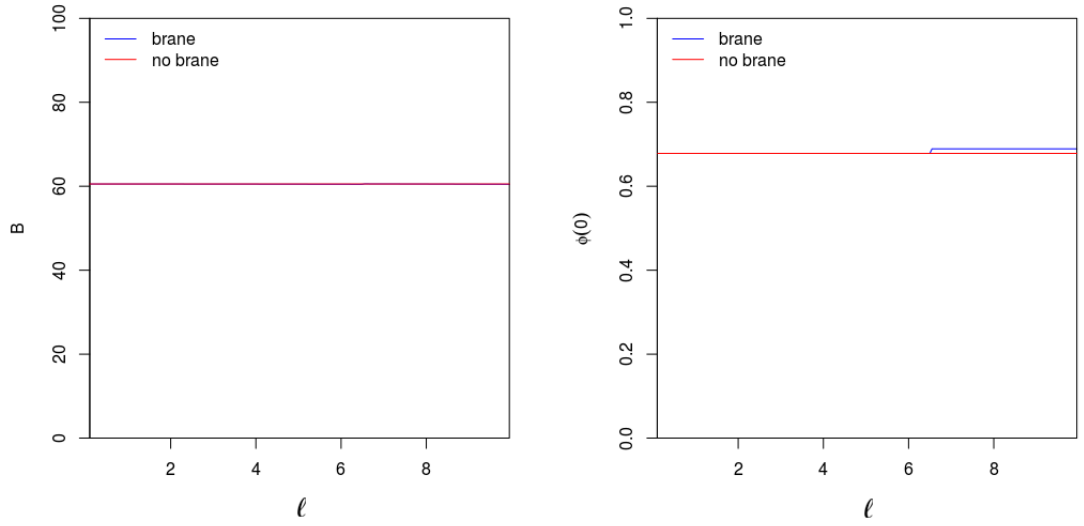

Figure 5.5: Change in the bounce action and change in ϕ_0 over a range $0 < \ell < 2.0$ for vacuum decay both with and without a brane.

$$0 = \ddot{\phi} + 3\frac{\dot{a}}{a}\phi' - \frac{dV}{d\phi} \tag{5.45}$$

$$\ddot{a} = \frac{8\pi G_5 a}{3}(\dot{\phi}^2 + V) \tag{5.46}$$

which are also solved numerically for comparison.

5.6 Results

Bounce solutions are obtained over a range $0 < \ell < 2.0$. Outside of this range, the sign change in $V + \sigma$ over the course of the integration means it is not possible to find solutions using the CdL method, though it is possible these solutions still exist.

Fig. 5.6 shows the tunnelling exponent for the quartic potential V_q given in chapter four with the parameter sets considered in §5.3, these are plotted as a function of the mass parameter $M_5 = M_p^{2/3}\ell^{-1/3}$, which determines the strength of gravity in five dimensions. The barrier is at the centre of the bubble $\phi_M = 0.4M_p$ and $\phi_M = 0.1M_p$. These test case examples show a reduction in B, hence an increase in the vacuum decay rate, due to the increasing influence of the extra dimension as M_5 becomes increasingly much smaller than M_p.

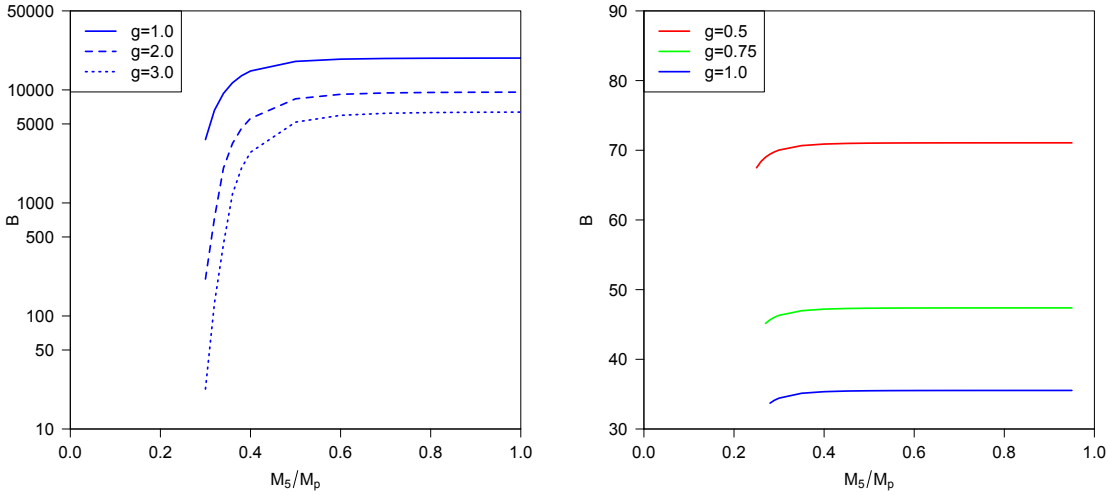

Figure 5.6: The vacuum decay exponent B for the quadratic potential plotted as a function of M_5 for barriers with $\phi_M = 0.4M_p$ (left) and $\phi_M = 0.1M_p$ (right). The exponent approaches the 4D value as M_5 approaches the 4D Planck mass M_p.

The edge of the plots denotes a minimum value of M_5 beyond which the numerical solutions cease to exist. If the value of M_5 is reduced any further, $V + \sigma$ undergoes a change of sign and the total surface tension on the brane becomes negative near the centre of the bubble. (Note: while it is not possible to obtain numerical solutions beyond this limit using the CdL method, this does not rule out their existence.) The increase in the vacuum decay rate only occurs when the potential is close to the Planck energy, but then the allowed range of M_5 is very narrow, as in the examples plotted above, and does not correspond to a significant hierarchy. Therefore, adding an extra dimension only affects the decay rate in very specialised situations.

For tunnelling in RS2, we plot the action of the bounce as a function of the anti-de Sitter radius. It can be seen from fig. 5.5 that as ℓ increases, the value of B tends to the same value as the 4-dimensional result, which has no dependence on ℓ.

$\tau = 0$ is defined as the centre of the bubble, and the field approaches its false vacuum value as $\tau \to \infty$. Bubble profiles are plotted from the instanton solutions for both the RS2 and 4-dimensional cases. From figures 5.8 and 5.9 these can be seen to have thick wall characteristics.

The value of the field at the centre of the bubble ϕ_0 in RS2 has a minor dependence on ℓ. ϕ_0 has no dependence on ℓ in four dimensions, but both cases show very similar bubble profiles that are not greatly affected by the presence of the fifth dimension.

Some results for the quadratic potential (5.32) are shown in fig. 5.6. The tunnelling

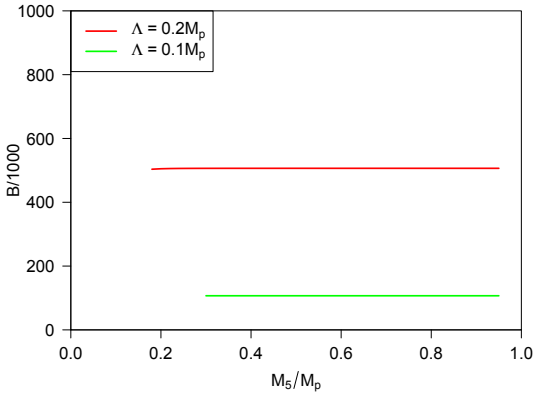

Figure 5.7: The vacuum decay exponent B plotted as a function of M_5 for Higgs potentials with a range of values of the instability scale Λ. There is no dependence on the extra dimension.

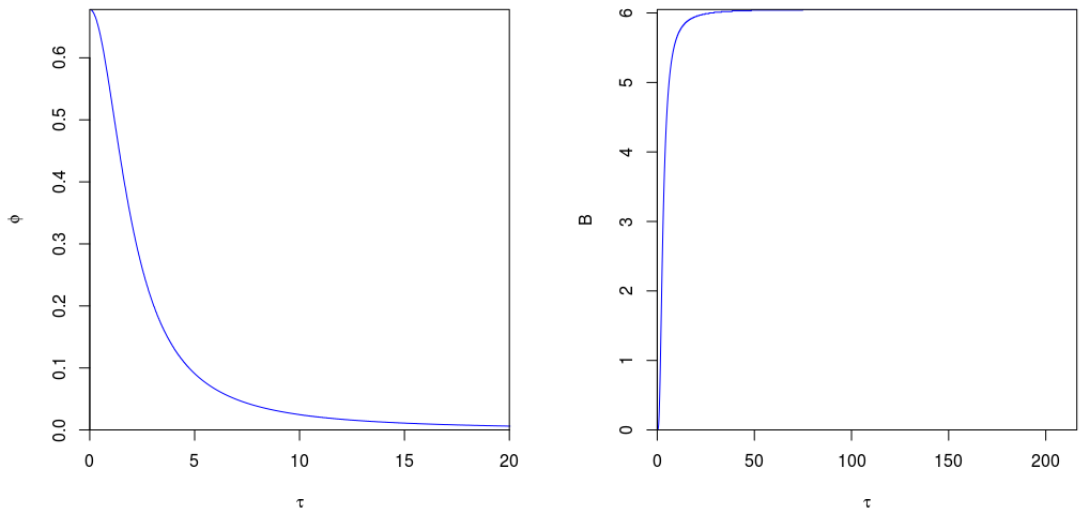

Figure 5.8: Plots of the bubble profiles on the brane and action vs radius for $\ell = 1$.

exponent has been plotted as a function of the mass parameter $M_5 = M_p^{2/3}\ell^{-1/3}$ which determines the strength of gravity in five dimensions. The barrier is at $\phi_M = 0.1M_p$ and $\phi_M = 0.2M_p$. These rather extreme examples show a reduction in B, and hence an increase in the vacuum decay rate, on reduction of the five dimensional Planck mass.

We also show the tunnelling exponent for the Higgs-style potential V_H, with parameters chosen within the Standard Model range in fig. 5.7. The Higgs potential is small at the Planck scale because the parameter g in the potential is so small. Consequently, vacuum

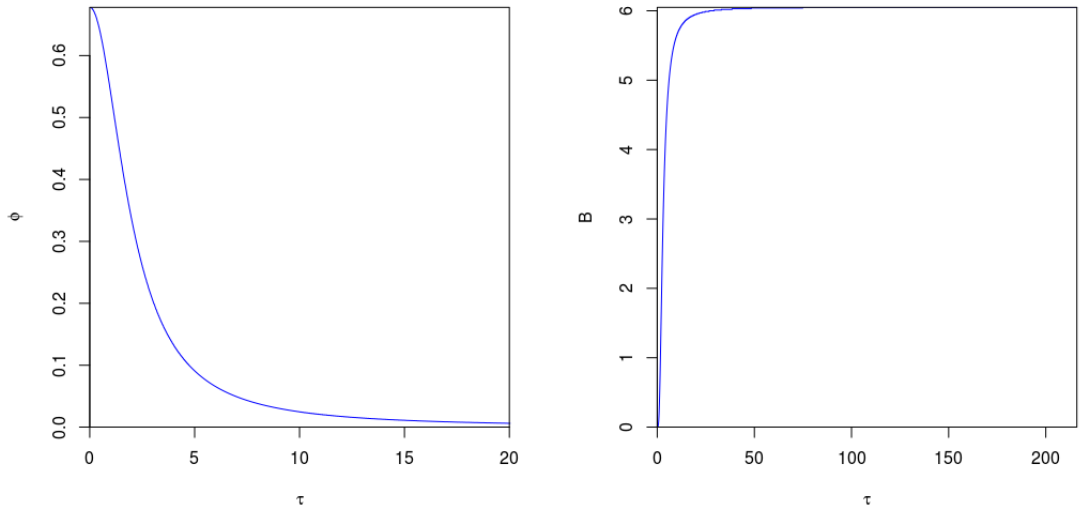

Figure 5.9: Plots of the bubble profiles in 4-dimensional flat space and action vs radius for $\ell = 1$.

decay rates with the Higgs potential show no dependence on the extra dimensions, as shown in fig. 5.7. However, this situation changes when we consider vacuum decay seeded by primordial black holes, as in ref. [38].

5.7 Conclusion

We have found instanton solutions for a field with an approximate Higgs potential in an RS2 braneworld, and used this to calculate transition rates. We explored general bubble solutions with a quartic potential, as well as an approximate Higgs potential, as outlined in chapter four. The tunnelling exponent is compared with that for phase transitions in 4-dimensional asymptotically flat space, and it is found that the influence of the fifth dimension on tunnelling rates is minor until the ratio M_5/M_p approaches the critical cut-off point beyond which numerical results could not be obtained.. This is consistent with Davis and Brechet's result when $V + \sigma > 0$.

Profiles of the true vacuum bubbles are also produced for both forms of the potential, with there being little change in the bubble properties or the value of the true vacuum after tunnelling compared with the 4D result.

One interesting feature of our numerical solutions was the sharp cut-off in the allowed value of M_5 due to the total brane tension becoming negative. This is possibly due to the fact we integrate out from $\tau = a = 0$, hence this method does not allow for a wormhole-type solution where the brane transitions from positive to negative tension as in [39, 40].

Chapter 6

Black Hole Instantons

This chapter presents work previously published in a paper by L. Cuspinera, R. Gregory, K. M. Marshall, and I. G. Moss, (2019). "Higgs vacuum decay from particle collisions?" *Physical Review D* **99**(2): 024046. arXiv:1803.02871v2 [hep-th].

6.1 Black Holes as bubble nucleation sites

Recent investigations of Standard Model Higgs vacuum decay would suggest that the exponential suppression of the tunnelling rate makes a phase transition within the lifetime of the universe unlikely, and Coleman's "ultimate ecological catastrophe" will not occur [12, 13, 14, 15, 16, 17, 18].

However, other work has looked at cases where this low tunnelling rate may be significantly enhanced – for fields in the presence of a black hole, the lifetime of the vacuum is greatly reduced and a tunnelling event becomes more likely [22, 23, 24, 25, 26, 27, 28, 29]

In this scenario, tunnelling is initiated by a black hole seed in the false vacuum, which decays to a remnant black hole while a true vacuum bubble nucleates with the black hole at its centre. The black hole remaining after the phase transition will have a smaller area and also lower entropy compared to the seed. This difference in areas allows the tunnelling rate to be determined – the tunnelling exponent B is given by the difference in actions between the initial and final configurations, which is equivalent to finding the difference in area between the seed and remnant black holes.

In this chapter, we will build on previous work in [23, 24, 25, 26] that looks at possible scenarios where vacuum decay is seeded by a black hole. It was found in [23, 24] that primordial black holes nearing the end of their lifetime may seed vacuum decay. Factoring in quantum gravity corrections to the Higgs, gravitational inhomogeneities give rise to

microscopic black holes that significantly reduce the barrier to vacuum decay. Here, we build on this picture by considering a scenario with a tidal black hole in a five dimensional Randall-Sundrum braneworld, while the Higgs field is localised to a four dimensional brane.

In this picture of vacuum decay, a key feature is the small size of the black holes needed in order to seed a phase transition. Such black holes may plausibly be produced in particle collisions, though current particle accelerators fall short of reaching the necessary energy scales. However, the most energetic of cosmic ray collisions at a scale of 10^{21} eV may provide the opportunity for such black holes to form – though these collisions are fortunately rare.

When investigating vacuum decay with black holes, we can compare the black hole's decay through Hawking evaporation to the vacuum decay rate. The vacuum decay rate is, as usual,

$$\Gamma_D = Ae^{-B} \tag{6.1}$$

and the Hawking evaporation rate of the black hole is given in [23] as

$$\Gamma_H \approx 3.6 \times 10^{-4}(G^2 M_s^3)^{-1} \tag{6.2}$$

where M_s is the mass of the seed black hole and G is the gravitational constant in the relevant number of dimensions.

We construct a picture of a Higgs field in the false vacuum close to the horizon of a static, spherically symmetric black hole. The field undergoes a phase transition to its true vacuum value, resulting in a bubble of true vacuum nucleating around the black hole. The presence of a bubble directly affects the black hole by reducing its radius and therefore its entropy. Both the black hole and the bubble have actions related to their area.

$$S_{bh} = -\frac{1}{4}A_{bh} + \beta M \tag{6.3}$$

$$S_b = -\frac{1}{4}A_b + \beta M \tag{6.4}$$

where A_{bh} is the area of the black hole and A_b is the area of the black hole remnant, and βM is a mass term [41, 42]. This result can be obtained from thermodynamics. We assume the action S_E is proportional to the free energy according to

$$S_E = \beta F \tag{6.5}$$

where β relates to the Hawking temperature T as $T = \beta^{-1}$. The free energy F then relates to enthalpy E, temperature T and entropy S, where the entropy can be expressed in terms of the black hole's area A.

$$F = E - TS \tag{6.6}$$
$$S = \frac{1}{4}A \tag{6.7}$$

The black hole's enthalpy is its mass M. The action is therefore

$$S_E = \beta\left(M - \frac{A}{4\beta}\right) \tag{6.8}$$
$$= \beta M - \frac{1}{4}A \tag{6.9}$$

With the βM terms cancelling, the difference in actions between the initial and final configurations can therefore be expressed in terms of a difference in the areas of the black holes:

$$\Delta S = S_b - S_{bh} \tag{6.10}$$

We can therefore rewrite the decay equation in terms of a reduction in the black hole's entropy ΔS

$$\Gamma_D \propto e^{\Delta S} \tag{6.11}$$

This result can also be proved directly – see appendix B.

6.2 The Euclidean Brane Black Hole Action

The action of any static black hole can be expressed entirely by surface terms – a result which also applies even with the presence of a cosmological constant, with matter, or with a conical singularity at the horizon.

This can be shown by first recalling the properties of the Euclidean Schwarzschild black

hole in four dimensions:

$$ds^2 = f(r)d\tau^2 + f(r)^{-1}dr^2 + r^2 d\Omega_{II}^2, \tag{6.12}$$

where

$$f(r) = 1 - \frac{2G_N M}{r} \tag{6.13}$$

and $d\Omega_{II}^2$ is the metric for a two-sphere. In order to explore the geometry near the 'horizon' $r_h = 2G_N M$, we expand using a new coordinate ϱ, defined by

$$\varrho = \sqrt{\frac{2(r - r_h)}{\kappa}} \tag{6.14}$$

where κ is the surface gravity, $\kappa = f'(r_h)/2$. To leading order $f(r) = \kappa^2\varrho^2 + O(\varrho^4)$, and close to the horizon,

$$ds^2 = d\varrho^2 + \varrho^2 d(\kappa\tau)^2 + r_h^2 d\Omega_{II}^2 + O(\varrho^4), \tag{6.15}$$

When $\kappa\tau$ is taken to be an angular coordinate with the usual range 2π, for small $\varrho \geq 0$, the metric is geometrically the product of a disc with a sphere. If $\kappa\tau$ has a different range, then the manifold has a conical singularity at r_h. Other than this, the Euclidean section is perfectly regular but only covers the exterior region of the original black hole. The *event* horizon of the original Lorentzian black hole is encoded in the topology of the Euclidean solution: the surface $\varrho = 0$ is a 2-sphere of radius r_h.

For the brane black hole in five dimensions, the metric is extended into an additional direction. This is parametrised by χ in Kudoh et al. [42], who numerically constructed small brane black holes with horizon size less than the AdS radius ℓ. In [42], the metric was written in the form

$$ds^2 = \frac{1}{(1 + \frac{\rho}{\ell}\cos\chi)^2}\left[T^2(\rho,\chi)d\tau^2 + e^{2B(\rho,\chi)}(d\rho^2 + \rho^2 d\chi^2) + e^{2C(\rho,\chi)}\rho^2\sin^2\chi d\Omega_{II}^2\right], \tag{6.16}$$

where the brane sits at $\chi = \pi/2$, and $\chi \leq \pi/2$ is kept as the bulk. In the small black hole limit, $\ell \to \infty$, we have the five dimensional Schwarzschild black hole [43]:

$$ds^2 = \left(\frac{\rho^2 - \rho_h^2}{\rho^2 + \rho_h^2}\right)^2 d\tau^2 + \left(\frac{\rho^2 + \rho_h^2}{\rho^2}\right)^2 \left[d\rho^2 + \rho^2 d\Omega_{III}^2\right] \tag{6.17}$$

written here in homogeneous co-ordinates, rather than the area gauge. $d\Omega_{III}^2$ is the metric for a three-sphere. The local Euclidean horizon coordinate is $\varrho = 2(\rho - \rho_h)$, and the

horizon has area $\mathcal{A} = 4\rho_h^2$, and surface gravity

$$\kappa = e^{-B(\rho_h)}T' \tag{6.18}$$

as given in [42], where the prime denotes the derivative with respect to ρ. At order ρ/ℓ the black hole is corrected by the conformal factor, and at order ρ_h/ℓ in the other metric functions close to the horizon. Kudoh and collaborators integrated the functions T, B and C numerically, and found that the T function to a very good approximation extends hyperspherically off the brane. Although B and C are not precisely the same, their difference is roughly of order ρ_h/ℓ as expected. At large ρ, $T, B, C \to 1$, and the metric is asymptotically AdS in the Poincaré patch.

Although we do not use the explicit form of the metric, the features we require from the solutions of [42] are that the event horizon is topologically hyperspherical with constant surface gravity, and that the braneworld black hole asymptotes to the Poincaré patch of AdS. The coordinate transformation between the local black hole coordinates and the Poincaré RS coordinates is

$$\rho^2 = r^2 + \ell^2(e^{|z|/\ell} - 1)^2, \qquad \tan\chi = \frac{r}{\ell(e^{|z|/\ell} - 1)}\,, \tag{6.19}$$

A slight bend in the brane 'trajectory' at ρ_h is expected due to the bending of the brane in response to the black hole, which gives rise to a four dimensional Newtonian potential as described in [34]. From the perspective of the $\{\rho, \chi\}$ coordinates, in which the brane sits at $\chi = \pi/2$, this will show up as a $1/\rho$ correction to T, B, C. We therefore take our asymptotic metric to be of the form

$$ds^2 = e^{-2|z|/\ell}\left[F(r,z)d\tau^2 + F(r,z)^{-1}dr^2 + r^2 d\Omega^2\right] + dz^2, \tag{6.20}$$

where $F \sim 1 - 2G_N M(z)/r + O(r^{-2})$. $M(z)$ can be thought of as coming from the brane bending term of M/ρ in the original coordinates.

6.2.1 Computing the Action

The action of the black hole instanton diverges, making it necessary to regulate it in some way. At large distances from the black hole, this is done by truncating the five dimensional manifold, taking a surface at large radius R on the brane and extending this along geodesics in the $\pm z$ directions orthogonal to the brane. This produces the outer boundary surface $\partial\mathcal{M}_R$ as shown in the cartoon in figure 6.1. The interior is denoted by $\mathcal{M}_R$ and the intersection of $\mathcal{M}_R$ with the brane world is denoted by $\mathcal{B}$.

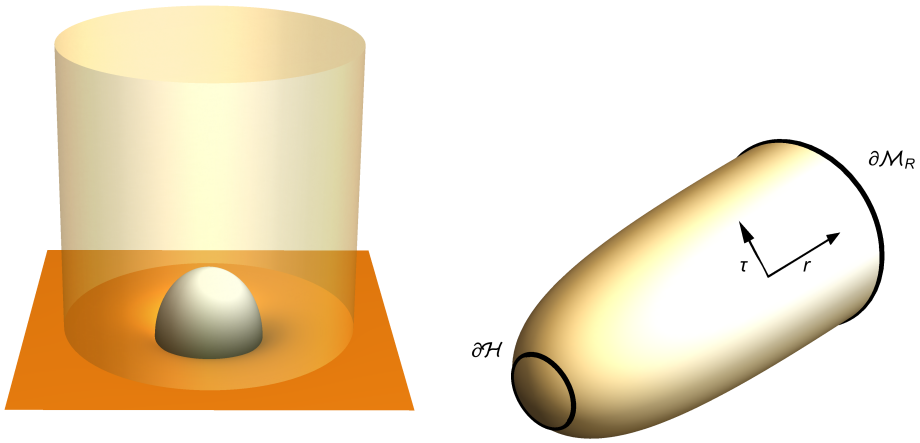

Figure 6.1: A cartoon of the Euclidean tidal black hole and the cut-off surfaces. On the left, the τ, θ coordinates are suppressed, and the cut-off surface is indicated relative to the brane and bulk black hole horizon. Only one half of the $\mathbb{Z}_2$ symmetric solution is shown. On the right, the Euclidean τ coordinate is shown but the bulk and angular coordinates are suppressed, and the "black hole cigar" geometry is indicated. Two circles denote the boundary $\partial\mathcal{H}$ of the region just outside the horizon and the boundary $\partial\mathcal{M}_r$ at large radius. Diagrams by Ruth Gregory.

The Euclidean action for this truncated instanton or black hole solution is

$$S_R = -\frac{1}{16\pi G_5}\int_{\mathcal{M}_R}(R_5 - 2\Lambda_5)\sqrt{g_5} + \int_{\mathcal{B}}\mathcal{L}_m\sqrt{g_4} + \frac{1}{8\pi G_5}\int_{\partial\mathcal{M}_R} K\sqrt{h}, \tag{6.21}$$

where K denotes the extrinsic curvature of the boundary surface $\partial\mathcal{M}_R$ defined with an *inward* pointing normal to the bulk manifold $\mathcal{M}_R$. The matter Lagrangian $\mathcal{L}_m$ includes the contribution from any nontrivial Higgs field profile, as well as the brane stress-energy tensor. The bulk integral ranges across all z, and includes the $\delta-$function curvature at the brane source in the spirit of the Israel approach. Numerical subscripts distinguish between bulk and brane geometry, with the gravitational constant in five dimensions given in terms of Newton's constant G_N by $G_5 = \ell G_N$.

The tunnelling exponent is given by the difference between the actions of the instanton geometry with a remnant black hole, and the false vacuum geometry with the seed black hole: $B = S_{\rm inst} - S_{\rm fv}$. This is finite in the limit $R \to \infty$.

To show this, we begin by introducing a small ball, $\mathcal{H}$, extending a proper distance of order $\mathcal{O}(\varepsilon)$ out from the black hole event horizon. This will deal with any conical deficits arising from a generic periodicity in Euclidean time. The action calculation is now split into two terms,

$$S_R = S_R^{\rm hor} + S_R^{\rm ext}, \tag{6.22}$$

where[1]

$$S_R^{\rm hor} = -\frac{1}{16\pi G_5}\int_{\mathcal{H}}(R_5 - 2\Lambda_5)\sqrt{g_5} + \int_{\mathcal{B}_{\mathcal{H}}}\mathcal{L}_m\sqrt{g_4} + \frac{1}{8\pi G_5}\int_{\partial\mathcal{H}}K\sqrt{h}, \tag{6.23}$$

$$\begin{aligned} S_R^{\rm ext} = &-\frac{1}{16\pi G_5}\int_{\mathcal{M}_R-\mathcal{H}}(R_5 - 2\Lambda_5)\sqrt{g_5} + \int_{\mathcal{B}-\mathcal{B}_{\mathcal{H}}}\mathcal{L}_m\sqrt{g_4} + \frac{1}{8\pi G_5}\int_{\partial\mathcal{H}}K\sqrt{h} \\ &+ \frac{1}{8\pi G_5}\int_{\partial\mathcal{M}_R}K\sqrt{h}, \end{aligned} \tag{6.24}$$

and $\mathcal{B}_{\mathcal{H}} = \mathcal{B}\cap\mathcal{H}$ is the intersection of the event horizon cap with the brane.

6.2.2 Near Horizon

To deal with the near-horizon contribution, we transform (6.16) to local horizon coordinates, analogous to the Euclidean Schwarzschild transformation, (6.14), so that

$$ds^2 \approx d\varrho^2 + A^2(\varrho,\xi)d\tau^2 + D^2(\varrho,\xi)d\Omega_{II}^2 + N^2(\varrho,\xi)d\xi^2, \tag{6.25}$$

where $\varrho < \varepsilon$ inside $\mathcal{H}$. Comparing to (6.16), we see $A = T/(1+\frac{\rho}{\ell}\cos\chi)$, $D = \rho\sin\chi e^C/(1+\frac{\rho}{\ell}\cos\chi)$, $N = e^B/(1+\frac{\rho}{\ell}\cos\chi)$, with $\varrho \approx (\rho-\rho_h)/(1+\frac{\rho_h}{\ell}\cos\chi)$ and $\xi = \chi + \mathcal{O}(\varrho^2)$. The brane sits at $\xi = \pi/2$, and on the horizon, $\xi\in[0,\pi]$.

As with the four dimensional Euclidean Schwarzschild, there is a natural periodicity of τ for which the Euclidean metric is nonsingular; this periodicity is $\beta_0 = 2\pi/\kappa$, where κ is the surface gravity of the black hole given in the original coordinates by (6.18), and in the horizon coordinates by $\partial A/\partial\varrho$. From nonsingularity of the geometry, we deduce $N \sim N_0(\xi) + \mathcal{O}(\varrho^2)$, $D \sim D_0(\xi) + \mathcal{O}(\varrho^2)$, and $A \sim \kappa\varrho + \mathcal{O}(\varrho^2)$. Now let us consider a general periodicity β for the Euclidean time τ, then we will have a conical singularity at $\varrho = 0$. In order to compute the action, we smooth this out by modifying the A function so that $A'(\varepsilon,\xi) = \kappa$, but $A'(0,\xi) = \kappa\beta_0/\beta$. Computing the curvature for this smoothed metric gives

$$\sqrt{g_5}(R_5 - 2\Lambda_5) = -2N_0(\xi)D_0(\xi)^2A''(\varrho) + \mathcal{O}(\varrho) \tag{6.26}$$

which gives the bulk contribution to $S_R^{\rm hor}$ as

$$-\frac{1}{16\pi G_5}\int_{\mathcal{H}}(R_5 - 2\Lambda_5)\sqrt{g_5} + \int_{\mathcal{B}_{\mathcal{H}}}\mathcal{L}_m\sqrt{g_4} \tag{6.27}$$

$$= \frac{\beta}{2G_5}[A'(\varepsilon) - A'(0)]\int N_0D_0^2d\xi + \mathcal{O}(\varepsilon^2) \tag{6.28}$$

$$= \frac{\kappa}{8\pi G_5}[\beta - \beta_0]\mathcal{A}_5 \tag{6.29}$$

[1]Note, the extrinsic curvature in the Gibbons-Hawking term is computed with an inward pointing normal, hence the *same* sign for that term in each expression.

where $\mathcal{A}_5 = 4\pi \int N_0 D_0^2 d\xi$ is the area of the braneworld black hole horizon extending into the bulk (on both sides of the brane). Note that the matter term on the left gives no contribution since the matter Lagrangian does not have a singularity at $\rho = 0$.

To compute the Gibbons-Hawking boundary term we note that the normal to $\partial\mathcal{H}$ is $n = -d\varrho$, hence the extrinsic curvature is

$$K = -A^{-1}A_{,\varrho} + \mathcal{O}(\varepsilon) \tag{6.30}$$

and

$$\frac{1}{8\pi G_5}\int_{\partial\mathcal{H}} K\sqrt{h} = -\frac{\kappa\beta}{2G_5}\int N_0 D_0^2 d\xi = -\frac{\kappa\beta\mathcal{A}_5}{8\pi G_5} \tag{6.31}$$

Thus the contribution to the action from the horizon region is

$$S_R^{\text{hor}} = -\frac{\kappa\beta_0\mathcal{A}_5}{8\pi G_5} = -\frac{\mathcal{A}_5}{4G_5} \tag{6.32}$$

6.2.3 External Region

The external part S_R^{ext} can be simplified by taking a canonical decomposition based on a foliation of the manifold by surfaces of constant τ and Σ_τ (see appendix B). The part of the action outside the horizon cylinder reduces to simple surface terms,

$$S_R^{\text{ext}} = \frac{1}{8\pi G_5}\int_0^\beta d\tau \left(\int_{C_R} {}^3K\,\sqrt{h} + \int_{C_\mathcal{H}} {}^3K\,\sqrt{h}\right). \tag{6.33}$$

where ${}^3K$ are the extrinsic curvatures of codimension two surfaces of constant r, regarded as submanifolds of surfaces of constant τ, Σ_τ as described in appendix B.1.

Close to the horizon, we use the metric (6.25) and find

$${}^3K = 2D^{-1}D_{,\varrho} + N^{-1}N_{,\varrho} \to 0, \tag{6.34}$$

at the horizon $\varrho = 0$ for the behaviour of the metric coefficients $D(\varrho,\xi)$ and $N(\varrho,\xi)$ given earlier. This boundary term gives no contribution to the action.

6.2.4 Large R

At large distances, the metric approaches the perturbed Poincaré form (6.20), and we find

$${}^3K = -\frac{2}{R}e^{|z|/\ell}F^{1/2}, \qquad \sqrt{h} = R^2 e^{-3|z|/\ell}F^{1/2}. \tag{6.35}$$

hence

$$S_R^{\rm ext} = -\frac{\beta}{G_N \ell} \int_0^\infty dz e^{-2z/\ell} \left(2R - 4G_N M(z) + O(R^{-1})\right). \tag{6.36}$$

Ideally, we would like to regularise this action either by background subtraction, or by adding in boundary counterterms along the lines of [44, 45]. However, the counterterms of [45] do not regulate this action, and one cannot replace the interior of $\mathcal{M}_R$ with a pure RS braneworld, due to the variation of $M(z)$ along $\partial\mathcal{M}_R$. Instead, we note that the Higgs fields on the brane in any instanton solution will die off exponentially for large r, so from the intuition that $M(z)/r \sim M_\infty/\rho = M_\infty/\sqrt{r^2 + \ell^2(e^{|z|/\ell} - 1)^2}$, we then deduce that the mass function $M(z)$ will be the same at leading order for both the false vacuum with the seed brane black hole, and the instanton solution, therefore the exterior terms will cancel when we take the difference between the instanton action and the false vacuum action:

$$B = S_{\rm inst} - S_{\rm fv} = \lim_{R\to\infty} \left[S_R^{\rm ext}\Big|_{\rm inst} - S_R^{\rm ext}\Big|_{\rm fv} \right] - \frac{\mathcal{A}_5^{\rm inst}}{4G_5} + \frac{\mathcal{A}_5^{\rm fv}}{4G_5} = \frac{\mathcal{A}_S}{4G_5} - \frac{\mathcal{A}_R}{4G_5} \tag{6.37}$$

where $\mathcal{A}_S$ and $\mathcal{A}_R$ refer to the areas of the seed and remnant black hole horizons respectively.

This is simply the reduction in entropy $-\Delta S$ caused by the decay process, and the tunnelling rate is recognisable as the probability of an entropy reduction $\propto \exp(\Delta S)$. The difficulty we face when applying (6.37) is that we have to relate the black hole area to the mass of the black hole triggering the vacuum decay and the physical parameters in the Higgs potential. This requires explicit solutions for the gravitational and Higgs fields.

6.3 Tidal black hole bubbles

The lack of any analytic brane black hole solutions presents the main obstacle to finding tunnelling instantons. The brane-vacuum equations are complicated by the reduced symmetry of the expected static, brane-rotationally symmetric geometry. Although we have numerical brane black hole solutions, the introduction of Higgs profiles on the brane would require these to be modified, and a new full numerical brane+bulk solution would have to be computed. Instead of attempting this considerable undertaking, we adopt a more practical alternative based on the tidal black hole solutions of Dadhich et al.[[46]].

As described, for example, by Maartens [47], one can take an approach of solving purely the brane "Einstein equations", i.e. the induced Einstein equations on the brane found by the Gauss Codazzi projection of the Einstein tensor in Shiromizu, Maeda and Sasaki [35] (hereafter referred to as SMS), which provide a suitable set of initial conditions on the brane for evolving into the bulk. These equations are similar to the four dimensional Einstein equations, but contain additional terms involving the square of the energy mo-

mentum of any matter on the brane, and an additional projected Weyl tensor , $\mathcal{E}_{\mu\nu}$, coming from a projection of electric part of the bulk Weyl tensor onto the brane. (For the full form of the Weyl tensor, see equation (B.21) in Appendix B.) The projected Weyl tensor for the tidal black hole satisfies the equations $\mathcal{E}_\mu{}^\mu = 0$ and $\nabla^\mu \mathcal{E}_{\mu\nu} = 0$. Following [47], one uses the symmetry of the physical set up to define functions $\mathcal{U}$ and Π and write the projected Weyl tensor as

$$\mathcal{E}^\mu_\nu = \mathrm{diag}\left(\mathcal{U}, -\frac{(\mathcal{U}+2\Pi)}{3}, \frac{\Pi-\mathcal{U}}{3}\right) \tag{6.38}$$

This is manifestly tracefree, and the 'Bianchi' identity implies a conservation equation for $\mathcal{U}, \Pi$. For the spherically symmetric static brane metric

$$ds^2_{\mathrm{brane}} = f(r)e^{2\delta(r)}d\tau^2 + f^{-1}(r)dr^2 + r^2 d\Omega^2_\Pi, \tag{6.39}$$

the conservation equation implies

$$(\mathcal{U}+2\Pi)' + \left(\frac{f'}{f} + 2\delta'\right)(2\mathcal{U}+\Pi) + \frac{6\Pi}{r} = 0\,. \tag{6.40}$$

Even for the vacuum brane this is not a closed system, but if one assumes an equation of state, one can find an induced brane solution [48]. The tidal black hole corresponds to the choice $\Pi = -2\mathcal{U}$, for which (6.40) is easily solved by $\mathcal{U} \propto 1/r^4$.

The tidal black hole of Dadhich et al. [46], has $\delta(r) \equiv 0$,

$$f(r) = 1 - \frac{2G_N M}{r} - \frac{r_Q^2}{r^2}\,, \tag{6.41}$$

and

$$\mathcal{E}_{\mu\nu}dx^\mu dx^\nu = -\frac{r_Q^2}{r^4}\left(f(r)d\tau^2 + f^{-1}(r)dr^2 - r^2 d\Omega^2\right), \tag{6.42}$$

where r_Q is a constant parameter related to the tidal charge Q of [46] by $r_Q^2 = -Q$. The motivation for this solution is clear: at large distances, the Newtonian potential of a mass source has the conventional $G_N M/r$ behaviour due to a "brane-bending" term identified by Garriga and Tanaka [34]; the interpretation being that the brane shifts relative to the bulk in response to matter on the brane. At small distances on the other hand we would expect the higher dimensional Schwarzschild potential to be more appropriate, hence the $-r_Q^2/r^2$ term. The event horizon is distorted by the projected Weyl tensor, hence the name. Other choices for the Weyl tensor lead to different brane solutions [48], however these tend to have either wormholes or singularities (or both), therefore we do not consider these here.

To obtain our bubble solution, we will need to find the fully coupled Higgs plus brane SMS-gravitational equations of motion in the spherically symmetric gauge (6.39). For this we will use the same *tidal* Ansatz for the equation of state of the projected Weyl tensor: $\mathit{\Pi} = -2\mathcal{U}$, meaning that even when the Higgs fields take a nontrivial bubble profile, the conservation equation for the Weyl tensor (6.40) is still solved by $\mathcal{U} = -r_Q^2/r^4$.

We also have some limited information about the form of the tidal black hole solution away from the brane from an expansion in the fifth coordinate. According to Maartens and Koyama, [49] the metric parallel to the brane at proper distance z from the brane is

$$\tilde{g}_{\mu\nu}(z) = g_{\mu\nu}(0) - (8\pi G_5 S_{\mu\nu})\, z + \left[(4\pi G_5)^2 S_{\mu\sigma}S^{\sigma}{}_{\nu} - 8\pi G_N S_{\mu\nu} - \mathcal{E}_{\mu\nu}\right] z^2 + \dots \tag{6.43}$$

where $S_{\mu\nu} = T_{\mu\nu} - \frac{1}{3}T g_{\mu\nu}$ is composed of the energy momentum tensor of brane matter. In the false vacuum state, we have $T_{\mu\nu} = 0$ and the metric expansion away from the brane reduces to

$$\begin{aligned} ds^2 &\approx e^{-2|z|/\ell}\left(g_{\mu\nu} - \mathcal{E}_{\mu\nu}z^2\right) + dz^2 \\ &\approx e^{-2|z|/\ell}\left\{\left(1 + \frac{r_Q^2 z^2}{r^4}\right)\left(f d\tau^2 + f^{-1}dr^2\right) + \left(1 - \frac{r_Q^2 z^2}{r^4}\right) r^2 d\Omega_{II}^2\right\} + dz^2 \end{aligned} \tag{6.44}$$

which shows clearly how the horizon area decreases in the z direction. The horizon forms into a true bulk black hole when the area vanishes for some value of z of order r_h^2/r_Q.

Although this tidal black hole has many attractive features, the main difficulty that has to be overcome when finding the bubble solutions is that the tidal constant r_Q is undetermined. Clearly a nonsingular brane black hole, if approximately tidal, should have a relation between the asymptotic mass measured on the brane, M, and the tidal charge r_Q^2. For very large black holes, we expect the horizon radius to be predominantly determined by M, and this ambiguity is not relevant, however for the small black holes we are interested in, the horizon radius is primarily dependent on r_Q, and we must confront this ambiguity.

We start by noting that the tidal black hole solution should be identical to the five dimensional Schwarzschild black hole in the limit that the AdS radius $\ell \to \infty$, as the brane stress-energy tensor, which is tuned to the cosmological constant, vanishes in this limit, and full $SO(4)$ rotational symmetry is restored. Since $G_N = G_5/\ell$, (6.41) implies that $r_Q^2 \to r_h^2$ in this limit. Intuitively, we also expect that for small black holes, the curvature is dominated by the black hole and the bulk AdS scale should be subdominant. The black hole should look (near the horizon at least) mainly like a five dimensional black hole which has radius r_Q, i.e. $r_Q^2 \to r_h^2$ as $r_h \to 0$. We will therefore assume analyticity in r_h/ℓ and

write

$$r_Q^2 = r_h^2 \left(1 - b\frac{r_h}{\ell} + \mathcal{O}\left(\frac{r_h^2}{\ell^2}\right)\right) \tag{6.45}$$

for small r_h/ℓ, where b is some constant independent of r_h and ℓ, expected to be roughly of order unity. For the tidal black hole, a trivial rewriting of (6.41) gives the relation

$$M = \frac{br_h^2}{2G_5} \tag{6.46}$$

in other words, we have expressed the ambiguity in the tidal parameter for small black holes by the parameter b, and the relationship between the asymptotic mass of the black hole as measured on the brane and the horizon radius explicitly factors in this ambiguity. As we now see, this uncertainty can be absorbed into a redefinition of the low energy Planck scale in the tunnelling rate.

The tunnelling process starts with the uniform false vacuum ϕ_{fv} and a seed black hole with mass M_S. This false vacuum configuration resembles the tidal black hole on the brane, and a slightly perturbed 5D Schwarzschild solution in the bulk [42]. The bubble solution represents the decay process to another state with the field asymptoting the same false vacuum at large distances but with the field approaching its true vacuum near the horizon of a remnant black hole with mass M_R, which remains after tunnelling.

Previously, we showed that the tunnelling exponent is given by

$$B = \frac{1}{4G_5}\left(\mathcal{A}_S - \mathcal{A}_R\right), \tag{6.47}$$

where S represents the five dimensional area of the seed black hole area and R that of the remnant black hole. To leading order in r_h/ℓ, the small black hole horizon has an approximately hyperspherical shape, therefore the area will be well approximated by $2\pi^2 r^3$, hence

$$B = \frac{\pi^2}{2G_5}\left(r_S^3 - r_R^3\right) = \frac{\pi^2 r_S^3}{2G_5}\left[1 - \left(\frac{M_R}{M_S}\right)^{\frac{3}{2}}\right] \tag{6.48}$$

using (6.46). In the limit that the difference in seed and remnant black hole masses is small, $(M_S - M_R)/M_S = \delta M/M_s \ll 1$, we finally arrive at

$$B \approx \frac{3}{4}\left(\frac{\pi M_S}{bM_5}\right)^{3/2}\frac{\delta M}{M_S}, \tag{6.49}$$

where $M_5 = (8\pi G_N \ell)^{-1/3}$ is the low energy Planck scale. The uncertainty in the value of the tidal charge parameter b can be absorbed into our uncertainty in the low energy Planck scale, and so we let $bM_5 \to M_5$.

The action B which gives the tunnelling exponent is therefore found from the taking the difference in actions of the black hole and the instanton.

$$\begin{aligned} B &= S_{bh} - S_b && (6.50)\\ &= 4\pi G M_{seed}^2 (r_{bh}^2 - r_b^2) && (6.51) \end{aligned}$$

6.3.1 Approximating ϕ'' near the horizon

Near the horizon of the black hole, it is necessary to use an analytical approximation for ϕ'' to solve the equations of motion. We take the spherically symmetric Euclidean metric as:

$$ds^2 = f(r)e^{2\delta(r)}d\tau^2 + \frac{dr^2}{f(r)} + r^2(d\theta^2 + \sin^2\theta d\phi^2) \tag{6.52}$$

Where f has the form

$$f = 1 - \frac{8\pi G\mu(r)}{3r^2} \tag{6.53}$$

The equations of motion for the bounce solution are

$$\begin{aligned} f\phi'' + \frac{3}{r}f\phi' + \delta' f\phi' + f'\phi' - \frac{\partial V}{\partial \phi} &= 0 && (6.54)\\ \delta' &= \frac{8\pi G}{3} r\phi'^2 && (6.55)\\ \mu' &= 2\pi^2 r^3 (\frac{1}{2}f\phi'^2 + V) && (6.56) \end{aligned}$$

To approximate ϕ, we rewrite f and perform a series expansion to second order, where we define $x = r - r_h$.

$$\begin{aligned} f &= f_1 x + f_2 x^2 + \dots && (6.57)\\ \phi &= \phi_h + a_1 x + a_2 x^2 + \dots && (6.58)\\ V &= V_h + V_{\phi h} a_1 x + \dots && (6.59)\\ V_\phi &= V_{\phi h} + V_{\phi\phi h} a_1 x + \dots && (6.60) \end{aligned}$$

By substituting these expansions into equation (6.56), this gives an approximation for ϕ

$$\phi'' = 2a_2 \tag{6.61}$$

where

$$a_2 = \frac{4\pi G}{3} r_h a_1^3 + \frac{a_1^2}{V_{\phi h}} \left[\frac{8\pi G}{3} V_h + \frac{1}{4} V_{\phi\phi h} \right] \tag{6.62}$$

6.3.2 Higgs bubbles on the brane

The Higgs bubble will correspond to a solution of the brane SMS equations with an energy momentum tensor derived from the (Euclidean) scalar field Lagrangian[2]

$$\mathcal{L}_m = \frac{1}{2} g^{\mu\nu} \phi_{,\mu} \phi_{,\nu} + V(\phi). \tag{6.63}$$

where $V(\phi)$ has a metastable false vacuum. The SMS equations for the bubble, assuming the general form (6.39) are derived in appendix B.2, and are

$$f\phi'' + f'\phi' + \frac{2}{r} f\phi' + f\delta'\phi' - V_{,\phi} = 0, \tag{6.64}$$

$$\mu' = 4\pi r^2 \left\{ \frac{1}{2} f\phi'^2 + V - \frac{2\pi G_N}{3} \ell^2 (\frac{1}{2} f\phi'^2 - V)(\frac{3}{2} f\phi'^2 + V) \right\}, \tag{6.65}$$

$$\delta' = 4\pi G_N r \phi'^2 \left\{ 1 - \frac{4\pi G_N}{3} \ell^2 (\frac{1}{2} f\phi'^2 - V) \right\}. \tag{6.66}$$

where, for comparison with the vacuum case (6.41), we have defined a "mass" function $\mu(r)$ by

$$f(r) = 1 - \frac{2G_N \mu(r)}{r} - \frac{r_Q^2}{r^2}. \tag{6.67}$$

These are integrated numerically from the black hole horizon r_h to $r \to \infty$ where ϕ is in the false vacuum, implementing the 'shooting' method described in chapter three. The remnant mass M_R and the tunnelling exponent B are determined in terms of the seed mass M_S, the potential V and the AdS radius ℓ.

The results presented in this section are based on the Higgs-like logarithmic potential described in the previous chapter, assuming that the standard model holds for energy scales up to the low energy Planck mass M_5.

Here we take a one parameter analytic fit to λ_{eff}, where the single parameter is the crossover scale Λ_ϕ:

$$\lambda_{\text{eff}} = g(\Lambda_\phi) \left\{ \left(\ln \frac{\phi}{M_p} \right)^4 - \left(\ln \frac{\Lambda_\phi}{M_p} \right)^4 \right\} \tag{6.68}$$

and $g(\Lambda_\phi)$, chosen to fit the high energy asymptote of λ_{eff}, varies very little across the range of $\Lambda_\phi$of relevance to the Standard Model λ_{eff}. In four dimensions, we can have a Higgs

[2]Note that we have defined the Euclidean Lagrangian to contain $+V$, meaning that the false vacuum solution will have energy-momentum $-V g_{\mu\nu}$, but that our 4D Einstein equations will have the conventional sign for the energy-momentum, i.e. $G_{\mu\nu} = 8\pi G_N T_{\mu\nu} + \ldots$.

instability scale very close to the Planck scale, however with large extra dimensions, new physics could potentially enter at the low-energy Planck scale M_5, thus to be consistent, we should restrict our parameters to the range $\Lambda_\phi < M_5 < M_p$.

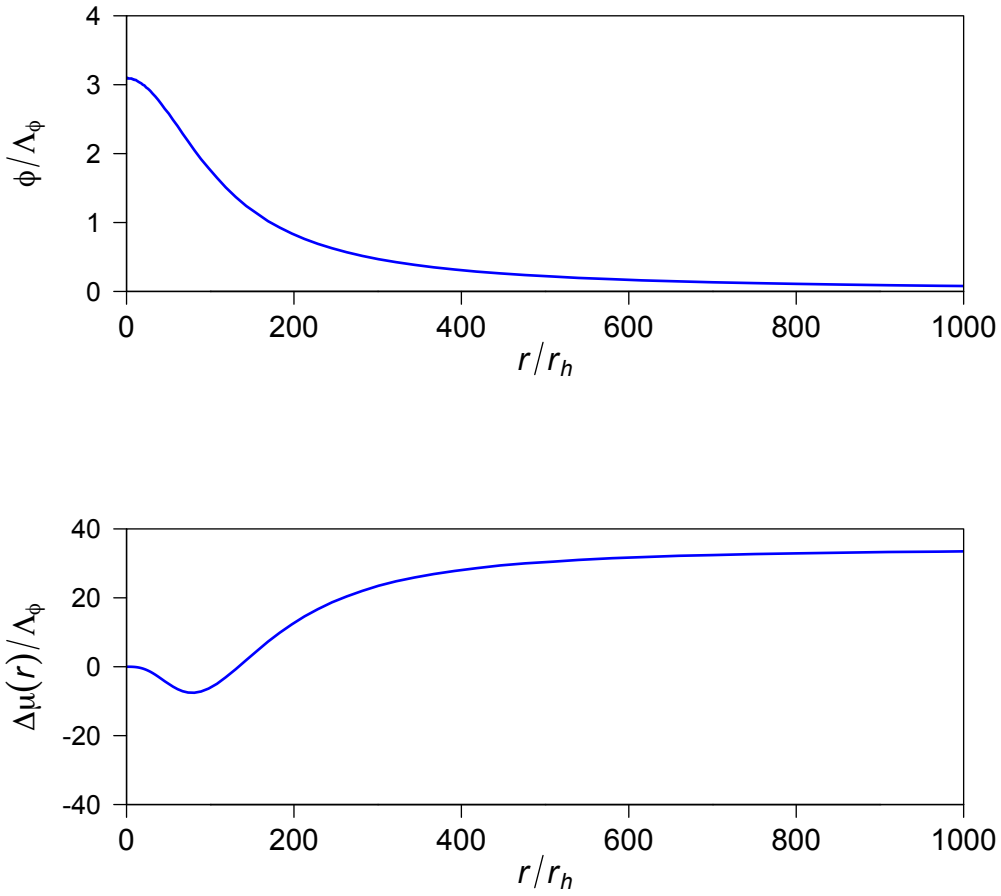

Figure 6.2: Profiles for the bubble and the mass term $\mu(r)$ outside the horizon r_h with $M_5 = 10^{15}$GeV, $\Lambda_\phi = 10^{12}$GeV and $r_h = 20000/M_p$. This particular solution has tunnelling exponent $B = 4.3$

Figure 6.2 gives profiles for a typical bubble centered on the black hole after tunnelling and for the mass term $\mu(r)$ beyond the horizon radius r_h. The field is in the true vacuum at the horizon and approaches the false vacuum as $r \to \infty$ with a characteristic thick wall profile. The bubble radius greatly exceeds the horizon of the black hole.

The change in the mass term is given by $\Delta\mu(r) = \mu(r) - \mu(r_h)$. Near the horizon, $\Delta\mu(r)$ is negative due to the negative potential V in equation (6.65). $\mu(r)$ becomes positive at large r where there is a positive contribution from the kinetic term and hence ΔM is positive.

6.3.3 Branching Ratios

The calculation of the vacuum decay rate assumes a stationary background which only makes sense when the decay rate exceeds the Hawking evaporation rate. The brane black hole can radiate in the brane or into the extra dimension, but if we consider a scenario as close as possible to the standard model then most of the radiation will be in the form of quarks and leptons radiated into the brane, simply because these are the most numerous particles. (For a review of Hawking evaporation rates in higher dimensions see [50].)

Black hole radiation is similar to the radiation from a black body with the same area as the black hole horizon and at the Hawking temperature, but with additional 'grey body' factors representing the effects of back-scattering of the radiation from the space-time curvature around the black hole. Following [50], we can express the energy loss rate due to evaporation as $\dot{E}$, where on dimensional grounds (since r_h is the only relevant dimensionful parameter)

$$|\dot{E}| = \gamma\, r_h^{-2}, \tag{6.69}$$

for some constant γ. The Hawking decay rate of the black hole Γ_H, using (6.46) to eliminate the radius, is

$$\Gamma_H = \frac{|\dot{E}|}{M_S} = \frac{4\pi\gamma M_5^3}{M_S^2} \tag{6.70}$$

The vacuum decay rate is given by the usual equation,

$$\Gamma_D = Ae^{-B}. \tag{6.71}$$

The pre-factor A contains a factor $(B/2\pi)^{1/2}$ from a zero mode and a vacuum polarisation term from the other modes, whose characteristic length scale is the bubble radius r_b. We estimate

$$\Gamma_D \approx \left(\frac{B}{2\pi}\right)^{1/2} \frac{1}{r_b} e^{-B}. \tag{6.72}$$

Transition rates seeded by the black hole seed are presented as a branching ratio of Γ_D and Γ_H, given in equation (6.2).

$$\frac{\Gamma_D}{\Gamma_H} \approx \frac{1}{\gamma}\left(\frac{B}{2\pi}\right)^{1/2}\left(\frac{M_S}{M_5}\right)^{3/2}\left(\frac{r_h}{r_b}\right)e^{-B} \tag{6.73}$$

Vacuum decay is important when this ratio is larger than one.

The contribution to Γ_H from a fermion in four dimensions is 7.88×10^{-4} for each degree of freedom [51]. In the Standard Model, there are a total of 90 fermions (quarks, leptons, and neutrinos) giving 90 fermion degrees of freedom. Harris and Kanti [52] find that Γ_H

for a five dimensional black hole is 14.2 times that for a four dimensional black hole, giving an approximate Γ_D in five dimensions

$$\Gamma_D \approx 14.2 \times 90 \times 7.88 \times 10^{-4} = 0.10. \tag{6.74}$$

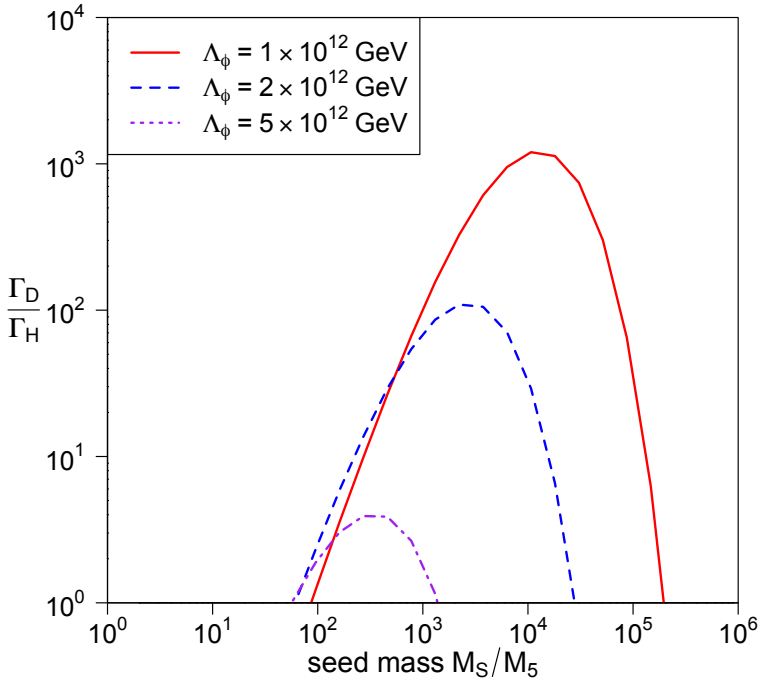

Figure 6.3: The branching ratio of the false vacuum nucleation rate to the Hawking evaporation rate as a function of the seed mass for a selection of Higgs models with $M_5 = 10^{15}$GeV.

The branching ratio is plotted in figure 6.3 for $M_5 = 10^{15}$GeV and Higgs instability scale around 10^{12} GeV (corresponding to a top quark mass of 172 GeV). Note that the decay rates in this parameter range are larger than M_5^3/M_S^2, i.e. they are extremely fast. The figure shows an example where black holes with masses between 10^{17} GeV and 10^{20} GeV, or 10^{-7} g to 10^{-4} g, would seed rapid Higgs vacuum decay.

6.4 Black hole seeded vacuum decay in four dimensions

To contrast the influence of a black hole in the bulk and a black hole on the brane for vacuum decay in RS2, we will also present results for vacuum decay seeded by a four dimensional black hole. For this subsection, we will revisit a toy model potential with two minima:

$$V = \frac{1}{2}m^2\phi^2 - \frac{1}{4}\lambda^2\phi^4 + \frac{1}{6}\hat{g}\phi^6 \tag{6.75}$$

where the free parameter $\hat{g}$ varies the height of the potential barrier and m and λ are self coupling parameters. We can rescale the variables to set $m = \lambda = 1$, and therefore the rescaled action $\hat{B}$ will be expressed in terms of the real action $\hat{B} = m\lambda B$ in plots. The effect of $\hat{g}$ on the decay rate in five dimensions is shown in figs. 6.6 and 6.7.

In four dimensions, the black hole's mass is presented as a ratio M_s/M_p of seed mass to Planck mass where $M_p^2 = (8\pi G)^{-1}$. In the bulk, the relevant parameter is the five dimensional Planck mass, and we consider the ratio M_s/M_5 where $M_5^3 = (8\pi G)^{-1}$.

We present these results to compare the influence of four and five dimensional black holes on vacuum decay rates, although we do not give results using the Higgs-like potential for a 4D case (which has been previously explored in [26]). Fig. 6.5 gives the action and branching ratios for vacuum decay seeded by a four dimensional black hole, which can be compared with the 5D results shown in figs. 6.6 and 6.7.

While the Higgs-like potential we have previously considered gives rise to bubbles that are characteristically thick walled, a quadratic potential allows for the nucleation of thin wall bubbles. The qualitative differences between a thick and thin wall bubble are shown in fig. 6.4, demonstrating how the thickness of the bubble wall may be much greater than its radius in the thick wall case.

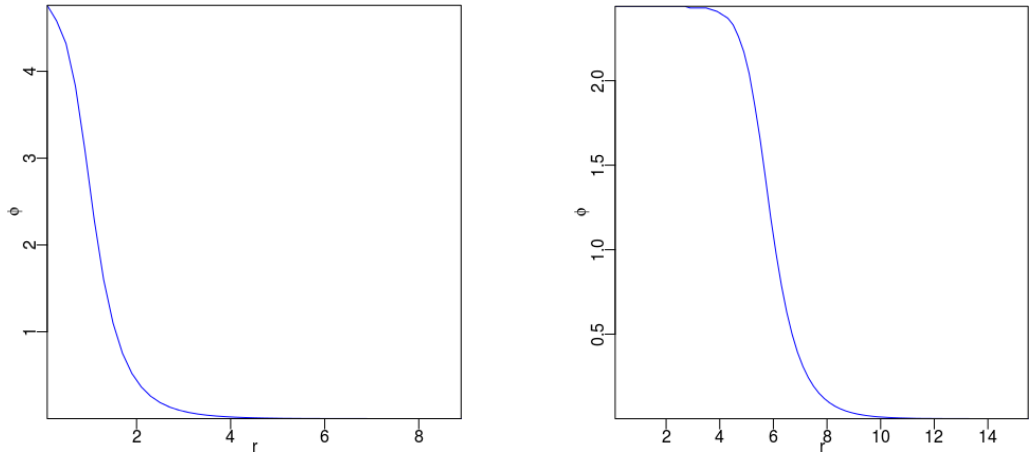

Figure 6.4: The bubble profiles for $\hat{g} = 0.04$ (left) and $\hat{g} = 0.14$ (right), which show a thick wall and thin wall bubble respectively.

6.4.1 Discussion

The tunnelling exponents and branching ratios are shown for two different values of the rescaled 5D Planck mass M_5 in figs. 6.6 and 6.7. The mass parameter M_D is defined

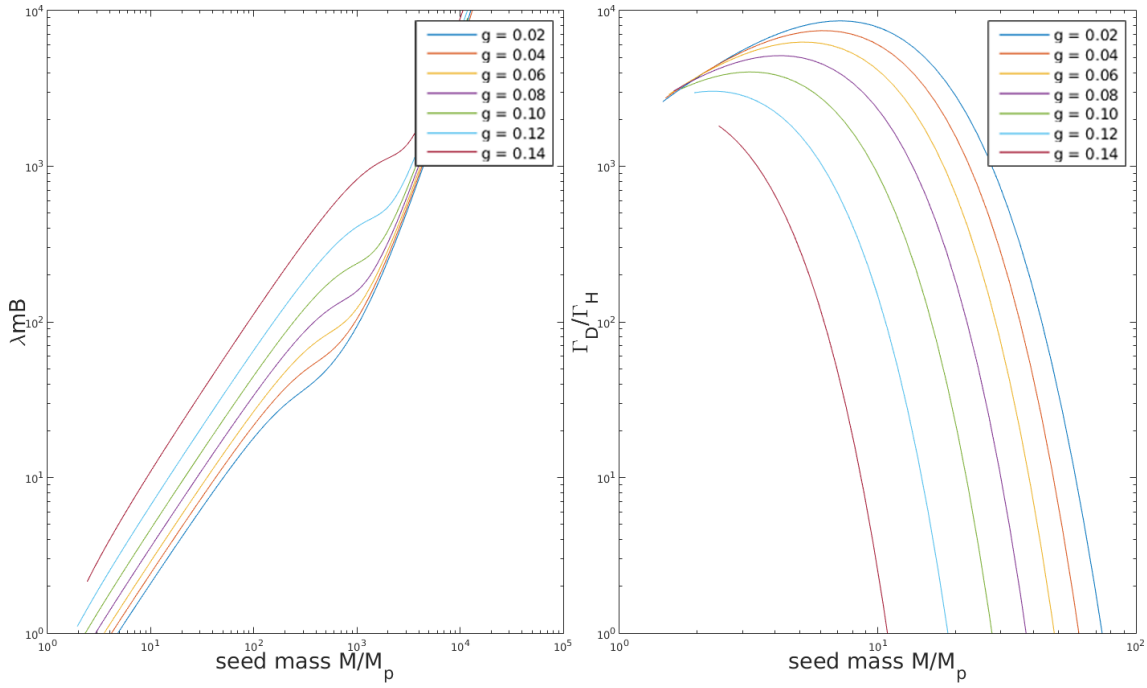

Figure 6.5: The tunnelling exponent as a function of seed mass (left) and the branching ratio of the false vacuum nucleation rate to the Hawking evaporation rate as a function of the seed mass (right), in four dimensions.

as $M_D = (\lambda m)^{2/3} M_5$ where M_5 is the five-dimensional Planck mass. λ and m are free parameters which can be varied by choosing a value for the rescaled $\hat{M}_5$. The effect of increasing the cube of the rescaled Planck mass by 10 from fig. 6.6 can be seen in fig. 6.7.

For the five dimensional case shown in 6.6, we see Hawking evaporation drive changes in the black hole's mass to a point where it is overtaken by vacuum decay. In the case of $M_5^3 = 10$, it is not possible to say which of vacuum decay or Hawking evaporation dominates across a range of seed masses, as both can be seen to drive mass changes across a narrow range depending on the self coupling parameter g. This range narrows further as the seed mass increases.

Increasing M_5 to $M_5^3 = 100$ widens the curves so that vacuum decay can be seen to dominate for smaller seed masses.

Compared to the four dimensional case, the convergence of the actions occurs at a lower seed mass, which would produce a higher tunnelling rate in five dimensions than in four for a black hole of the same mass.

For both four and five dimensional fields, when the black hole seed mass is sufficiently large, the action will tend towards a large value independent of $\hat{g}$. This has the effect of quenching the tunnelling rate.

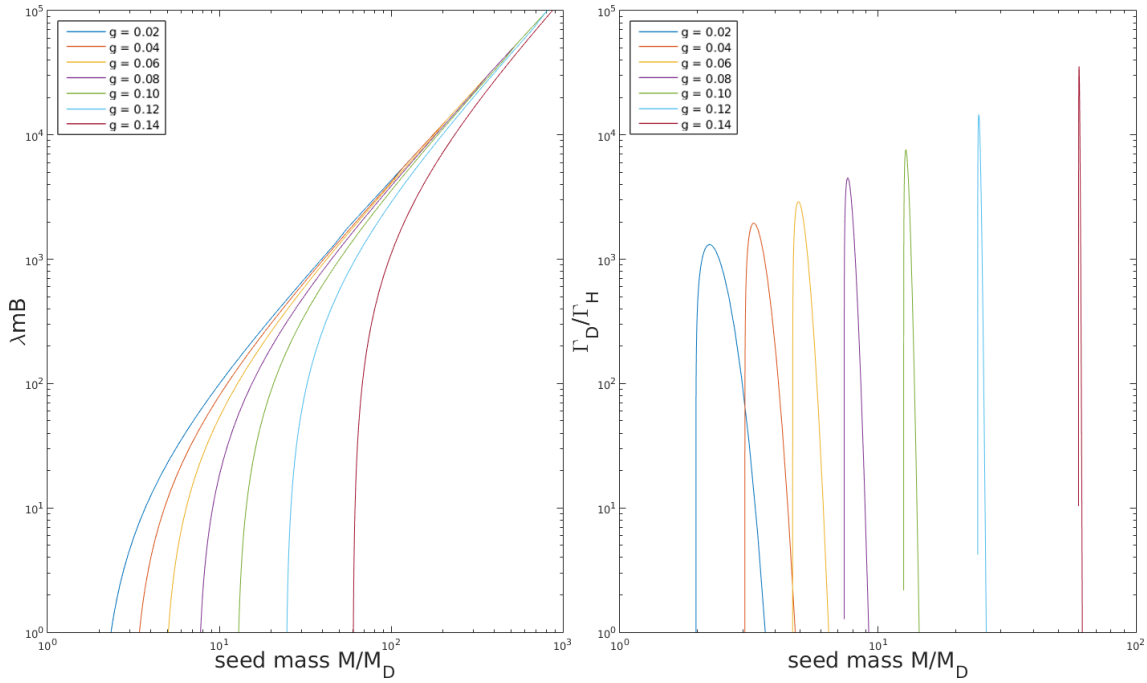

Figure 6.6: The tunnelling exponent as a function of seed mass (left) and the branching ratio of the false vacuum nucleation rate to the Hawking evaporation rate as a function of the seed mass (right), in five dimensions. $M_D = (\lambda m)^{2/3} M_5$, $M_5^3 = 10$.

6.5 Conclusion

In this chapter, we have used the Randall-Sundrum model to explore black hole seeded vacuum decay in five dimensions, and found that for a Higgs-like potential, black holes with masses in the approximate range $10^2 < M_s/M_5 < 10^5$ rapidly seed vacuum decay. The branching ratio plot shown in figure 6.3 demonstrates that small black holes in higher dimensions are overwhelmingly likely to initiate vacuum decay once they have radiated away sufficient mass to enter this range. As was found to be the case for 4D in [26], any small black hole, formed either in the early universe or in a high energy cosmic ray collision, will radiate, lose mass, then become sufficiently light that it seeds decay with a rate of order $10^{3-5} T_5$.[3]

Due to the much lower Planck mass M_5 in five dimensions ($M_5 \lesssim 10^9$GeV), it is possible that black holes light enough to trigger vacuum decay could be produced in high energy cosmic ray collisions. For example, the highest energy cosmic ray collisions [53, 54, 55] observed have an energy in excess of 10^{11}GeV, which could be sufficient to produce black holes of this scale.

Since the probability of vacuum decay occurring as a result of the existence of these small

[3]Here, $T_5 = (c^3/8\pi G_5 \hbar)^{1/3}$ is the 5D Planck time.

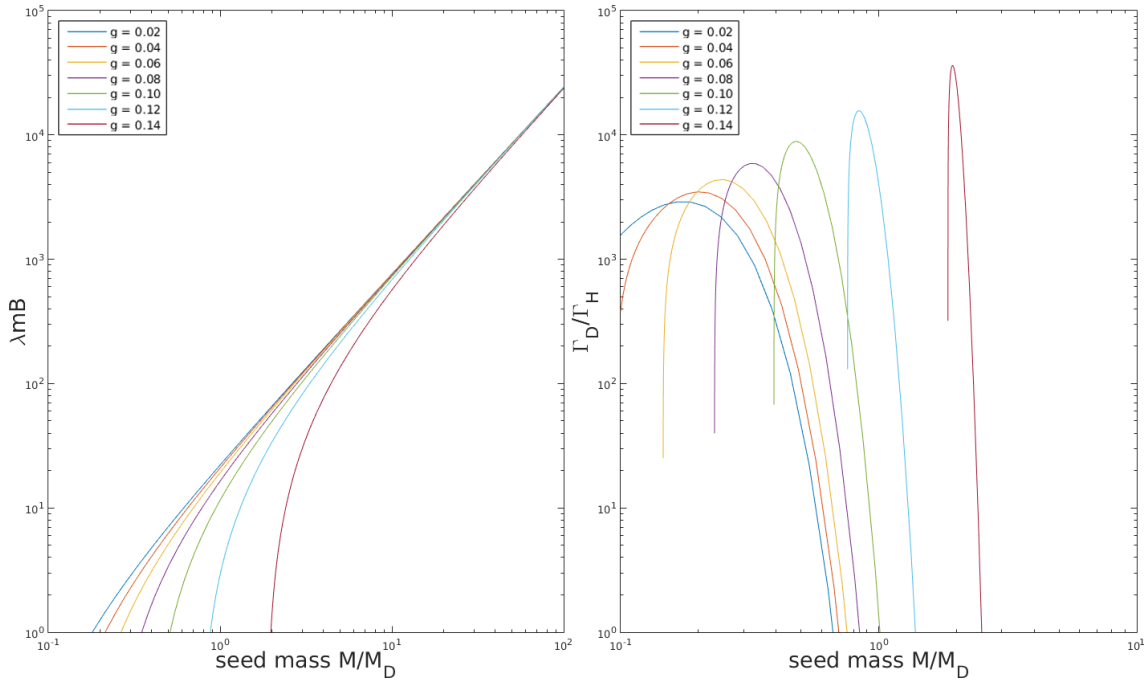

Figure 6.7: The tunnelling exponent as a function of seed mass (left) and the branching ratio of the false vacuum nucleation rate to the Hawking evaporation rate as a function of the seed mass (right), with increased M_5. $M_D = (\lambda m)^{2/3} M_5$, $M_5^3 = 100$.

black holes is so high, we can conclude that either:

- there were no microscopic primordial black holes capable of seeding vacuum decay, as the present day universe exists in a metastable false vacuum state;
- or, we do not live in an RS2 braneworld where the reduced 5D Planck scale allows for such black holes to be produced in the highest energy cosmic ray collisions.

Our results were presented as a branching ratio of the Hawking evaporation rate Γ_H to tunnelling rate Γ_D, which required calculating the tunnelling exponent B. Although the solution for a brane black hole is not known analytically, we were nonetheless able to construct an argument from thermodynamics that the action for tunnelling would still be the difference in areas of the black hole horizons (an alternative derivation of this is given in Appendix B).

Chapter 7

Negative Modes

This chapter presents work previously published in a paper by R. Gregory, K. M. Marshall, F. Michel and I. G. Moss, (2018). "Negative modes of Coleman–De Luccia and black hole bubbles." *Physical Review D* **98**(8): 085017. arXiv:1808.02305v2 [hep-th].

7.1 Bubbles with negative modes

In previous chapters, we have worked with a model of vacuum decay in which a phase transition is interpreted as the nucleation of a true vacuum bubble on a false vacuum background. A key feature of this picture is the existence of a negative mode of field perturbations corresponding to a scaling of the bubble radius up or down. However, for decay in asymptotically de Sitter space, a problem arises with the emergence of an infinite number of negative modes and the question of how this can be physically interpreted.

Previously, the negative mode problem has been investigated numerically for vacuum decay in asymptotically de Sitter spacetimes. This chapter presents the first results for negative modes for an asymptotically flat instanton. We also give a new analytic result for the first negative mode in the thin wall bubble limit.

Here we look at two different Higgs vacuum decay scenarios: vacuum decay in empty space and vacuum decay seeded by black holes. For the first scenario, vacuum decay rates with gravitational back-reaction in empty space have previously been examined by [16, 56, 57, 58]. The gravitational back reaction becomes significant when Λ approaches the Planck scale. Here we present an analysis of the negative modes that includes the possibility of non-minimal coupling of the Higgs field to gravity.

Numerical calculations show there are two possible cases for the modes of the solutions: either a single negative mode, or infinitely many. The second case is seen for vacuum

decay in asymptotically de Sitter space, where a change in sign for the kinetic terms in the action of the perturbations gives rise to the infinite stack of negative modes.

In the second scenario we investigate, we return to the case of black hole seeded vacuum decay. Here, vacuum decay is enhanced by the presence of a microscopic black hole left over from the early universe. This effect has previously been investigated for vacuum decay in de Sitter space [22], and later for more general scenarios including asymptotically flat space [23, 24, 25].

In both the empty space and black hole scenarios, the dominant decay process is one that produces static O(3) symmetric bubbles. Numerical analysis of the negative modes for vacuum decay with an asymptotically flat black hole nucleation seed finds only one negative mode. The kinetic term in the action of the perturbations is always positive. We can conclude from this that vacuum decay seeded by black holes has a single negative mode and will likely be consistent in the bounce solutions.

7.2 Tunnelling and negative modes

We consider decay of the false vacuum state of a scalar field ϕ with potential $V(\phi)$. The path integral formalism from Coleman (summarised in chapter two) is used to find bounce solutions ϕ_b to the scalar field equations, with imaginary time coordinate τ [2]. Recalling equation (2.41) from chapter two, evaluating the path integral for a single bubble solution gives a contribution to the vacuum decay amplitude of the form

$$S_{\text{bubble}} \approx \frac{1}{2} i \Omega T \left| \frac{\det' S_E''[\phi_b]}{\det S_E''[\phi_{\text{fv}}]} \right|^{-1/2} \frac{B^2}{4\pi^2} e^{-B} S_{\text{fv}}, \tag{7.1}$$

where S_E'' denotes the second functional derivative of the Euclidean action, and $\det'$ denotes omission of zero modes from the determinant. The zero modes give factors Ω and T for the total volume and time period, along with a Jacobian factor $B^2/4\pi^2$. The factor i arises from the negative mode. This would become i^n if there were n negative modes. The vacuum decay rate Γ can be calculated by summing multiple bubble amplitudes, and the result is [8, 59]

$$\Gamma \approx \left| \frac{\det' S_E''[\phi_b]}{\det S_E''[\phi_{\text{fv}}]} \right|^{-1/2} \frac{B^2}{4\pi^2} e^{-B}. \tag{7.2}$$

The negative mode can be explained easily in the thin-wall limit, when the bubble solution consists of a true vacuum region ϕ_{tv} surrounded by a relatively narrow wall where the field transitions to the false vacuum. This approximation is valid when the difference in energy ε of the true and false vacua is small compared to a combination of barrier height and width. The field is represented by a bubble Ansatz of the form $\phi = \phi(\tau; R) \simeq \phi_0(\tau - R)$,

with τ being the radial distance from the centre of the bubble and R being the bubble radius, where $\phi_0(x)$ solves the 'planar' domain wall equation

$$\phi'' \approx \frac{\partial V}{\partial \phi}\,. \tag{7.3}$$

For tunnelling in empty space, we have the boundary conditions:

- $\phi_b \to \phi_{\rm fv}$ when $\tau \to \pm\infty$
- at spatial infinity: $\phi_b \to \phi_{\rm fv}$ as $|\mathbf{x}| \to \infty$

where $\phi_{\rm fv}$ is the value of the field at the false vacuum.

From Coleman [2], the tunnelling exponent B is related to the change in Euclidean action by $B = S_E[\phi_b] - S_E[\phi_{\rm fv}]$, where

$$B = \int_{-\infty}^{\infty} d\tau \int d^3x \left(\frac{1}{2}(\partial_\tau \phi_b)^2 + \frac{1}{2}(\boldsymbol{\nabla}\phi_b)^2 + V(\phi_b) \right). \tag{7.4}$$

In [2] Coleman showed that there exists a bubble solution with $O(4)$ symmetry that has the smallest action, and hence the largest tunnelling rate, compared to other bounce solutions. This solution has exactly one negative mode [8] and is a saddle point of the Euclidean action, as shown in Coleman and Callan's second paper covered in chapter two (see equation (2.41) in §2.4).

Using the thin wall approximation, we can integrate the tunnelling exponent in terms of the bubble radius R (see §2.3),

$$B(R) = 2\pi^2 \sigma R^3 - \frac{1}{2}\pi^2 \varepsilon R^4. \tag{7.5}$$

where ϵ is the difference in height between the two minima and σ is the bubble wall tension. The action has an extremum $B' = 0$ at $R = 3\sigma/\varepsilon$. Here, σ is the action per unit area of the bubble wall, which can be found in terms of an integral of the potential $V(\phi)$ by

$$\sigma = \int_{\phi_{\rm fv}}^{\phi_{\rm tv}} |2\Delta V(\phi)|^{1/2} d\phi \tag{7.6}$$

using $\frac{1}{2}\phi_0'^2 = \Delta V$ found from integrating equation (7.3). The bubble solution is given by the extremum at the radius $R_b = R_0 \equiv 3\sigma/\varepsilon$, where B has a maximum.

The negative mode corresponds to changes in ϕ that increase or decrease the radius of the

bubble solution,

$$\delta\phi = \frac{d\phi}{dR}\delta R. \tag{7.7}$$

The overall change in B is related to the negative eigenvalue λ_0 of the perturbations about the bounce by,

$$\delta B \approx \frac{1}{2}B''(R)\delta R^2 \tag{7.8}$$

$$= \frac{1}{2}\sum c_n^2\lambda_n \approx \frac{1}{2}c_0^2\lambda_0, \tag{7.9}$$

where $\delta\phi$ is defined by a sum over u_n modes

$$\delta\phi = \sum c_n u_n. \tag{7.10}$$

(The derivation of the eigenvalue equation for perturbations about the bounce will be dealt with later.) The norm of a function $f(x)$ is defined by

$$\|f\|^2 = \int f(x)^2\, d^4x, \tag{7.11}$$

Eq. 7.10 is normalised so that

$$||u_n||^2 = 1 \tag{7.12}$$

As we require a negative expression for δB, we pick out λ_0 as the single negative mode and rewrite $\|\delta\phi\|^2$,

$$\|\delta\phi\|^2 = \|c_0 u_0\|^2 = c_0^2 \tag{7.13}$$

and therefore δB

$$\delta B \approx \frac{1}{2}c_0^2\lambda_0 \approx \frac{1}{2}||\delta\phi||^2\lambda_0 \tag{7.14}$$

Combining all of the above gives an expression for the negative eigenvalue λ_0,

$$\lambda_0 = \frac{B(R)''\delta R^2}{||\delta\phi||^2} \tag{7.15}$$

Using equation (7.7), this gives us a simple formula for the negative eigenvalue in the thin-wall approximation,

$$\lambda_0 \approx \left.\frac{B(R)''}{||d\phi/dR||^2}\right|_{R=R_b} \tag{7.16}$$

This can be taken further using our approximation for the bubble wall profile. The field

at distance τ relates to its true vacuum value according to

$$\phi = \frac{1}{2}\phi_{tv}\left(1 - \tanh\left[\frac{3\sigma}{\phi_{tv}^2}(\tau - R)\right]\right) \tag{7.17}$$

as given by (2.68) in chapter two. The action has a maximum at $R = R_b$. Using equation (7.17), we can write

$$\left|\left|\frac{d\phi}{dR}\right|\right|^2 \approx 2\pi^2\sigma R^3 \tag{7.18}$$

Substituting this into equation (7.16), the negative eigenvalue can be expressed as

$$\lambda_0 = \frac{\frac{1}{2}B''(R_b)}{3\pi^2 R_b^3\sigma}. \tag{7.19}$$

We now substitute B'' from equation (7.5) into this expression to get

$$\lambda_0 \approx -\frac{3}{R_b^2}. \tag{7.20}$$

This result is remarkably simple! From this new approach, we confirm the findings of Coleman and Callan in [8]. The approximation is valid when the thickness of the wall is small compared to the bubble radius, which translates to $\varepsilon \ll 9\sigma^2/\phi_{\mathrm{tv}}^2$.

7.2.1 Gravitational back-reaction

We will look at bubble solutions with gravitational back-reaction. These can be found by extremising the Einstein-scalar action,

$$S_E = \int\left[-\frac{\mathcal{R}}{16\pi G} + \frac{1}{2}\left(\partial\phi\right)^2 + V(\phi)\right]\sqrt{g}d^4x, \tag{7.21}$$

where $\mathcal{R}$ is the Ricci scalar. Bubble solutions with $O(4)$ symmetry can be described by a 'radial' solution of scalar field, $\phi(\tau)$, and geometry:

$$ds^2 = d\tau^2 + a^2(\tau)d\Omega_{III}^2 \tag{7.22}$$

where ϕ and a tend towards the true vacuum form as $\tau, a(\tau) \to 0$, and the false vacuum form for large τ.

When finding the bounce solutions, B is given by the difference in actions between the bubble and the false vacuum, and we assume this is still true when considering the case of a single bubble.

There are two scenarios to consider depending on whether the Euclidean metric is compact

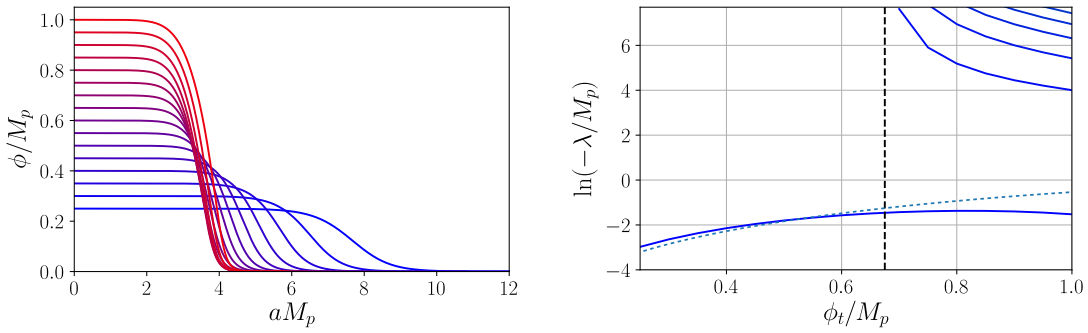

Figure 7.1: Left panel: O(4)-symmetric instantons obtained with the quartic potential (7.53) for $\lambda_q = 128$ and $\phi_t/\phi_m = 2.5$. The value of ϕ_t in Planck units increases from blue to red. Right panel: Negative eigenvalues for these solutions. The dashed curve shows the thin wall approximation (7.35). The vertical dashed line shows the value ϕ_c of ϕ_t above which Q_b takes negative values. Plots by Florent Michel.

or infinite:

1. The compact case, where the scalar field never quite reaches the false vacuum value outside the bubble.

2. The infinite case, where the scalar field asymptotically approaches the false vacuum value as $a \to \infty$.

In the compact case, the possible bubble solutions are restricted by regularity conditions on the metric at the two points where $a = 0$. For this case we impose the boundary conditions:

$$\phi'(0) = 0 \tag{7.23}$$

$$\phi_{\text{final}} = 0 \tag{7.24}$$

$$a(0) = a_{\text{final}} = 0 \tag{7.25}$$

$$a'(0) = 1 \tag{7.26}$$

In the infinite case, $B = S_E[\phi_b] - S_E[\phi_{\text{fv}}]$ may also become infinite without constraints on the metric. We require that the Euclidean metric approaches the same form at infinity for the bounce and for false vacuum to ensure that B remains finite. It is not necessary to introduce boundary terms here as they will cancel when evaluating B.

We use Coleman and de Luccia's formalism to obtain bounce solutions in the thin wall limit. The thin wall approximation assumes that the scalar field oscillates rapidly between false and true vacuum values. At the centre of the bubble wall, the bubble radius R is the scale factor a. Provided the local curvature within a bubble wall with width w and

tension σ is below the Planck scale $w\sigma \ll M_p^2$, the thin wall approximation still holds [60] (here we used the reduced Planck mass $M_p^2 = 1/(8\pi G)$).

The curved-space bubble solutions can be represented by the form $\phi = \phi(a; R)$ where $\phi \approx \phi_0(\tau - \tau_b)$ for the thin wall, and τ_b is the coordinate location of the bubble centre: $a(\tau_b) = R$.

The scale factor is approximated by a piecewise differentiable function

$$a(\tau) = a_{\rm tv}(\tau)\,\Theta[\tau_b - \tau] + a_{\rm fv}(\tau)\,\Theta[\tau - \tau_b]\,, \tag{7.27}$$

where $a_{\rm tv}(\tau_b) = a_{\rm fv}(\tau_b) = R$.

We compute the difference in actions between the bubble and the false vacuum to find B as before.

In the compact case, we will consider a phase transition where the vacuum decays from a de Sitter universe into flat space. The potential V is therefore constructed such that the false vacuum has positive energy ε while the energy of the true vacuum is zero.

The scale factors for the true vacuum at the centre of the bubble and the false vacuum outside the bubble can be written in terms of τ:

$$a_{\rm tv} = \tau \tag{7.28}$$

$$a_{\rm fv} = \ell \sin((\tau - \tau_0)/\ell) \tag{7.29}$$

where $\ell = \sqrt{3/(8\pi G\varepsilon)}$ is the de Sitter radius and τ_0 is a introduced to satisfy $a_{\rm tv}(\tau_b) = a_{\rm fv}(\tau_b) = R$. The tunnelling exponent can be directly calculated as (see also [3])

$$B(R) = \frac{4}{3}\pi^2\varepsilon\ell^4\left\{1 \mp (1 - R^2/\ell^2)^{3/2}\right\} - 2\pi^2\varepsilon\ell^2R^2 + 2\pi^2\sigma R^3, \tag{7.30}$$

and is plotted in figure 7.2.

- The upper sign applies when the false vacuum region is larger than a hemisphere, and the true vacuum bubble occupies a smaller volume than the false vacuum region (a "small bubble" situation, following the terminology of ref. [61]).
- The lower sign applies when the false vacuum covers less than a hemisphere, and the true and false vacuum regions have a similar volume (a "large bubble" situation)

The tunnelling exponent (7.30) has one extremum R_b away from the origin,

$$R_b = \frac{R_0}{1 + (R_0/2\ell)^2}, \tag{7.31}$$

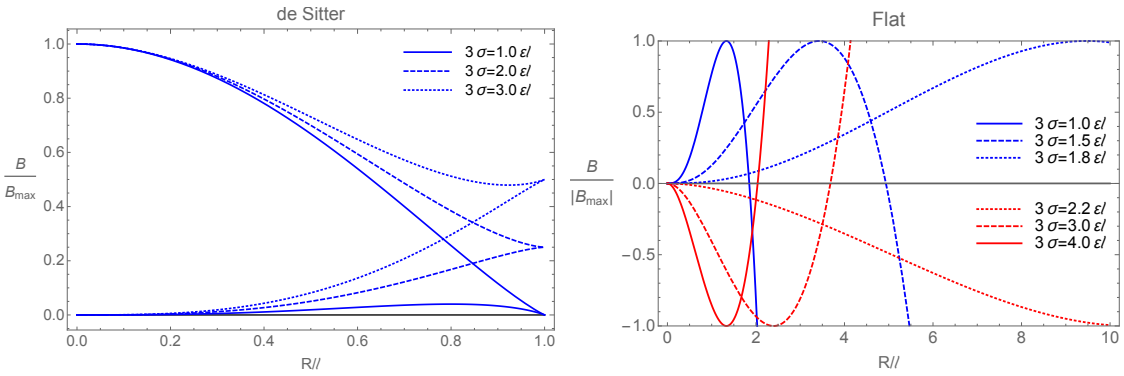

Figure 7.2: Left panel: The tunnelling exponent $B(R)$ for a thin-wall bubble of flat vacuum in de Sitter space. The large and small bubble exponents are superposed. Right panel: The tunnelling exponent $B(R)$ for a thin-wall bubble of anti-de Sitter vacuum in flat space. ℓ is the AdS radius, ε is the barrier height, and σ the bubble wall tension. Plots by Florent Michel.

where $R_0 = 3\sigma/\varepsilon$ is the bubble radius without the gravitational back reaction. Bubble solutions always exist, but the extremum becomes a minimum when $3\sigma/\varepsilon > 2\ell$. The thin-wall approximation therefore predicts the disappearance of the negative mode, and we can estimate the value of the mode in a similar way to the probe case. Since the bubble wall is determined by $\tau = R$, and the geometry inside the bubble is flat, we find that the eigenvalue is well approximated here by the flat space value 7.16. Numerical investigations have shown that new sets of spherically symmetric negative modes start to appear [62, 63, 64, 61, 65]. The first set are fluctuations localised near the bubble wall, called 'wall modes' in Ref [61]. The second set are localised near the maximum radius of the instanton in the 'large bubble' case.

In the non-compact case, the true vacuum has negative energy $-\varepsilon$ and the false vacuum has zero energy. This represents vacuum decay from flat space to anti de Sitter space, and we have $a_{\rm tv} = \ell \sinh \tau/\ell$, $a_{\rm fv} = \tau + (R - \tau_b)$ in (7.27). This time we find

$$B(R) = \frac{4}{3}\pi^2 \varepsilon \ell^4 \left\{1 - (1 + R^2/\ell^2)^{3/2}\right\} \pm 2\pi^2 \varepsilon \ell^2 R^2 + 2\pi^2 \sigma R^3, \tag{7.32}$$

plotted in the right panel of figure 7.2. The upper sign corresponds to $3\sigma/\varepsilon < 2\ell$, and the bubble matches an interior of AdS to an *exterior* of an S^3 in $\mathbb{R}^4$, i.e. a conventional bubble. For $3\sigma/\varepsilon > 2\ell$ we can still find a solution, provided we match the interior of an AdS sphere to an *interior* of a three-sphere in $\mathbb{R}^4$: clearly this does not have an intuitive interpretation as a vacuum decay bubble, and is similar to the situation of dS tunnelling above, where the false vacuum covers less than a hemisphere of dS. We note simply that these solutions do not have a negative mode, hence are not tunnelling instantons, and do

not consider them further. For $3\sigma/\varepsilon < 2\ell$ the bubble has radius [3]

$$R_b = \frac{R_0}{1-(R_0/2\ell)^2}. \tag{7.33}$$

Whenever a bubble solution exists the extremum is always a maximum and the negative mode we had originally should remain. This time, in our estimate of the negative eigenvalue, we note $R = \ell \sinh \tau_b/\ell$, hence

$$\left\| \frac{d\phi}{dR} \right\|^2 = \left\| \frac{d\phi}{d\tau_b} \right\|^2 \left(\frac{d\tau_b}{dR} \right)^2 = 2\pi^2 \sigma R^3 (1 + R^2/\ell^2)^{-1} \tag{7.34}$$

We can substitute this into the general formula (7.16), with the exponent $B(R)$ from (7.32), and evaluate the result at the bubble radius R_b from (7.33), to get

$$\lambda_0 \approx -\frac{3}{R_0^2} \left\{ 1 - \left(\frac{R_0}{2\ell} \right)^4 \right\}, \tag{7.35}$$

where $R_0 = 3\sigma/\varepsilon$ as before.

7.2.2 Model and field equations

In order to consider a wide variety of models relevant to Higgs cosmology, we generalise the gravitational action (7.21) to include non-minimal coupling between the scalar field and gravity,

$$S = \int \left[-\frac{\hat{R}}{16\pi G} + \frac{\xi}{2}\hat{R}\phi^2 + \frac{\hat{g}^{\mu\nu}}{2}(\partial_\mu\phi)(\partial_\nu\phi) + V(\phi) \right] \sqrt{\hat{g}} d^4x \tag{7.36}$$

where ξ is a non-minimal coupling coefficient and hats denote the choice of metric commonly referred to as the Jordan frame. We consider potentials such that $V(0) = V'(0) = 0$, $V''(0) > 0$, and assume V takes negative values in some interval of ϕ so that the bubble solutions will be non-compact. To find numerical solutions and study their perturbations, it is convenient to go to the Einstein frame by rescaling the metric:

$$g_{\mu\nu} = \left(1 - 8\pi G \xi \phi^2\right) \hat{g}_{\mu\nu} \tag{7.37}$$

(for an analysis of solutions in the Jordan frame see [16, 58]). The action becomes

$$S = \int \left(-\frac{R}{16\pi G} + \frac{f(\phi)^2}{2} \left(\partial_\mu \phi\right) \left(\partial^\mu \phi\right) + W(\phi) \right) \sqrt{g} d^4x, \tag{7.38}$$

where

$$f(\phi) = \frac{\sqrt{1 - 8\pi G\xi\,(1-6\xi)\,\phi^2}}{1 - 8\pi G\xi\phi^2} \tag{7.39}$$

and the modified potential is

$$W(\phi) = \frac{V(\phi)}{\left(1 - 8\pi G\xi\phi^2\right)^2}. \tag{7.40}$$

In all the cases we will consider, $f(\phi)$ remains strictly positive. We look for O(4)-symmetric solutions, and slightly change the form of our metric to add a lapse function:

$$ds^2 = N(\tau)^2 d\tau^2 + a(\tau)^2 d\Omega_{III}^2, \tag{7.41}$$

The lapse function N allows us to recover the full set of Einstein equations from extremisation of the action, which will be convenient when deriving the eigenvalue equation. Substituting in the form of the metric (7.41), and integrating out over the angular variables, we obtain

$$S = 2\pi^2 \int \left[\frac{f(\phi)^2}{2N^2}\phi'^2 + W(\phi) - \frac{3}{8\pi G}\left(\frac{1}{a^2} + \left(\frac{a'}{aN} \right)^2 \right) \right] a^3 N d\tau, \tag{7.42}$$

Variation with respect to ϕ and N give the system of equations:

$$f(\phi)\left(f(\phi)\frac{a^3}{N}\phi' \right)' = Na^3 W', \tag{7.43}$$

$$\frac{a'^2}{N^2} = 1 + \frac{8\pi G}{3}a^2\left(\frac{f(\phi)^2}{2N^2}\phi'^2 - W(\phi) \right). \tag{7.44}$$

Variation with respect to a gives a Bianchi Identity[1]. The system (7.43,7.44) can also be obtained from the full set of Einstein equations after eliminating redundancies, showing that there is no independent constraint. For boundary conditions, we look for asymptotically flat instantons, with $\phi(\infty) = \phi_{FV}$ and $a(\tau) \sim \tau$ as $\tau \to \infty$. We choose to place the centre of the instanton at $\tau = 0$, where $a(0) = 0$ and for regularity at the origin we must have $\phi'(0) = 0$. Equation (7.44) can be rewritten as:

$$\frac{1 - 8\pi G a^2 W(\phi)/3}{1 - 4\pi G a^2 (\partial_a \phi)^2/3} = \frac{a'^2}{N^2}. \tag{7.45}$$

This shows that the left-hand side, which will play an important role in the following, is always non-negative, and cannot vanish if a is strictly monotonic.

The lapse function $N(\tau)$ represents some of the freedom we have to choose the coordinate

[1] Using Eq. (7.43), it is equivalent to the derivative of Eq. (7.44).

gauge. We will focus on instantons where a is a strictly increasing function of the distance to the centre of the bubble, which allows us to choose a as radial coordinate. Setting $\tau = a$, the action (7.42) becomes

$$S = 2\pi^2 \int_0^\infty N a^3 \left(\frac{f(\phi)^2 \phi'^2}{2N^2} + W(\phi) \right) da - \frac{3\pi}{4G} \int_0^\infty \left(N + \frac{1}{N} \right) a da \tag{7.46}$$

Variation with respect to N and ϕ gives back the system (7.43,7.44), showing that no physical degree of freedom has been lost.

Since the derivative of N does not appear in Eq. (7.46), one can express N as a function of ϕ and ϕ':

$$N = \left(\frac{1 - 4\pi G a^2 f(\phi)^2 \phi'^2/3}{1 - 8\pi G a^2 W(\phi)/3} \right)^{1/2}. \tag{7.47}$$

This quantity is always real. The expression in the denominator is a recurring and important combination for the eigenvalue problem, hence we write

$$Q[\phi] \equiv 1 - \frac{8\pi G}{3} a^2 W(\phi). \tag{7.48}$$

Plugging Eq. (7.47) into Eq. (7.46), we obtain an unconstrained action for the scalar field ϕ,

$$S = -\frac{3\pi}{2G} \int_0^\infty \mathrm{sgn}\left(Q[\phi]\right) \left[Q[\phi] \left(1 - \frac{4\pi G a^2}{3} f(\phi)^2 \phi'^2 \right) \right]^{1/2} a da. \tag{7.49}$$

Extremization of this action gives back Eq. (7.43) with the explicit form of N given by Eq. (7.44).

This expression for the action can be conveniently used to derive the eigenvalue equation. To this end, let us assume we have an exact solution $\phi = \phi_b$. We look for a perturbed solution of the form[2] $\phi = \phi_b + \varphi / f(\phi_b)$. To quadratic order in φ, the action reads $S = S^{(0)} + S^{(2)} + O\left(\varphi^3\right)$, where $S^{(0)}$ is the action of the background instanton and

$$S^{(2)} = 2\pi^2 \int_0^\infty \frac{a^3}{N_b} \left[\left(D^2 W + \frac{8\pi G a^2}{3 Q_b} (DW)^2 + \frac{8\pi G f}{3 Q_b} \phi_b' DW \right) \frac{\varphi^2}{2 Q_b} + \frac{1}{N_b^2 Q_b} \frac{\varphi'^2}{2} \right] da. \tag{7.50}$$

where $Q_b = Q[\phi_b]$, and $D = f^{-1} d/d\phi$. The simplest way to derive (7.50) is to regard ϕ as a coordinate on a one dimensional manifold with metric

$$\mathfrak{g} = f(\phi)^2 d\phi^2. \tag{7.51}$$

The action can be evaluated in a coordinate frame with $f = 1$, and then the general ex-

[2]Notice that $\varphi(a)$ is the geodesic distance, in the metric (7.51), between the perturbed and background fields.

pression is recovered by replacing derivatives with respect to ϕ by the covariant derivative D.

The corresponding eigenvalue equation obtained from the perturbed action is

$$\frac{1}{N_b\, a^3}\left(\frac{a^3}{N_b^3\, Q_b}\varphi'\right)' = \left[\frac{1}{N_b^2 Q_b}\left(D^2W + \frac{8\pi G a^2}{3Q_b}\,(DW)^2 + \frac{8\pi G a^2 f}{3Q_b}\phi_b' DW\right) - \lambda\right]\varphi, \tag{7.52}$$

where λ is the eigenvalue.

By definition, N_b is always positive. However, Q_b will be negative wherever $a^2W(\phi_b) > 3/(8\pi G)$. When Q_b is negative, the quadratic action is unbounded from below. (In fact, it can reach arbitrarily high negative values even for square integrable perturbations of unit L^2 norm provided the latter oscillate sufficiently fast in the region where $Q_b < 0$.) As was shown in [61, 65] for instantons in de Sitter space, if the eigenmode equation has no singularity, negativity of the kinetic term implies the existence of an infinite number of negative eigenvalues.

The existence of this infinite tower of negative modes can be qualitatively understood as follows. In regions where the kinetic term is positive, for sufficiently large negative values of λ, φ increases or decreases exponentially with a, with growth rate $N_b^2\sqrt{Q|\lambda|}$. Let us call the boundaries of the interval in which Q is negative a_- and a_+. φ is exponentially increasing or decreasing for $a > a_+$, and oscillating for $a_- < a < a_+$. The global solution will be decreasing at infinity provided the oscillating solution for a just below a_+ can be matched with the decaying one for $a > a_+$. This occurs twice each time we add one wavelength in the interval $[a_-, a_+]$. If the kinetic term is positive everywhere, the boundary conditions at $a = 0$ and $a \to \infty$ can not be simultaneously satisfied. If the kinetic term reaches negative values, however, φ becomes oscillatory in some interval, allowing us to match an exponentially decreasing function for $a \to \infty$ with a hyperbolic cosine for $a \approx 0$. More precisely, they will match provided the difference between the phases of the oscillations at both ends of the region where the kinetic term is negative exactly compensates the difference between the ratios φ'/φ for the hyperbolic cosine on the left and the exponential on the right.

It must be noted, however, that these negative modes may be physically relevant only for very thin bubbles. Indeed, negativity of the kinetic term requires that $|af(\phi_b)\phi_b'|$ reaches values above the Planck mass. In many models, ϕ_b is limited to be less than 1 in Planck units, so that the semiclassical analysis should not break down. These negative modes may thus be physically meaningful only if $|af(\phi_b)\phi_b'| \gg |\phi_b|$, i.e., either when the width of the bubble is much smaller than its radius or when f is large. The latter case can occur when ξ is large and negative. In the following section we will see examples that realise

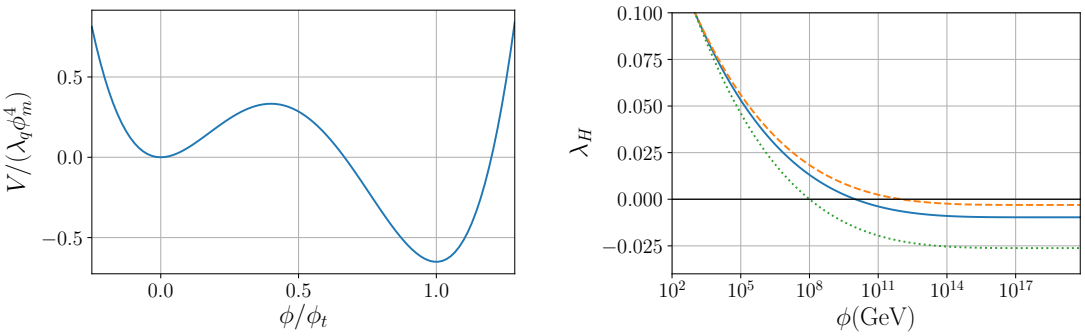

Figure 7.3: Left panel: Quartic potential (7.53) for $\phi_m = M_p/10$, $\phi_t = M_p/4$, and $\lambda_q = 10/3$. Right panel: Effective coupling for the Higgs-like potential (7.56) for $\Lambda = 10^8$GeV (green, dotted), $\Lambda = 10^{10}$GeV (blue, continuous), and $\Lambda = 10^{12}$GeV (orange, dashed), and q chosen so that $\lambda(\phi = 10^3\text{GeV}) = 0.1$. Plots by Florent Michel.

both of these possibilities.

7.3 Eigenvalues of negative modes

We turn now to the numerical solution of the system (7.43,7.44) and eigenvalue equation (7.52) with two different shapes for the potential V. Recall from chapter four the quartic potential

$$V_q(\phi) = \frac{1}{4}\lambda_q\phi^4 - \frac{1}{3}\lambda_q(\phi_m + \phi_t)\phi^3 + \frac{1}{2}\lambda_q\phi_m\phi_t\phi^2, \tag{7.53}$$

been parameterised by ϕ_m and ϕ_t, the field values at the maximum and the non-zero minimum respectively. The parameter λ_q sets the overall scale. The origin $\phi = 0$ is a false vacuum, and ϕ_t is the true vacuum when $\phi_t > 2\phi_m$. One example is shown in the left panel of Fig. 7.3. The thin wall approximation is not used to obtain the numerical results, though can provide a useful check. The thin wall approximation is valid when $\phi_t \sim 2\phi_m$.

An important derived parameter is the AdS radius of the true vacuum ℓ. For minimal coupling ($\xi = 0$),

$$\ell^2 = -\frac{3M_p^2}{V(\phi_t)}. \tag{7.54}$$

For example, we expect gravitational back-reaction to be important when the bubble radius is comparable to the AdS radius. In the thin-wall approximation, the 'flat-space' bubble radius $R_0 = 3\sigma/\epsilon$ and the ratio R_0/ℓ is,

$$\frac{R_0}{\ell} = \frac{1}{\sqrt{2}}\frac{\phi_t}{M_p}\left(1 - 2\frac{\phi_m}{\phi_t}\right)^{-1/2}. \tag{7.55}$$

Note that this is independent of the overall scale parameter λ_q. It is possible to scan through different values of R_0/ℓ by fixing ϕ_m/ϕ_t and scanning through different values of ϕ_t.

While the quartic potential is convenient for illustrative purposes, obtaining results which may be applicable to the Standard Model requires a more realistic one. We thus also used a Higgs-like potential with the form given in chapter four,

$$V_H(\phi) = \frac{\lambda_H(\phi)}{4}\phi^4, \quad \lambda_H(\phi) = q\left(\left(\ln\frac{\phi}{M_p}\right)^4 - \left(\ln\frac{\Lambda}{M_p}\right)^4\right). \tag{7.56}$$

In this expression, $\Lambda > 0$ is the scale at which the coupling and the potential vanish, and q is a strictly positive number. Like the quartic potential $V_q(\phi)$, this potential has a local minimum at $\phi = 0$. Plots of the function λ_H for three different choices of (q, Λ) are shown in the right panel of Fig. 7.3. They approximate the next-to-next-to-leading order calculations reported in [11] with different values of the top quark mass.

The height of the Higgs potential barrier is small compared to Λ^4, making the bubble solutions shallow, with thick walls, and Higgs values inside the bubble extend beyond the barrier but do not reach a true vacuum. The potential inside the bubble is roughly of order Λ^4 and the bubble size is of order Λ^{-1}, so that the 'effective' value of R_0/ℓ in this case is around Λ/M_p.

We first work with the quadratic potential and $\xi = 0$, i.e., with a minimal coupling between the scalar field ϕ and gravity. In Fig. 7.1 we show the negative eigenvalues with fixed ratio $\phi_t/\phi_m = 2.5$, $\lambda_q = 128$, and ϕ_t ranging from $0.25M_p$ to M_p. Below a critical value ϕ_c, here close to $0.67M_p$, there is only one negative mode. The dashed line shows the negative mode obtained for the thin-wall approximation using (7.35), which agrees quite well with the numerical result despite the walls not being particularly thin.

The quantity Q defined in (7.48) is positive for the bubble solutions with $\phi_t < \phi_c$, but for $\phi_t > \phi_c$, Q takes negative values in a finite interval of a. Correspondingly, we find new negative eigenvalues, all but one going to $-\infty$ in the limit $\phi_t \to \phi_c$. The numerical evidence therefore supports the existence of infinitely many negative eigenvalues for $\phi_t > \phi_c$.

Results with nonminimal coupling are shown in Fig. 7.4. Here the parameters of the potential are fixed to $\phi_m = 0.36$, $\phi_t = 0.84$, and $\lambda_4 = 10/3$, and the nonminimal coupling ξ is varied between -0.5 and 0.9. At the level of the instanton solution, the main effect of a negative value of ξ seems to be to increase the radius of the bubble, while a positive value increases $\phi(0)$. Its role is more dramatic when considering the negative modes: as shown in the right panel of the figure, there is a critical value ξ_c, here close to 0.2, above which only one negative mode is present, but below which there is an infinite number of

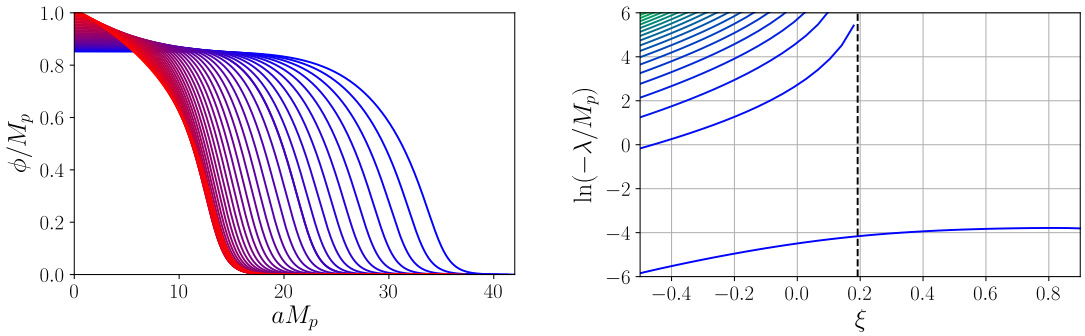

Figure 7.4: Left panel: O(4)-symmetric instantons obtained with the quartic potential (7.53) for $\phi_m = 0.36$, $\phi_t = 0.84$, and $\lambda_q = 10/3$, for different values of the nonminimal coupling ξ ranging from -0.5 to 0.9. The value of ξ increases from blue to red. Right panel: Negative eigenvalues for these solutions. The vertical dashed line shows the value ξ_c of ξ below which Q_b takes negative values. Plots by Florent Michel.

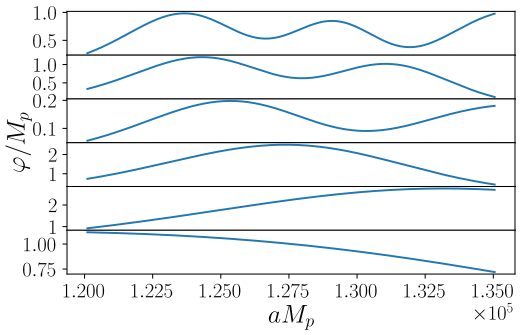

Figure 7.5: Plots of the first six negative modes in the region where the kinetic term is negative. We use the Higgs-like potential (7.56) with $q = 10^{-7}$ and $\Lambda = 0.3$, and a minimal coupling $\xi = -5.3$, slightly below the critical one $\xi_c \approx -4.8$ for this potential. (The normalization is arbitrary.) Plot by Florent Michel.

them. As already noticed when varying ϕ_t, the first case corresponds to a positive Q, while in the second case this function takes negative values in a finite interval of a. As in the previous case also, all but one negative eigenvalues go to negative infinity when approaching the threshold $\xi \to \xi_c$.

Figures 7.5, 7.6, and 7.7 show results obtained with the potential V_H. To ease the numerical resolution, they are made with relatively high values of Λ, close to unity in Planck units. We found a similar behavior for smaller values of this parameter. In Fig. 7.5 are shown the first six negative modes for fixed potential and a minimal coupling ξ slightly smaller than ξ_c, in the region where $Q < 0$. The main information is that, as expected, negative modes are oscillatory in this region, and that the n^{th} one has approximately $n/2$ wavelengths for sufficiently large n.

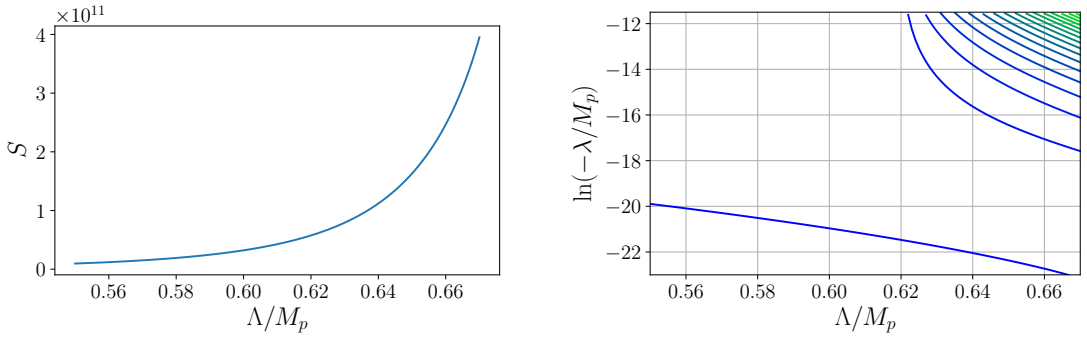

Figure 7.6: Euclidean action (left panel) and negative eigenvalues (right panel) of an asymptotically flat O(4)-symmetric instanton with the Higgs potential (7.56) with $q = 10^{-7}$ and $\xi = 0$. Plots by Florent Michel.

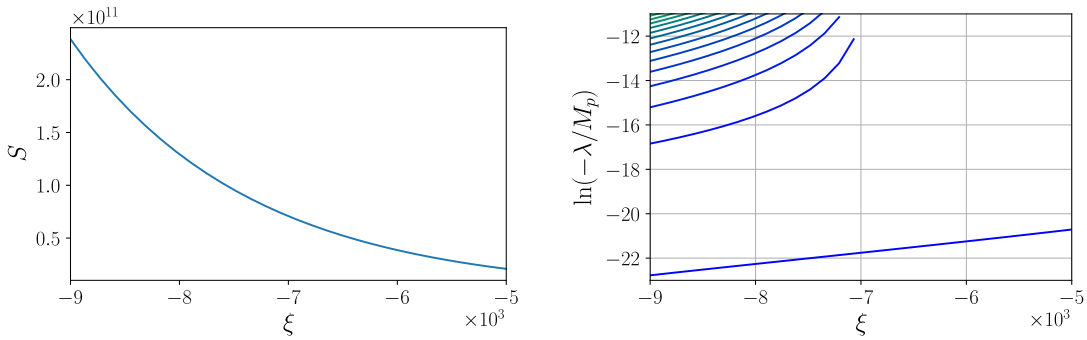

Figure 7.7: Euclidean action (left panel) and negative eigenvalues (right panel) of an asymptotically flat O(4)-symmetric instanton for the Higgs potential (7.56) with $q = 10^{-7}$ and $\Lambda = 0.5$. Plots by Florent Michel.

Figures 7.6 and 7.7 shows the Euclidean action and negative eigenvalues of instantons as functions of Λ and ξ respectively, for $q = 10^{-7}$. As can be seen on the left panels and more generally in Figure 7.8, the Euclidean action of instantons supporting infinitely many negative modes is huge, making the transition rate negligible. We found the same holds for all parameters we tried. It thus seems that, for realistic potentials, the appearance of an infinite number of negative eigenvalues requires such a strong back-reaction from gravity on the instanton that the probability of bubble nucleation becomes negligibly small. Conversely, all instantons we found which gave non-negligible decay rates have only one negative eigenvalue.

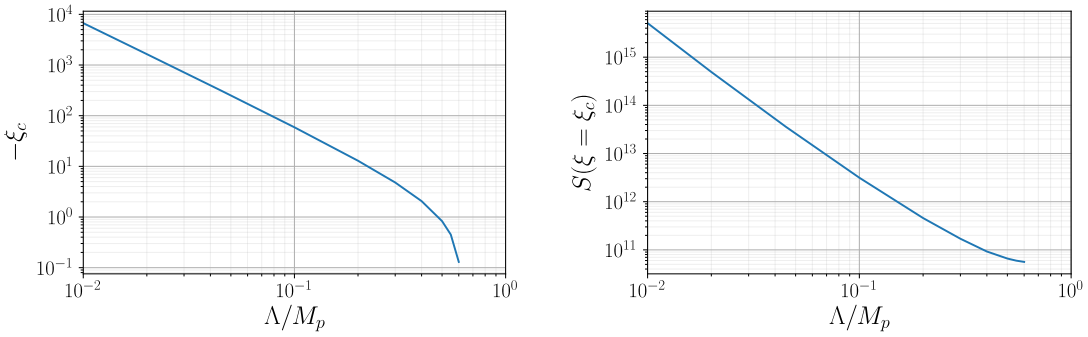

Figure 7.8: Left panel: Dependence of the critical value ξ_c of the nonminimal coupling below which an infinite number of negative modes is present in the scale Λ at which the Higgs potential vanishes. The potential is given by (7.56) with $q = 10^{-7}$. For larger values of Λ, ξ_c is formally positive, but ϕ reaches values close to the Planck scale so that the semi-classical approximation is not expected to be valid. Right panel: Euclidean action of the critical instanton with $\xi = \xi_c$ for the same values of Λ. Plots by Florent Michel.

7.3.1 Negative modes of black hole seeded instantons

We also present the results for the negatives modes of instantons seeded by black holes.[3] Recall from chapter six the metric:

$$ds^2 = f(r)^{2\delta(r)}d\tau^2 + \frac{dr^2}{f(r)} + r^2 d\Omega_2^2, \tag{7.57}$$

where τ is the Euclidean time, f is a smooth positive function, and $d\Omega_2^2$ is the metric on a two-dimensional sphere. We define the function μ by

$$f(r) = 1 - \frac{2G\mu(r)}{r}, \tag{7.58}$$

and the Einstein equations are as given previously

$$\left(r^{2\delta} f\phi'\right)' = r^2 e^{\delta} V'[\phi], \tag{7.59}$$

$$\mu' = 4\pi r^2 \left(\frac{1}{2} f\phi'^2 + V[\phi]\right), \tag{7.60}$$

$$\delta' = 4\pi G\, r\phi'^2. \tag{7.61}$$

We look for asymptotically flat black hole solutions, for which $f(r)$ vanishes at the horizon $r = r_h$ and ϕ approaches the false vacuum as $r \to \infty$. Without loss of generality (up to a global rescaling of τ), we can impose the condition $\delta(r_h) = 0$. The final boundary

[3] This part of the project was done by Florent Michel and has been included for completeness.

condition is given by a regularity condition at the horizon [25]:

$$\phi'(r_h) = \frac{r_h V'[\phi(r_h)]}{1 - 8\pi G r_h^2 V[\phi(r_h)]}. \tag{7.62}$$

To express the eigenvalue equation, we write $\phi = \phi_b + \phi_1$, $\mu = \mu_b + \mu_1$, and $\delta = \delta_b + \delta_1$, where $(\phi_b, \mu_b, \delta_b)$ is an exact solution of equations (7.59 – 7.61). We define $f_b \equiv 1 - 2G\mu_b/r$. The eigenvalue equation is:

$$\frac{e^{-\delta_b}}{r^2}\frac{d}{dr}\left(r^2 e^{\delta_b} f_b \phi_1'\right) = \left(\mathcal{V}(r) - \lambda\right)\phi_1. \tag{7.63}$$

where

$$\mathcal{V}(r) \equiv V''[\phi_b] + 16\pi G r V'(\phi_b)\phi_b' - 8\pi G r f_b' + \delta_b' f_b + \frac{f_b}{r}\phi_b'^2. \tag{7.64}$$

We solved the system (7.59 – 7.61) and the eigenvalue equation (7.63) in the two potentials (7.53) and (7.56). Results for the tunnelling exponent B and negative eigenvalues λ are shown in Figs. 7.9 and 7.10.

Notice that in the case of the quartic potential (7.53) we have an approximate symmetry when the effects of gravity are sufficiently small. The differences between the curves shown in each panel of Fig. 7.9 are thus entirely due to the gravitational back-reaction, which has the tendency to increase the tunnelling exponent B and decrease the absolute value of λ.

For both potentials, in the whole range of parameters that were tried we always found only one negative mode, as could be expected from the fact that the kinetic term in the eigenvalue equation (7.63) is always positive outside the horizon, and the background solution has no node. This suggests that the static instantons with black holes found in [22, 24, 25] can be safely interpreted as the dominant contribution to the decay rate of the false vacuum in the presence of small black holes.

Three solutions corresponding to different values of r_h are shown in Fig. 7.11 for the Higgs-like potential with $\Lambda = 10^{-10}$. Each of them has only one node, which confirms there should exist one and only one negative mode over each instanton.

7.4 Conclusion

In this section, we have studied negative modes of instantons for the case of asymptotically flat O(4)-symmetric Coleman-de Luccia type instantons, including a non-minimal coupling of the scalar, and also presented the results for negative modes of instantons seeded by black holes, such as those developed in [23, 24, 25].

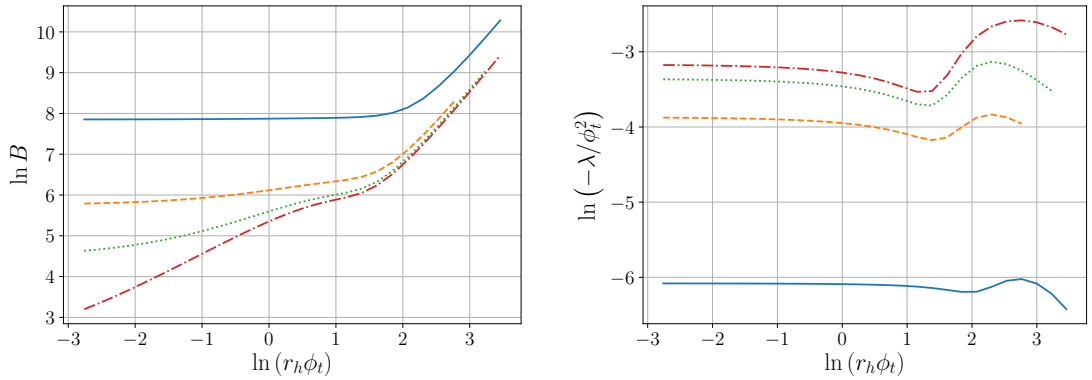

Figure 7.9: Tunnelling exponent for seeded nucleation (left panel) and negative eigenvalue (right panel) of the instanton with black hole for the quartic potential (7.53) with the parameters $a_4 = 1$, $\phi_t = 2\alpha$ and $\phi_m = 0.6\alpha$, where $\alpha = 1$ (blue), $10^{-1/4}$ (orange), $10^{-1/2}$ (green), and 10^{-1} (red). Plots by Florent Michel.

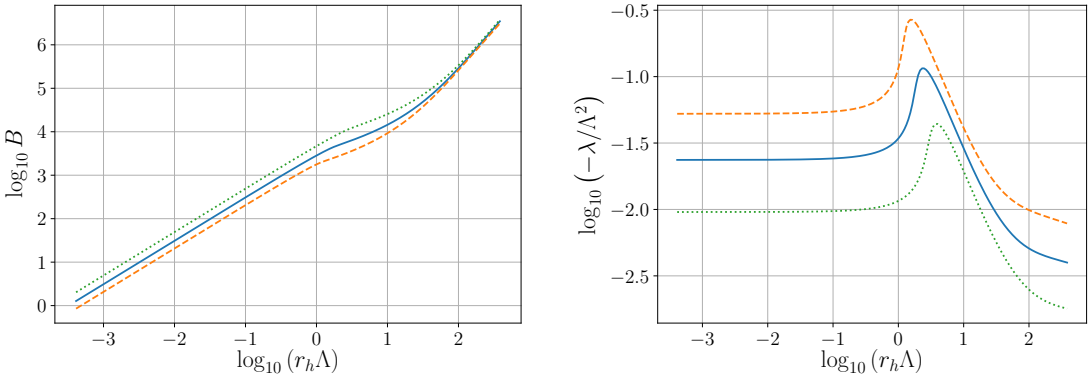

Figure 7.10: Tunnelling exponent for seeded nucleation (left panel) and negative eigenvalue (right panel) obtained for the Higgs potential (7.56) for the same values of the parameters as in Fig. 7.3, right panel. Plots by Florent Michel.

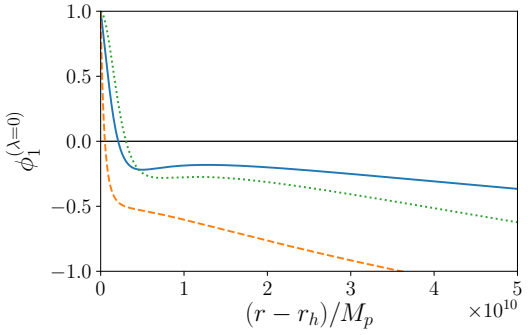

Figure 7.11: Solutions for the tunnelling exponent with $\lambda = 0$ for the Higgs-like potential (7.56) with $\Lambda = 10^{-10}$. The Schwarzschild radius r_h is equal to $0.1\Lambda^{-1}$ (orange), Λ^{-1} (blue), and $10\Lambda^{-1}$ (green). Plot by Florent Michel.

For the O(4)-symmetric asymptotically flat instantons, we explored a wide range of parameter space with a conventional quartic potential, as well as a more phenomenologically realistic analytic fit to the Standard Model Higgs potential. For any value of the nonmimimal coupling parameter ξ, it is always possible to find a region of parameter space in the potential that has an infinite tower of negative modes for the corresponding instanton. However, these parameter values correspond to energies close to the Planck scale.

In the case of the black hole instantons, this problem of infinite negative modes did not occur as the kinetic term of the quadratic action is always positive outside the horizon, and we therefore confirmed numerically that there is always only one negative mode. A change in the potential due to nonmininal coupling would not change the sign of the kinetic term, and therefore, while we did not explicitly consider it here, we would expect the number of negative modes to remain exactly one should it be included.

As already noted in [61, 65, 66], the infinite tower of negative modes that arises when the kinetic term of the quadratic action reaches negative values remains mysterious, although it is intriguing that the tower of modes appear approximately at the self-compactification scale corresponding to a domain wall topological defect of tension σ [67, 68]. Using an analytical estimate for the large negative eigenvalues in the O(4)-symmetric case, we argue that these infinite negative modes induce a divergence in quadratic observables, which seems to support the argument that they may signal a breakdown of the semiclassical approximation.

Assuming asymptotic flatness in both the O(4)-symmetric and black-hole cases, we have found that realistic instantons always have exactly one negative mode. It therefore seems to be a safe interpretation that the leading contribution to the tunnelling rate comes from the lowest-action instanton.

Chapter 8

Conclusions and Further Work

8.1 Conclusions

A general description of vacuum decay was presented in chapter one. Current measurements of the Higgs and top quark masses suggest our universe exists in a metastable false vacuum state, i.e. that the shape of the Higgs potential exhibits a potential barrier and the Higgs field may spontaneously transition to a lower energy state. Such a vacuum decay event was described by Coleman as "the ultimate ecological catastrophe", and this thesis has addressed the possibility that such an event may occur for different spacetimes and for different potentials, including a close approximation to the Higgs potential at high energies.

Chapter two outlined the methods from Coleman and de Luccia [3] that were used throughout this thesis to obtain instanton solutions and the exponent B that gives the dominant contribution to vacuum decay in the tunnelling equation. Profiles of the bubble were obtained by solving the equations of motion for the field, while the difference in action between the bubble and false vacuum states is used to find the tunnelling rate. This technique for finding exact numerical solutions to the bounce was applied in later chapters to tunnelling in de Sitter space, anti-de Sitter space, and a Randall-Sundrum braneworld both with and without the presence of a black hole.

In chapter three, the effects of back reaction were examined for a scalar field in a toy model potential featuring two minima. In this model, there were three free parameters that were varied to determine the effects of back reaction: V_0, that set the height of the potential at $\phi(0) = 0$, the rescaled Planck mass M_p, and a self-coupling parameter g. It was found that:

- For tunnelling in de Sitter space, the spacetime backreacts with the bubble.

- Of the three free parameters V_0, M_p and g, varying the rescaled Planck mass has a lesser effect on the bubble than by varying the parameters in the potential.
- The tunnelling rate is enhanced by increasing the relative difference between the two minima.
- Increasing V_0 has the effect of decreasing the relative difference between the two minima, therefore suppressing vacuum decay.
- Potentials with a taller barrier give rise to thin wall bubbles, while smaller barriers produce thick wall bubbles.
- The thin wall approximation only holds for values of the self-coupling g between 0 and 3/16.

The potentials we consider for vacuum decay in higher dimensions are defined in chapter four. The two potentials of interest are a quartic potential with a well defined false vacuum, resulting in the nucleation of thin wall bubbles, and also a Higgs-like potential that allows for investigation of decay of the Higgs field, where the parameter g can be tuned to fit the Higgs approximation to the actual Higgs potential calculated from two-loop beta functions for a range of top masses. These potentials are then used to investigate vacuum decay in higher dimensions both with and without a black hole.

In chapter five, we considered the case of vacuum decay on the brane and compared this to the regular result for four dimensional asymptotically flat space. For a field in a Randall-Sundrum braneworld featuring a single brane, it was found that the presence of the fifth dimension had very little effect on either the shape of the bubble or the tunnelling rates in the range $0.4 < M_5/M_p < 1.0$, with only a very minor dependence on the AdS radius ℓ. The extra dimension enhances the tunnelling rate when $M_5 << M_p$, but for larger values of M_5 the usual 4D result is reproduced, consistent with the findings of [30].

Chapter six expanded on previous work to investigate the behaviours of four and five dimensional scalar fields around black holes. For large black hole masses, the probability of a bubble nucleating with large enough radius to exceed the black hole horizon rapidly tends to zero, therefore all but eliminating any chances of the black hole seeding vacuum decay. However, black holes that decay rapidly to reach a small mass in the range $10^2 < M_s/M_5 < 10^5$ are extremely likely to trigger a phase transition. The main conclusions of this chapter are:

- Decay rates are presented as branching ratios Γ_D/Γ_H, as the evaporation rate of the seed black holes must be taken into account.
- The tunnelling exponent B is given by the difference in area between the seed and

remnant black holes, a result that can be derived from thermodynamics.

- Black holes at the TeV scale are sufficiently small to seed vacuum decay.
- Current particle accelerators do not operate at high enough energies to seed vacuum decay, though it is possible that such particles may be produced in the most highly energetic cosmic ray collisions.
- The high likelihood of vacuum decay occurring should such TeV black holes exist rules out the possibility of microscopic primordial black holes.

Comparing with the results from chapter five, where it was found that the presence of an extra dimension does not enhance the decay rate, we can conclude that it is the presence of the black hole rather than the extra dimension that seeds vacuum decay.

The final chapter investigated the emergence of negative modes of O(4) and black hole instantons and presented a first look at negative modes with curvature coupling. The main conclusion of this chapter is the new result for the negative eigenvalue λ_0 found analytically using the thin wall approximation, $\lambda_0 \approx -\frac{3}{R_b^2}$.

When exploring the O(4) instantons, for any value of the non-mimimal coupling parameter ξ, an infinite tower of negative modes emerged when parameters were tuned to correspond to energies close to the Planck scale. This was true both for the quartic potential and the potential approximating the Higgs. While the precise reason for the appearance of this infinite stack of negative modes remains a mystery, it appears to be the case that in asymptotically flat space the most realistic instantons (energies not approaching the Planck scale) have only one negative mode. The leading contribution to the decay rate is given by the instanton with the lowest action.

Comparing this briefly to the result for black hole instantons, it was confirmed that for tunnelling in the presence of a black hole, the kinetic term of the action remained positive and thus the instanton only featured a single negative mode.

8.2 Further Work

This thesis has considered vacuum decay for a variety of spacetimes, encompassing both four and five dimensions and incorporating black holes, as well as considering both Higgs-like potentials and potentials with well defined minima. Further work could continue to explore vacuum decay for other models, or address particular problems that arose in the course of this research, such as:

- how to obtain instanton solutions on the brane when $V + \sigma < 0$;

- how to interpret an infinite stack of negative modes.

In chapter five, it was not possible to use the Coleman-de Luccia method to obtain instanton solutions at large AdS radii for negatives values of $V + \sigma$, though it is possible such solutions still exist. A means to confirm or disprove their existence is not currently known, though future work may search for alternate methods of obtaining instanton solutions.

The work in chapter six examining black hole seeded vacuum decay considered the case of spherically symmetric Schwarzchild black holes. Further work may consider vacuum decay seeded by rotating or charged black holes, or consider vacuum decay on a brane in RS1 rather than RS2.

The infinite stack of negative modes that emerges for O(4) instantons at energies near the Planck scale in chapter seven thus far eludes a satisfactory physical interpretation, though future work could investigate this problem further, such as studying time-dependent perturbations around the bounce.

Appendix A

Israel junction conditions

A.1 Israel junction conditions on the brane

In this appendix, we derive the equations of motion for vacuum decay on the brane in RSII from the Israel junction conditions. (A detailed explanation of how junction conditions may be used to derive field equations can be found in [69].) These give us information about the brane's curvature. From [37] the five-dimensional bulk has the Euclidean metric

$$ds^2 = hdt^2 + h^{-1}dr^2 + r^2 d\Omega_3^2 \tag{A.1}$$

On the brane, the metric is

$$ds^2 = d\tau^2 + r^2 d\Omega_3^2 \tag{A.2}$$

The Israel junction conditions are

$$\Delta K_{ab} = 8\pi G_5[\Sigma_{ab} - \frac{1}{3}\Sigma h_{ab}] \tag{A.3}$$

where $\Delta K_{ab} = K_{ab}^+ - K_{ab}^-$ is the jump in the extrinsic curvature and h_{ab} the four-dimensional metric. The indices a and b run over the brane, while we later use the indices μ and ν that run over the bulk. K has the form

$$K = -K_{\tau\tau} + \frac{3}{r^2}K_{\chi\chi} \tag{A.4}$$

The subscript τ denotes imaginary time while χ is the is the radial coordinate of the 3-sphere appearing in equation (5.5).

A.2 Extrinsic Curvature

A.2.1 $K_{\chi\chi}$

We will first derive the $K_{\chi\chi}$ component of the curvature

We define a tangent vector t^a

$$t^a = \dot{t}\partial_t + \dot{r}\partial_r \tag{A.5}$$

where the dot denotes the derivative with respect to imaginary time. From the metric, it is therefore possible to write

$$h\dot{t}^2 + \frac{\dot{r}^2}{h} = 1 \tag{A.6}$$

This allows us to define

$$\dot{t} = \rho/h \tag{A.7}$$

where $\rho = (h - \dot{r}^2)^{\frac{1}{2}}$.

Integrating the stress-energy tensor for the brane, we define

$$\Sigma_{\mu\nu} = \int T_{\mu\nu} dl \tag{A.8}$$

using the stress-energy tensor $T_{\mu\nu}$, where

$$\phi = \phi(\tau) \tag{A.9}$$

$$(\nabla\phi)^2 = \dot{\phi}^2 \tag{A.10}$$

The trace of Σ is given by

$$\Sigma = -\left(\dot{\phi}^2 + 4V + 4\sigma\right) \tag{A.11}$$

while $\Sigma_{\chi\chi}$ can also be written

$$\Sigma_{\chi\chi} = -r^2\left(\frac{1}{2}\dot{\phi}^2 + V + \sigma\right) \tag{A.12}$$

The curvature $K_{\chi\chi}$ has dependence on both the brane and bulk, but can be found from the metric on the brane by taking the non-zero Christoffel symbols and defining a normal

vector n_i

$$\begin{aligned} K_{\chi\chi} &= h^a_\chi h^b_\chi \left(n_{a,b} - \Gamma^c_{ab} n_c\right) && \text{(A.13)} \\ &= \Gamma^c_{\chi\chi} n_c && \text{(A.14)} \\ &= \Gamma^t_{\chi\chi}\dot{r} - \Gamma^r_{\chi\chi}\dot{t} && \text{(A.15)} \\ &= -\frac{1}{2} g^{rr}\left(g_{r\chi,\chi} + g_{r\chi,\chi} - g_{\chi\chi,r}\right)\dot{t} && \text{(A.16)} \\ &= h\dot{t}r && \text{(A.17)} \end{aligned}$$

Therefore, by replacing $\dot{t} = \rho/h$, we can write

$$K_{\chi\chi} = \rho r \tag{A.18}$$

We now use this to find the equations of motion. From the Israel junction conditions we have

$$[K_{\chi\chi}]^+_- = 8\pi G_5 (\Sigma_{\chi\chi} - \frac{1}{3}\Sigma g_{\chi\chi}) \tag{A.19}$$

The curvature is assumed to be equal on both sides of the brane. By symmetry from $K^+_{\chi\chi} = K^-_{\chi\chi}$ we can write

$$\begin{aligned} 8\pi G_5 (\Sigma_{\chi\chi} - \frac{1}{3}\Sigma g_{\chi\chi}) &= 2K_{\chi\chi} && \text{(A.20)} \\ &= 2\rho r && \text{(A.21)} \\ &= 2r\sqrt{h - \dot{r}^2} && \text{(A.22)} \end{aligned}$$

$$\begin{aligned} 2r\sqrt{h-\dot{r}^2} &= 8\pi G_5 \left[-r^2\left(\frac{1}{2}\dot{\phi}^2 + V + \sigma\right) + \frac{1}{3}r^2\left(\dot{\phi}^2 + 4V + 4\sigma\right)\right] && \text{(A.23)} \\ \sqrt{h-\dot{r}^2} &= \frac{4}{3}\pi G_5 r\left[\sigma + \left(V - \frac{1}{2}\dot{\phi}^2\right)\right]. && \text{(A.24)} \end{aligned}$$

Squaring both sides:

$$h - \dot{r}^2 = \left(\frac{4}{3}\pi G_5\right)^2 r^2 \left[\sigma^2 + 2\sigma\left(V - \frac{1}{2}\dot{\phi}^2\right) + \left(V - \frac{1}{2}\dot{\phi}^2\right)^2\right] \tag{A.25}$$

We can then substitute $h = 1 + r^2/\ell^2$ into this equation to get

$$1 + \frac{r^2}{\ell^2} - \dot{r}^2 = \left(\frac{4}{3}\pi G_5\right)^2 r^2 \left[\sigma^2 + 2\sigma\left(V - \frac{1}{2}\dot{\phi}^2\right) + \left(V - \frac{1}{2}\dot{\phi}^2\right)^2\right] \tag{A.26}$$

Equating the r^2 terms then gives an expression in terms of the AdS radius ℓ and the brane

tension σ.

$$\frac{r^2}{\ell^2} = \left(\frac{4\pi G_5}{3}\right)^2 r^2\sigma^2 \tag{A.27}$$

$$\frac{1}{\ell^2} = \left(\frac{4\pi G_5}{3}\right)^2 \sigma^2 \tag{A.28}$$

Taking out the r^2 terms in (A.26) leaves

$$1-\dot{r}^2 = \left(\frac{4\pi G_5}{3}\right)^2 r^2 \left(\frac{6}{4\pi G_5\ell}\left(V-\frac{1}{2}\dot{\phi}^2\right)+\left(V-\frac{1}{2}\dot{\phi}^2\right)^2\right) \tag{A.29}$$

$$= \left(\frac{8\pi G_5}{3\ell}\right)^2 r^2 \left(\frac{6}{4\pi G_5\ell}\left(V-\frac{1}{2}\dot{\phi}^2\right)+r^2\frac{4}{3}\pi G_5\left(V-\frac{1}{2}\dot{\phi}^2\right)^2\right) \tag{A.30}$$

Dividing through by r^2 gives an expression equivalent to the SMS equations as given in [36], where the induced Einstein equations on the brane are found by the Gauss Codazzi projection of the Einstein tensor.

$$\frac{1-\dot{r}^2}{r^2} = \frac{8\pi G_N}{3}\left(V-\frac{1}{2}\dot{\phi}^2\right)+\frac{4\pi G_5}{3}\left(V-\frac{1}{2}\dot{\phi}^2\right)^2 \tag{A.31}$$

A.2.2 $K_{\tau\tau}$

We now look to find the $K_{\tau\tau}$ component of the curvature. $K_{\tau\tau}$ has the form

$$K_{\tau\tau} = t^a t^b n_{a,b} - \Gamma^c_{ab} n_c \tag{A.32}$$

$$= t^t\partial_t n_t + t^r\partial_t n_r - \left(\ddot{t}^2\Gamma^c_{tt} + 2\dot{t}r\Gamma^c_{tr} + r^2\Gamma^c_{rr}\right)n_c \tag{A.33}$$

$$= \dot{t}\ddot{r} - \dot{r}\ddot{t} - 2\dot{t}\dot{r}^2\Gamma^t_{rt} + \dot{t}^3\Gamma^r_{tt} + t\dot{r}^2\Gamma^r_{rr} \tag{A.34}$$

The non-zero Christoffel symbols are

$$\Gamma^t_{rt} = \frac{1}{2}\frac{h'}{h} \tag{A.35}$$

$$\Gamma^r_{tt} = \frac{1}{2}h'h \tag{A.36}$$

$$\Gamma^r_{rr} = -\frac{1}{2}\frac{h'}{h} \tag{A.37}$$

Substituting these into (A.34) and substituting $\dot{t} = \rho/h$ gives

$$K_{\tau\tau} = \dot{t}\ddot{r} - \dot{r}\ddot{t} - 2\dot{t}\dot{r}^2\frac{h'}{h} + \dot{t}^3\frac{1}{2}h'h - t\dot{r}^2\frac{1}{2}\frac{h'}{h} \tag{A.38}$$

$$= \dot{t}\ddot{r} - \dot{r}\ddot{t} - \frac{3}{2}\dot{t}\dot{r}^2\frac{h'}{h} + \frac{\dot{t}^3}{2}h'h \tag{A.39}$$

$$= \frac{\rho}{h}\ddot{r} - \dot{r}\left(\frac{\rho}{h}\right)^{\cdot} - \frac{3\rho h'}{2h^2}\dot{r}^2 + \frac{\rho^3}{2}h'h^2 \tag{A.40}$$

Using (A.6), we now make the substitutions $\rho = \left(h - \dot{r}^2\right)^{\frac{1}{2}}$ and $\dot{\rho} = \frac{1}{2}(h'r - 2\dot{r}\ddot{r})\rho^{-1}$. This gives

$$\left(\frac{\rho}{h}\right)^{\cdot} = \frac{\dot{\rho}}{h} - \frac{\rho h'\dot{r}}{h^2} \tag{A.41}$$

which we substitute into (A.40)

$$K_{\tau\tau} = \frac{\rho}{h}\ddot{r} - \frac{\rho}{h}\dot{r} + \frac{\rho h'}{h^2}r\dot{r} - \frac{3\rho h'}{2h^2}\dot{r}^2 + \frac{\rho^3 h'}{2h^2} \tag{A.42}$$

$$= \frac{\rho}{h}\ddot{r} - \frac{\dot{r}}{2h\rho}\left(h'\dot{r} - 2\dot{r}\ddot{r}\right) + \frac{\dot{r}^2\rho h'}{h^2} - \frac{3\dot{r}^2\rho h'}{2h^2} + \frac{\rho^3 h'}{2h^2} \tag{A.43}$$

$$= \ddot{r}\left(\frac{\rho}{h} + \frac{\dot{r}^2}{h\rho}\right) - \frac{\dot{r}^2 h'}{2h\rho} - \frac{\rho h' h}{2h^2} \tag{A.44}$$

$$= \frac{\ddot{r}}{\rho} - \frac{\dot{r}^2 h'}{2h\rho} - \frac{\rho h'}{2h} \tag{A.45}$$

$$= \frac{\ddot{r}}{\rho} - \frac{h'}{2\rho} \tag{A.46}$$

We arrive at a final expression for $K_{\tau\tau}$

$$K_{\tau\tau} = \frac{\ddot{r} - h'/2}{\rho} \tag{A.47}$$

We can use this to find an expression for $\ddot{r}$. From the Israel junction conditions we have

$$2K_{\tau\tau} = 8\pi G_5(\Sigma_{\tau\tau} - \frac{1}{3}Sg_{\tau\tau}) \tag{A.48}$$

where $g_{\tau\tau} = 1$. $\Sigma_{\mu\nu}$ has the form

$$\Sigma_{\mu\nu} = \phi_{,\mu}\phi_{,\nu} - g_{\mu\nu}\left(\frac{1}{2}(\nabla\phi)^2 + V + \sigma\right) \tag{A.49}$$

where we write the stress-energy tensor in terms of the brane tension σ. The trace of $\Sigma_{\mu\nu}$ is

$$\Sigma = \Sigma^{\mu}_{\mu} = -\left(\dot{\phi}^2 + 4V + 4\sigma\right) \tag{A.50}$$

$\Sigma_{\tau\tau}$ is

$$\Sigma_{\tau\tau} = \frac{1}{2}\dot{\phi}^2 - V - \sigma \tag{A.51}$$

We can therefore write

$$\begin{aligned} 2K_{\tau\tau} &= 8\pi G_5 \left(\frac{1}{2}\dot{\phi}^2 - V - \sigma + \frac{1}{3}\left(\dot{\phi}^2 + 4V + 4\sigma\right)\right) && \text{(A.52)} \\ &= 8\pi G_5 \left(\frac{5}{6}\dot{\phi}^2 + \frac{1}{3}V + \frac{1}{3}\sigma\right) && \text{(A.53)} \end{aligned}$$

We now make the substitution $K_{\tau\tau} = (\ddot{r} - h'/2)/\rho$ from (A.47).

$$2\ddot{r} - h' = 8\pi G_5 \rho \left(\frac{1}{2}\dot{\phi}^2 - V - \sigma + \frac{1}{3}\left(\dot{\phi}^2 + 4V + 4\sigma\right)\right) \tag{A.54}$$

We can now replace ρ using

$$\rho = \frac{4\pi G_5 r}{3}\left(\sigma + V - \frac{1}{2}\dot{\phi}^2\right) \tag{A.55}$$

from the expression for $K_{\chi\chi}$. This gives

$$\begin{aligned} 2\ddot{r} - h' &= \frac{2}{3}(4\pi G_5)^2 r \left(V - \frac{1}{2}\dot{\phi}^2 + \sigma\right)\left(\frac{5}{6}\dot{\phi}^2 + \frac{1}{3}V + \frac{1}{3}\sigma\right) && \text{(A.56)} \\ &= 2\left(\frac{4\pi G_5}{3}\right)^2 r \left[\sigma^2 + 2\sigma\left(\dot{\phi}^2 + V\right) + \left(V - \frac{1}{2}\dot{\phi}^2\right)\left(\frac{1}{3}V + \frac{5}{6}\dot{\phi}^2\right)\right] && \text{(A.57)} \end{aligned}$$

We now make the substitution

$$h' = \frac{2r}{\ell^2} = 2\left(\frac{4\pi G_5}{3}\right)^2 r\sigma^2 \tag{A.58}$$

and replace σ using

$$\sigma = \frac{3}{4\pi G_N \ell^2} \tag{A.59}$$

This gives

$$2\ddot{r} - \frac{2r}{\ell^2} = -\frac{2r}{\ell^2} + \frac{16\pi G_5}{3\ell}(\dot{\phi}^2 + V) + \frac{2r}{3}(4\pi G_5)^2 \left(V - \frac{1}{2}\dot{\phi}^2\right)\left(\frac{1}{3}V + \frac{5}{6}\dot{\phi}^2\right) \tag{A.60}$$

The σ^2 terms now cancel.

$$\ddot{r} = \frac{8\pi G_5 a}{3\ell} a(\dot{\phi}^2 + V) + \frac{r}{3}(4\pi G_5)^2 \left(V - \frac{1}{2}\dot{\phi}^2\right)\left(\frac{1}{3}V + \frac{5}{6}\dot{\phi}^2\right) \tag{A.61}$$

Appendix B

Canonical decomposition

B.1 Canonical decomposition

In this appendix we review and extend the ideas given in [70] that provide a canonical decomposition of a manifold (in our case a Euclidean one) by a foliation of hypersurfaces Σ_τ to recast the gravitational action in its Hamiltonian version.

The gravitational equations on a manifold $\mathcal{M}$ with boundary $\partial\mathcal{M}$ are obtained by the extremisation of the usual Einstein-Hilbert action plus a Gibbons-Hawking surface term:

$$I = -\frac{1}{16\pi G_5}\int_{\mathcal{M}} (R_5 - 2\Lambda_5)\sqrt{g_5} + \int_{\mathcal{B}} \mathcal{L}_m(g,\phi)\sqrt{g_4} + \frac{1}{8\pi G_5}\int_{\partial\mathcal{M}} \sqrt{h}K, \tag{B.1}$$

here $\mathcal{L}_m$ is the matter Lagrangian, $h_{ab} = g_{ab} - n_a n_b$ is the induced metric and $K = g^{ab}K_{ab} = g^{ab}h_a{}^c h_b{}^d \nabla_c n_d$ is the trace of the extrinsic curvature of the boundary $\partial\mathcal{M}$ with normal vector n_a pointing *in* to $\mathcal{M}$.

To simplify this action we make a foliation of the spacetime $\mathcal{M}$ by codimension one time-slices Σ_τ, labelled by a periodic Euclidean time function τ which runs from $\tau = 0$ to $\tau = \beta$. The induced metric on the time-slices is written as

$$\mathfrak{h}_{ab} = g_{ab} - u_a u_b, \tag{B.2}$$

where u^a is a unit normal vector to the slice Σ_τ. In general, $\partial/\partial\tau$ and u^a will not be aligned, but we can decompose $\partial/\partial\tau$ into components along the normal and tangential directions,

$$\left(\frac{\partial}{\partial\tau}\right)^a = N u^a + N^a \tag{B.3}$$

The *lapse function*, N, measures the rate of flow of proper time with respect to the

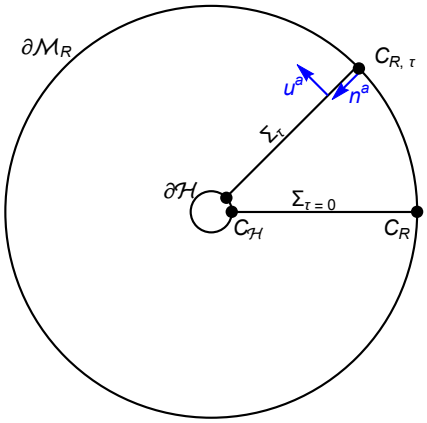

Figure B.1: An illustration of the foliation of the Euclidean $\{\tau, r\}$ section of the brane black hole. The normals u^a and n^a of, respectively, the foliation Σ_τ and manifold boundaries are shown, together with the codimension two surfaces $C_{R,\tau}$ that are regarded as a codimension one submanifold of the Σ_τ surfaces.

coordinate time τ as one moves through the family of hypersurfaces. We construct the time-slices Σ_τ to meet the boundary $\partial\mathcal{M}$ orthogonally for convenience. In the case of the region outside the horizon for I_R^{ext} (6.24), the boundary $\partial\mathcal{M}$ is composed of two surfaces of constant radius, $\Sigma_{\mathcal{H}}$ near the horizon, and Σ_R at large radius.

We use the Gauss identity to relate the Riemann tensor of g_{ab} in five dimensions to the Riemann tensor of $\mathfrak{h}_{ab}$ in four, and the extrinsic curvatures of the constant time slices $\mathcal{K}_{ab} = \mathfrak{h}^c{}_a \mathfrak{h}^d{}_b \nabla_c u_d$, as

$$R_4{}^a{}_{bcd} = \mathfrak{h}^a{}_{a'} \mathfrak{h}_b{}^{b'} \mathfrak{h}_c{}^{c'} \mathfrak{h}_d{}^{d'} R_5{}^{a'}{}_{b'c'd'} + \mathcal{K}^a{}_c \mathcal{K}_{db} - \mathcal{K}^a{}_d K_{cb}. \tag{B.4}$$

Notice this $\mathcal{K}$ is distinct from the extrinsic curvature of Σ_R in (B.1). Contracting (B.4) gives

$$R_5 = R_4 + 2R_{5ab} u^a u^b - (\mathcal{K}^2 - \mathcal{K}^{ab}\mathcal{K}_{ab}), \tag{B.5}$$

and we obtain a relation between the second term of this expression and the extrinsic curvature by commuting covariant derivatives of the normal vector

$$R_{5ab} u^a u^b = 2u^b \nabla_{[c} \nabla_{b]} u^c = \mathcal{K}^2 - \mathcal{K}^{ab}\mathcal{K}_{ab} - \nabla_a (u^a \nabla_c u^c) + \nabla_c (u^a \nabla_a u^c). \tag{B.6}$$

Combining these two expressions leads to the identity,

$$R_5 = R_4 - (\mathcal{K}^{ab}\mathcal{K}_{ab} - \mathcal{K}^2) - 2\left[\nabla_a (u^a \nabla_c u^c) - \nabla_c (u^a \nabla_a u^c)\right], \tag{B.7}$$

which forms the basis of all canonical decompositions of the Einstein-Hilbert action.

When substituted in (B.1), the last two terms of (B.7) are reduced to boundary contributions on $\partial\mathcal{M}$. The first of these vanishes due to orthogonality of $\partial\mathcal{M}_R$ and Σ_τ. The second combines with $\int_{\partial\mathcal{M}} K$ from the original action, and gives on $\partial\mathcal{M}_R$ (with a similar expression for $\partial\mathcal{H}$)

$$\begin{aligned}\frac{1}{8\pi G_5}\int_{\partial\mathcal{M}_R} d^4x\sqrt{h}\left(\nabla_a n^a + n_b u^a\nabla_a u^b\right) &= \frac{1}{8\pi G_5}\int_{\partial\mathcal{M}_R} d^4x\sqrt{h}(g^{ab}-u^a u^b)\nabla_a n_b \\ &= \frac{1}{8\pi G_5}\int_{\partial\mathcal{M}_R} d^4x\sqrt{h}\;\mathfrak{h}^{ab}\nabla_a n_b, \end{aligned} \tag{B.8}$$

but this four dimensional integral can be viewed as an integral over τ of a three dimensional integrand that is precisely the three dimensional extrinsic curvature ${}^3K$ of a family of surfaces $C_R(\tau) = \partial\mathcal{M}_R \cap \Sigma_\tau$ living in the boundary $\partial\mathcal{M}_R$. A similar term is obtained for the $\partial\mathcal{H}$ surface near the horizon however, for the black hole metrics, it turns out that ${}^3K \to 0$ as $r \to r_h$, and so this term does not contribute to the action.

Noticing that $\sqrt{g} = N\sqrt{\mathfrak{h}}$, and introducing a metric ${}^3\mathfrak{h}$ on C_R, we can divide the spacetime integral into space and time, to express the action (B.1) as

$$\begin{aligned} I = -\int N d\tau \Bigg\{ &\frac{1}{16\pi G_5}\int_{\Sigma_\tau}\sqrt{\mathfrak{h}}\left[R_4 - (\mathcal{K}^{ab}\mathcal{K}_{ab} - \mathcal{K}^2) - 2\Lambda_5 - 16\pi G_5\mathcal{L}_m\right] \\ &-\frac{1}{8\pi G_5}\int_{C_R}\sqrt{{}^3\mathfrak{h}}\;{}^3K - \frac{1}{8\pi G_5}\int_{C_\mathcal{H}}\sqrt{{}^3\mathfrak{h}}\;{}^3K\Bigg\}. \end{aligned} \tag{B.9}$$

Furthermore, we can see how the extrinsic curvature is related to the Lie derivative of the intrinsic metric with respect to τ via (B.3):

$$\mathcal{K}_{ab} = \frac{1}{2}\pounds_u\mathfrak{h}_{ab} = \frac{1}{2N}\left(\pounds_\tau\mathfrak{h}_{ab} - \pounds_N\mathfrak{h}_{ab}\right) = \frac{1}{2N}\left(\dot{\mathfrak{h}}_{ab} - 2D_{(a}N_{b)}\right), \tag{B.10}$$

where $\dot{\mathfrak{h}}_{ab} = \mathfrak{h}^c_a\mathfrak{h}^d_b\pounds_\tau\mathfrak{h}_{cd}$ and D_a is the derivative associated with $\mathfrak{h}_{ab}$.

To obtain the Hamiltonian form of I we define the canonical momentum π^{ab} conjugate to the intrinsic metric as

$$\pi^{ab} \equiv \frac{\delta I}{\delta\dot{\mathfrak{h}}_{ab}} = \sqrt{\mathfrak{h}}(\mathcal{K}^{ab} - \mathcal{K}\mathfrak{h}^{ab}), \tag{B.11}$$

This allows us to recast (B.9) in terms of the canonical momentum

$$\begin{aligned} I = -\int_0^\beta N d\tau \Bigg\{ &\frac{1}{16\pi G_5}\int_{\Sigma_\tau}\sqrt{\mathfrak{h}}\left[R_4 - \frac{1}{\mathfrak{h}}\left(\pi^{ab}\pi_{ab} - \frac{1}{3}\pi^2\right) - 2\Lambda_5 - 16\pi G_5\mathcal{L}_m\right] \\ &-\frac{1}{8\pi G_5}\int_{C_R}\sqrt{{}^3\mathfrak{h}}\;{}^3K - \frac{1}{8\pi G_5}\int_{C_\mathcal{H}}\sqrt{{}^3\mathfrak{h}}\;{}^3K\Bigg\}. \end{aligned} \tag{B.12}$$

Now we are ready to perform a Legendre transformation of the Lagrangian and using

(B.10) and (B.11) to obtain the Hamiltonian formulation.

$$\begin{aligned} I = \frac{1}{8\pi G_5}\int_0^\beta d\tau \Big\{ \frac{1}{2}\int_{\Sigma_\tau} \sqrt{\mathfrak{h}}\left(\pi^{ab}\dot{\mathfrak{h}}_{ab} - N\mathcal{H} - N^a\mathcal{H}_a\right) \\ + \int_{C_R}\sqrt{{}^3\mathfrak{h}}(N\ {}^3K + N^a\pi_{ab}n^b) + \int_{C_\mathcal{H}}\sqrt{{}^3\mathfrak{h}}(N\ {}^3K + N^a\pi_{ab}n^b)\Big\}, \end{aligned} \tag{B.13}$$

with the *Hamiltonian constraint* function $\mathcal{H}$ and the *momentum constraint* function $\mathcal{H}^a$ given by

$$\mathcal{H}^a = -2D_b\left(\frac{1}{\sqrt{\mathfrak{h}}}\pi^{ab}\right) \tag{B.14}$$

$$\mathcal{H} = R_4 - 2\Lambda_5 + \frac{1}{\mathfrak{h}}\left(\pi^{ab}\pi_{ab} - \frac{1}{3}\pi^2\right) - 16\pi G_5\mathcal{L}_m. \tag{B.15}$$

Finally, for a static spacetime we have $\dot{\mathfrak{h}}_{ab} = 0$ and in the non-rotating case $N^a = 0$. The metric is a solution to the field equations, so that in particular we have the constraint equations $\mathcal{H} = \mathcal{H}^a = 0$. The only non-vanishing part of the action are the two boundary terms ${}^3K$,

$$I = \frac{1}{8\pi G_5}\int_0^\beta d\tau\left(\int_{C_R}{}^3K\sqrt{h} + \int_{C_\mathcal{H}}{}^3K\sqrt{h}\right). \tag{B.16}$$

For our black hole solutions, this diverges in the limit $R\to\infty$, with R being the radius of the surface C_R in fig. B.1. However, the matter contributions to the black hole instanton solutions die off exponentially at large radii, so that the boundary terms cancel when we calculate the difference in actions between the instanton solutions and the false vacuum solutions with the same mass and periodicity β.

B.2 Brane equations for the instanton bubble

Following the work done in [35, 46] we briefly review the derivation of the equations (6.64-6.66), which describe the dynamics of the bubble-brane system analysed on Section 6.3.

The Einstein equations for a five dimensional RS braneworld can be written as

$${}^{(5)}G_{ab} = -\Lambda_5 g_{ab} + 8\pi G_5\delta(z)(-\sigma h_{ab} + T_{ab}), \tag{B.17}$$

where z is a coordinate defined by taking the proper distance from the brane into the bulk, $G_5 = G_N\ell$ and the cosmological constant of the bulk $\Lambda_5 = -6/\ell^2$ is given in terms of the AdS_5 radius ℓ. Notice that we use latin indices for the bulk spacetime whereas greek indices will be reserved for objects living on the brane. The brane is located at $z = 0$ and

has an induced metric h_{ab}, defined by

$$h_{ab} = g_{ab} - n_a n_b \tag{B.18}$$

where n^a is a unit vector in the $z-$direction. The energy momentum tensor of the brane carries the effect of the tension σ and has a contribution T_{ab}, coming from the fields living in the brane.

The Israel junction conditions for the brane allow us to write down a set of four dimensional Einstein equations (see [35]),

$$G_{\mu\nu} = 8\pi G_N \tilde{T}_{\mu\nu} - \mathcal{E}_{\mu\nu} - \Lambda_{\text{eff}} h_{\mu\nu}, \tag{B.19}$$

where Λ_{eff} is an effective four dimensional cosmological constant on the brane,

$$\Lambda_{\text{eff}} = -\frac{3}{\ell^2} + \frac{(4\pi G_5 \sigma)^2}{3}\,, \tag{B.20}$$

and $\mathcal{E}_{\mu\nu}$ is the projection of the five dimensional Weyl tensor onto the brane

$$\mathcal{E}_{\mu\nu} = {}^{(5)}C^{\alpha}{}_{\beta\rho\sigma} n_\alpha n^\rho h_\mu{}^\beta h_\nu{}^\sigma, \tag{B.21}$$

carrying information about the extra dimensional geometry to the brane. $\mathcal{E}_{\mu\nu}$ is divergence free due to the Bianchi identities. Due to the properties of the Weyl tensor, $\mathcal{E}_{\mu\nu}$ is traceless and divergence free. In the critical RS brane that will be our false vacuum, the tension of the brane is tuned so as to set Λ_{eff} to zero, i.e.

$$\sigma = \frac{3}{4\pi G_5 \ell}\,. \tag{B.22}$$

Finally, the effective energy momentum tensor, $\tilde{T}_{\mu\nu} = T_{\mu\nu} + \pi_{\mu\nu}$ consists of the standard energy momentum tensor, together with second order terms

$$\pi_{\mu\nu} = \frac{1}{\sigma}\left(-\frac{3}{2}T_{\mu\alpha}T^{\alpha}_{\nu} + \frac{1}{2}TT_{\mu\nu} + \frac{3}{4}h_{\mu\nu}T_{\alpha\beta}T^{\alpha\beta} - \frac{1}{4}h_{\mu\nu}T^2\right). \tag{B.23}$$

As discussed in section 6.3, we consider static, spherically symmetric solutions on the brane, with metric (6.39), and make the tidal Ansatz for the Weyl tensor:

$$\mathcal{E}_{\mu\nu}dx^\mu dx^\nu = \mathcal{U}(r)\left(fe^{2\delta}d\tau^2 + f^{-1}dr^2 - r^2 d\Omega_{II}^2\right) \tag{B.24}$$

where the conservation equation gives

$$\mathcal{U}(r) = -\frac{r_Q^2}{r^4}. \tag{B.25}$$

where r_Q is a constant parameter related to the tidal charge Q of [46] by $r_Q^2 = -Q$. The metric functions $f(r)$ and $\delta(r)$ are determined by the effective Einstein equations (B.19). Following [25], we define a "mass function" $\mu(r)$ by

$$f = 1 - \frac{2G_N\mu(r)}{r} - \frac{r_Q^2}{r^2}, \tag{B.26}$$

where we have explicitly factored out the tidal term r_Q^2/r^2. The relevant components of the Einstein tensor are

$$G^t{}_t = -\frac{2G_N\mu'}{r^2} + \frac{r_Q^2}{r^4} \quad , \quad G^r{}_r - G^t{}_t = \frac{2f}{r}\delta' \tag{B.27}$$

For the instanton scalar profile with potential $V(\phi)$, the energy-momentum tensor for the scalar field is

$$T_{\mu\nu} = \phi'^2\delta^r_\mu\delta^r_\nu - h_{\mu\nu}\left(\frac{1}{2}f\phi'^2 + V\right), \tag{B.28}$$

thus inputting the form of f, we see that the tidal contribution is cancelled by the tidal tensor, and we finally obtain the equations of motion (6.64-6.66) used in the numerical integration:

$$0 = f\phi'' + \frac{2}{r}f\phi' + \delta' f\phi' + f'\phi' - \frac{\partial V}{\partial\phi} \tag{B.29}$$

$$\mu'(r) = 4\pi r^2\left[\frac{1}{2}f\phi'^2 + V - \frac{2\pi G_N}{3}\ell^2(\frac{1}{2}f\phi'^2 - V)(\frac{3}{2}f\phi'^2 + V)\right], \tag{B.30}$$

$$\delta' = 4\pi G_N r\phi'^2\left[1 - \frac{4\pi G_N}{3}\ell^2(\frac{1}{2}f\phi'^2 - V)\right]. \tag{B.31}$$

Bibliography

[1] P. W. Higgs. Broken Symmetries and the Masses of Gauge Bosons. *Physical Review Letters*, 13:508–509, October 1964.

[2] Sidney R. Coleman. The Fate of the False Vacuum. 1. Semiclassical Theory. *Phys. Rev.*, D15:2929–2936, 1977. [Erratum: Phys. Rev.D16,1248(1977)].

[3] Sidney R. Coleman and Frank De Luccia. Gravitational Effects on and of Vacuum Decay. *Phys. Rev.*, D21:3305, 1980.

[4] I. Yu. Kobsarev, L. B. Okun, and Ya. B. Zeldovich. Spontaneous cp-violation and cosmology. *Phys. Lett.*, 50B:340–342, 1974.

[5] I. Yu. Kobzarev, L. B. Okun, and M. B. Voloshin. Bubbles in Metastable Vacuum. *Sov. J. Nucl. Phys.*, 20:644–646, 1975. [Yad. Fiz.20,1229(1974)].

[6] Joan Elias-Miro, Jose R. Espinosa, Gian F. Giudice, Gino Isidori, Antonio Riotto, and Alessandro Strumia. Higgs mass implications on the stability of the electroweak vacuum. *Phys. Lett.*, B709:222–228, 2012.

[7] Jose R. Espinosa, Gian F. Giudice, Enrico Morgante, Antonio Riotto, Leonardo Senatore, Alessandro Strumia, and Nikolaos Tetradis. The cosmological Higgstory of the vacuum instability. *JHEP*, 09:174, 2015.

[8] Curtis G. Callan and Sidney R. Coleman. The Fate of the False Vacuum. 2. First Quantum Corrections. *Phys. Rev.*, D16:1762–1768, 1977.

[9] Alessandro Strumia and Nikolaos Tetradis. Bubble nucleation rates for cosmological phase transitions. *JHEP*, 11:023, 1999.

[10] Moshe Carmeli and Tanya Kuzmenko. Value of the cosmological constant in the cosmological relativity theory. *International Journal of Theoretical Physics*, 41(1): 131–135, Jan 2002.

[11] Giuseppe Degrassi, Stefano Di Vita, Joan Elias-Miro, Jose R. Espinosa, Gian F. Giudice, Gino Isidori, and Alessandro Strumia. Higgs mass and vacuum stability in the Standard Model at NNLO. *JHEP*, 08:098, 2012.

[12] Ilya V. Krive and Andrei D. Linde. On the Vacuum stability problem in gauge theories. *Nucl. Phys.*, B432:265, 1976.

[13] Nicola Cabibbo, Luciano Maiani, Giorgio Parisi, and Roberto Petronzio. Bounds on the Fermions and Higgs Boson Masses in Grand Unified Theories. *Nucl. Phys.*, B158: 295–305, 1979.

[14] H. David Politzer and Stephen Wolfram. Bounds on particle masses in the Weinberg-Salam model. *Physics Letters B*, 82(2):242 – 246, 1979.

[15] Gino Isidori, Giovanni Ridolfi, and Alessandro Strumia. On the metastability of the standard model vacuum. *Nucl. Phys.*, B609:387–409, 2001.

[16] Arttu Rajantie and Stephen Stopyra. Standard Model vacuum decay with gravity. *Phys. Rev.*, D95(2):025008, 2017.

[17] Anders Andreassen, William Frost, and Matthew D. Schwartz. Scale Invariant Instantons and the Complete Lifetime of the Standard Model. *Phys. Rev.*, D97(5): 056006, 2018.

[18] Vincenzo Branchina, Filippo Contino, and Apostolos Pilaftsis. Protecting the stability of the electroweak vacuum from Planck-scale gravitational effects. *Phys. Rev.*, D98 (7):075001, 2018.

[19] M. Tanabashi et al. Review of Particle Physics. *Phys. Rev.*, D98(3):030001, 2018.

[20] Dario Buttazzo, Giuseppe Degrassi, Pier Paolo Giardino, Gian F. Giudice, Filippo Sala, Alberto Salvio, and Alessandro Strumia. Investigating the near-criticality of the Higgs boson. *JHEP*, 12:089, 2013.

[21] Kfir Blum, Raffaele Tito D'Agnolo, and JiJi Fan. Vacuum stability bounds on Higgs coupling deviations in the absence of new bosons. *JHEP*, 03:166, 2015.

[22] Ruth Gregory, Ian Moss, and Benjamin Withers. Black holes as bubble nucleation sites. *JHEP*, 03:081, 2014.

[23] Philipp Burda, Ruth Gregory, and Ian Moss. Gravity and the stability of the Higgs vacuum. *Phys. Rev. Lett.*, 115:071303, 2015.

[24] Philipp Burda, Ruth Gregory, and Ian Moss. Vacuum metastability with black holes. *JHEP*, 08:114, 2015.

[25] Philipp Burda, Ruth Gregory, and Ian Moss. The fate of the Higgs vacuum. *JHEP*, 06:025, 2016.

[26] Ruth Gregory and Ian G. Moss. The Fate of the Higgs Vacuum. *PoS*, ICHEP2016: 344, 2016.

[27] Nikolaos Tetradis. Black holes and Higgs stability. *JCAP*, 1609(09):036, 2016.

[28] Pisin Chen, Guillem Domènech, Misao Sasaki, and Dong-han Yeom. Thermal activation of thin-shells in anti-de Sitter black hole spacetime. *JHEP*, 07:134, 2017.

[29] Kyohei Mukaida and Masaki Yamada. False Vacuum Decay Catalyzed by Black Holes. *Phys. Rev.*, D96(10):103514, 2017.

[30] Stephen C. Davis and Sylvain Brechet. Vacuum decay on a brane world. *Phys. Rev.*, D71:104023, 2005.

[31] Lisa Randall and Raman Sundrum. A Large mass hierarchy from a small extra dimension. *Phys. Rev. Lett.*, 83:3370–3373, 1999.

[32] Lisa Randall and Raman Sundrum. An Alternative to compactification. *Phys. Rev. Lett.*, 83:4690–4693, 1999.

[33] W. Israel. Singular hypersurfaces and thin shells in general relativity. *Nuovo Cim.*, B44S10:1, 1966. [Nuovo Cim.B44,1(1966)].

[34] Jaume Garriga and Takahiro Tanaka. Gravity in the brane world. *Phys. Rev. Lett.*, 84:2778–2781, 2000.

[35] Tetsuya Shiromizu, Kei-ichi Maeda, and Misao Sasaki. The Einstein equation on the 3-brane world. *Phys. Rev.*, D62:024012, 2000.

[36] Misao Sasaki, Tetsuya Shiromizu, and Kei-ichi Maeda. Gravity, stability and energy conservation on the Randall-Sundrum brane world. *Phys. Rev.*, D62:024008, 2000.

[37] Peter Bowcock, Christos Charmousis, and Ruth Gregory. General brane cosmologies and their global space-time structure. *Class. Quant. Grav.*, 17:4745–4764, 2000.

[38] Leopoldo Cuspinera, Ruth Gregory, Katie M. Marshall, and Ian G. Moss. Higgs vacuum decay from particle collisions? *Phys. Rev. D*, 99:024046, Jan 2019.

[39] Daisuke Ida, Tetsuya Shiromizu, and Hirotaka Ochiai. Semiclassical instability of the brane world: Randall-Sundrum bubbles. *Phys. Rev.*, D65:023504, 2002.

[40] Hirotaka Ochiai, Daisuke Ida, and Tetsuya Shiromizu. Quantum creation of the Randall-Sundrum bubble. *Prog. Theor. Phys.*, 107:703–715, 2002.

[41] Hideaki Kudoh and Yasunari Kurita. Thermodynamics of four-dimensional black objects in the warped compactification. *Phys. Rev.*, D70:084029, 2004.

[42] Hideaki Kudoh, Takahiro Tanaka, and Takashi Nakamura. Small localized black holes in brane world: Formulation and numerical method. *Phys. Rev.*, D68:024035, 2003.

[43] Robert C. Myers and M. J. Perry. Black Holes in Higher Dimensional Space-Times. *Annals Phys.*, 172:304, 1986.

[44] Vijay Balasubramanian and Per Kraus. A Stress tensor for Anti-de Sitter gravity. *Commun. Math. Phys.*, 208:413–428, 1999.

[45] Roberto Emparan, Clifford V. Johnson, and Robert C. Myers. Surface terms as counterterms in the AdS / CFT correspondence. *Phys. Rev.*, D60:104001, 1999.

[46] Naresh Dadhich, Roy Maartens, Philippos Papadopoulos, and Vahid Rezania. Black holes on the brane. *Phys. Lett.*, B487:1–6, 2000.

[47] Roy Maartens. Cosmological dynamics on the brane. *Phys. Rev.*, D62:084023, 2000.

[48] Ruth Gregory, Richard Whisker, Kris Beckwith, and Chris Done. Observing braneworld black holes. *JCAP*, 0410:013, 2004.

[49] Roy Maartens and Kazuya Koyama. Brane-World Gravity. *Living Rev. Rel.*, 13:5, 2010.

[50] Panagiota Kanti and Elizabeth Winstanley. Hawking Radiation from Higher-Dimensional Black Holes. *Fundam. Theor. Phys.*, 178:229–265, 2015.

[51] Don N. Page. Particle Emission Rates from a Black Hole: Massless Particles from an Uncharged, Nonrotating Hole. *Phys. Rev.*, D13:198–206, 1976.

[52] Chris M. Harris and Panagiota Kanti. Hawking radiation from a (4+n)-dimensional black hole: Exact results for the Schwarzschild phase. *JHEP*, 10:014, 2003.

[53] John Linsley. Evidence for a primary cosmic-ray particle with energy 10**20-eV. *Phys. Rev. Lett.*, 10:146–148, 1963.

[54] M. Nagano and Alan A. Watson. Observations and implications of the ultrahigh-energy cosmic rays. *Rev. Mod. Phys.*, 72:689–732, 2000.

[55] Alexander Aab et al. Measurement of the Cosmic Ray Spectrum above 4×10^{18} eV Using Inclined Events Detected with the Pierre Auger Observatory. *JCAP*, 1508:049, 2015.

[56] Gino Isidori, Vyacheslav S. Rychkov, Alessandro Strumia, and Nikolaos Tetradis. Gravitational corrections to standard model vacuum decay. *Phys. Rev.*, D77:025034, 2008.

[57] Alberto Salvio, Alessandro Strumia, Nikolaos Tetradis, and Alfredo Urbano. On gravitational and thermal corrections to vacuum decay. *JHEP*, 09:054, 2016.

[58] Arttu Rajantie and Stephen Stopyra. Standard Model vacuum decay in a de Sitter Background. *Phys. Rev.*, D97(2):025012, 2018.

[59] Sidney R. Coleman, V. Glaser, and Andre Martin. Action Minima Among Solutions to a Class of Euclidean Scalar Field Equations. *Commun. Math. Phys.*, 58:211, 1978.

[60] David Garfinkle and Ruth Gregory. Corrections to the Thin Wall Approximation in General Relativity. *Phys. Rev.*, D41:1889, 1990.

[61] Hakjoon Lee and Erick J. Weinberg. Negative modes of Coleman-De Luccia bounces. *Phys. Rev.*, D90(12):124002, 2014.

[62] George V. Lavrelashvili, V. A. Rubakov, and P. G. Tinyakov. Tunneling transitions with gravitation: breaking of the quasiclassical approximation. *Phys. Lett.*, 161B: 280–284, 1985.

[63] Takahiro Tanaka and Misao Sasaki. False vacuum decay with gravity: Negative mode problem. *Prog. Theor. Phys.*, 88:503–528, 1992.

[64] George V. Lavrelashvili. Negative mode problem in false vacuum decay with gravity. *Nucl. Phys. Proc. Suppl.*, 88:75–82, 2000.

[65] Michael Koehn, George Lavrelashvili, and Jean-Luc Lehners. Towards a Solution of the Negative Mode Problem in Quantum Tunnelling with Gravity. *Phys. Rev.*, D92 (2):023506, 2015.

[66] Lorenzo Battarra, George Lavrelashvili, and Jean-Luc Lehners. Negative Modes of Oscillating Instantons. *Phys. Rev.*, D86:124001, 2012.

[67] G. W. Gibbons. Global structure of supergravity domain wall space-times. *Nucl. Phys.*, B394:3–20, 1993.

[68] Filipe Bonjour, Christos Charmousis, and Ruth Gregory. Thick domain wall universes. *Class. Quant. Grav.*, 16:2427–2445, 1999.

[69] Eric Poisson. A relativist's toolkit. *A Relativist's Toolkit, by Eric Poisson, Cambridge, UK: Cambridge University Press, 2007*, 12 2007.

[70] S. W. Hawking and Gary T. Horowitz. The Gravitational Hamiltonian, action, entropy and surface terms. *Class. Quant. Grav.*, 13:1487–1498, 1996.